FINAL PROGRESS REPORT

Principal Investigator Information:
Mark Redfern, Ph.D.
University of Pittsburgh
826 Cathedral of Learing
Pittsburgh, PA 15260
412-624-9019
mredfern@pitt.edu

Institution to which award was made:
University of Pittsburgh
Office of Research
University Club, B21
University Place
Pittsburgh, PA 15261

Project Information:

Title: Developing a Computational Model for Shoe-Floor Friction Related to Slipping Accidents
Project Director: Mark Redfern, PhD
Co-Investigators: Kurt Beschorner, PhD
Sponsor: National Institute of Occupational Safety and Health
Grant number: R01OH008986
Start date: 8/1/2010; End date: 7/31/2014

Final Progress Report Submitted in October, 2014.

A.Table of Contents

B.List of Terms and Abbreviations

A_c: Contact area
$COF_{adhesion}$: Coefficient of friction due to adhesion
COF_{asp}: Coefficient of friction between contacting asperities
$COF_{asymptote}$: Asymptotic coefficient of friction at high sliding speeds
COF_{BL}: Boundary lubrication coefficient of friction
E': Elastic modulus
$F_{N(tot)}$: Total normal force across shoe-floor fluid interface
$F_{adhesion}$: Friction force due to adhesion
$F_{fr(fluid)}$: Friction force from the fluid
F_{dry}: Friction force under dry conditions
$F_{hysteresis}$: Friction force due to hysteresis
$F_{N(asp)}$: Normal force between contacting asperities.x
$F_{SAE75W-140}$: Friction force when SAE75W-140 fluid contaminant is present
G(t): Shear modulus as a function of time.
G_∞: Long-term shear modulus
G_0: Short-term shear modulus
H_{min}: Minimum film thickness
NF_{fluid}: Normal force supported by the fluid
p: Hydrodynamic pressures
R': Radius of curvature
S_{eq}: Shear force between contacting asperities
v: sliding velocity
Δx: distance between fluid pressure scans
Δy: distance between fluid pressure samples
Δt: time between fluid pressure samples
τ_{hydro}: Decay constant relating sliding speed and COF
η: Fluid viscosity

C.Abstract

Slip and fall accidents are among the leading and fastest growing sources of occupational injuries. Slip and fall accidents typically occur when the available friction between the shoe and the floor is less than the friction that is required during walking or performing some task. Existing methods of evaluating shoe and floor slip-resistance are limited to using tribometers to measure the coefficient of friction (COF). This approach is limited because COF is a gross approximation of several tribological mechanisms and cannot guide interventions. Over the past four years, our team has created shoe-floor friction models and performed experimental studies to identify and quantify the underlying tribological contributions to shoe-floor COF. These studies were performed at the microscopic scale (Aim 1), the whole-shoe scale (Aim 2) and during laboratory studies of human subjects (Aim 3). These studies revealed two mechanisms by which fluid contaminants can cause a slip: hydrodynamic lubrication and boundary lubrication. Each was explored from the microscopic level through to human biomechanical slip evaluations.

Hydrodynamic lubrication occurs when fluid between the shoe and the floor becomes pressurized and reduces COF. This effect was confirmed by fluid modeling and experimental studies at the microscopic scale, experimental studies at the whole shoe scale, and by human slipping studies. Specifically, at the microscopic scale, shoe-floor COF decreased with increasing sliding speed and fluid viscosity consistent with the film thickness that were estimated by hydrodynamic models. At the whole-shoe scale, a novel method of measuring under-shoe fluid pressures was implemented to evaluate the factors that influence hydrodynamic lubrication. Shoe tread and fluid viscosity were identified as the critical factors influencing under-shoe fluid pressures. The finding that shoe tread reduces under-shoe fluid pressures and slipping risk was confirmed in human subject studies using an unexpected slipping paradigm.

Boundary lubrication occurs when a fluid does not become pressurized but still reduces the COF between the surfaces. The two main contributors to boundary lubrication friction were identified as adhesion and hysteresis COF. High viscosity fluid contaminants drastically reduced the adhesion COF and caused the shoe-floor interface to become slippery. Adhesion in the presence of a fluid was modeled as a function of the fluid and the amount of dry adhesion at the microscopic model. Furthermore, finite element analysis was used to model the amount of dry adhesion and hysteresis friction at the microscopic scale. This model showed strong correlation with experimental data. Furthermore, this model was used to explain the independent effects of shoe hardness, roughness, floor roughness, speed and vertical loading on coefficient of friction. Boundary lubrication COF values for different shoe materials were found to predict slipping risk using a human-slipping paradigm, confirming the relevance of this mechanism for shoe-floor friction.

The findings from this study can be applied to improve shoe design, selection and maintenance. For example, shoes that maintain a rough outsole and that contain at least 1.5 mm of tread will reduce fluid pressures and maximize boundary lubrication COF for environments that commonly experience greasy or oily contaminants (i.e., restaurant kitchens).

Section 1 of the Final Progress Report

D.Significant (Key) Findings:

Key findings were made for each of the three proposed specific aims. Initially, the tribological mechanisms that were relevant to shoe-floor friction were more precisely defined and described. These initial experiments and models were then used to guide the modeling process by focusing on modeling the most relevant mechanisms. Human studies were then performed to validate the key findings related to the two relevant tribological mechanisms.

Key Finding 1: Boundary and mixed lubrication are relevant to shoe-floor coefficient of friction (COF). Microscopic models (Aim 1) of the fluid were conducted to explain the response of COF to fluid viscosity and sliding speed during pin-on-disk experiments [1]. This study determined that mixed-lubrication was only relevant at high sliding speeds and with high viscosity fluids (e.g., oil), while boundary lubrication was relevant at lower speeds and with lower viscosity fluids (e.g., water). Macroscopic experiments (Aim 2) that measured under-shoe fluid pressures (an indicator of mixed-lubrication) confirmed that mixed lubrication was only relevant in the presence of high-viscosity fluids [2]. This study further found that boundary lubrication was also the dominant friction mechanism regardless of fluid viscosity when considering treaded shoes.

Key Finding 2: Worn shoe tread causes an increase in fluid pressure, which is associated with increased slip risk. The impact of shoe tread wear was evaluated using a mechanical slip-tester (Aim 2) [2] and an unexpected slipping paradigm using human subjects (Aim 3) [3]. In both experiments, under-shoe fluid pressures were measured. The mechanical slip-testing experiments revealed that fluid pressures were negligible in conditions where all or half of the shoe tread was present; however, fluid pressure became significant when no shoe tread remained. Human slip-testing experiments confirmed that fluid pressures were substantial for shoes with completely worn tread and were negligible for shoes with full tread. This study also found a relationship between the under-shoe fluid pressures and the slipping severity, indicating that under-shoe fluid pressures are predictive of slip risk.

Key Finding 3: Microscopic modeling of shoe-floor asperity contact explains impact of shoe materials and roughness on adhesion and hysteresis COF. We developed a microscopic finite element analysis model that simulates the contact between shoe and floor asperities and used this model to explain experimental findings (Aim 1) [4]. For example, shoe roughness is a strong covariate with shoe hardness, which prevented experimental studies from determining which factor explained the relationship between shoe material and COF. The developed model was able to isolate the effects of material and roughness, and predict their impacts on COF in the boundary lubrication regime, for both adhesion and hysteresis. The model revealed that adhesion friction was positively correlated with shoe hardness and negatively correlated with shoe roughness, while hysteresis friction was negatively correlated with hardness and positively correlated with roughness. For example, softer shoe materials with a rough surface have increased hysteresis friction because their increased roughness more than offsets the impact of soft shoe materials. One implication is that to optimize hysteresis friction, new shoe materials would need to be developed that are hard but maintain a high roughness level.

Key Finding 4: Shoe materials with higher boundary lubrication reduce slip risk. The impact of shoe material on slip risk in boundary lubrication was evaluated using a human subject unexpected slipping protocol (Aim 3). Treaded shoes were made using three different outsole shoe materials with different hardness levels. COF measurements confirmed that the softest shoe material had the highest COF when contaminated with a 50% glycerol/50% water solution (Aim 2). The unexpected slipping paradigm found that the softest shoe material led to the fewest number of slips, consistent with the microscopic model (Aim 1) and the measurements of macroscopic testing (Aim 2). We intend to expand these findings by

quantifying how well predicted friction from a macroscopic model that is currently being completed (Aim 2) can predict these slipping outcomes. The development of the macroscopic model was delayed by a change in modeling approach given that boundary lubrication was highly relevant to slip-resistance, but should be completed within the next year.

Translation of Findings:

Replacing Worn Shoes: Our finding that worn shoes dramatically increase slipping risk in the presence of viscous fluids is currently being translated to industry. This finding has been incorporated into a training program (funded by the OSHA Susan Harwood program) that is being disseminated through a train-the-trainer approach to electric utility, gas utility and power plant employees. In addition, the Co-I (Beschorner) has disseminated these results to three major footwear companies. The research team has submitted a new R01 study to build on these findings in order to precisely identify replacement limits of shoes and identify the factors that contribute to shoe wear to improve the specificity of industry recommendations.

Novel Testing Methods: The measurement of under-shoe fluid pressures is currently being translated into a standard shoe testing method. We are working to commercialize this technology through an SBIR grant from the National Institute of Health and to develop a standard through the slip-testing standards committee (ANSI/NFSI B101.7). This technology allows for the measurement of drainage capacity of new and used shoes.

Boundary Lubrication Model: The boundary lubrication model offers the potential as a tool for improving the design of slip-resistant shoes. This tool has teased out the contributions of hardness and roughness on COF and to examine how sliding speed and contact pressure each independently contribute to COF. The following findings have been communicated to shoe companies: hard and rough shoe and floor surfaces contribute to increased COF under oily conditions; soft and smooth shoe and floor surfaces increase COF under dry and water-contaminated conditions; rough floors increase COF under oily conditions; and better load distribution increases both COF across all conditions. We continue to work with these companies to translate these fundamental findings to impact shoe design.

Outcomes/ Impact:

Potential Outcomes:

- The findings about shoe wear have the potential to lead to improved safety practices. Specifically, the finding that worn shoes increase slip risk can be used by employees to check shoe tread and replace shoes once tread has been worn. This finding also has the potential to modify administrative controls by guiding workplaces to check employees' shoes and replace them once they become too worn.
- The findings from the boundary lubrication model can be used to guide development of novel materials and tread designs. For example, new materials that are both rough and hard are predicted to maximize oily coefficient of friction. Also, new tread designs that enhance load distribution can also be used to enhance dry and oily coefficient of friction.
- Lastly, broad adaptation of the novel methods used evaluating under-shoe fluid pressures in this grant has the potential to lead to improved shoe selection by shoe users and more rigorous testing standards for shoe producers. Therefore, these methods are expected to lead to improved slip-resistance of shoes that will reduce slip and fall accidents.

Intermediate Outcomes

- The findings related to shoe wear have been integrated into safety training programs that are currently being disseminated. A train-the-trainer paradigm is being utilized for this dissemination to achieve broad impact.

End Outcomes

- No end outcomes are noted at this time. Future research is required to determine the effectiveness of the intermediate outcomes on end outcomes.

Section 2 of the Final Progress Report: Scientific Report.

E. Background

E.1. Problem Statement and Significance

Falls continue to be among the leading generators of work-related injuries. Britain ranked slips, trips and falls as the most frequent event leading to fatal and non-fatal major accidents, accounting for 30% of all job-related injuries in 1997/1998 (Health and Safety Executive, 1998). In Sweden, 22% of all occupational accidents were attributed to falls, once again the most numerous type of job-related accidents (National Board of Occupational Safety and Health, 1998). The US Bureau of Labor Statistics (BLS) reported that falls accounted for an average 17% of non-fatal injuries and 12% of deaths (Department of Labor, 1998). Injuries from falls are often severe. More than 25% of workers that sustain falling injuries miss 31 days at work or more [5]. Falls are often listed as the cause of the most disabling conditions (e.g. fractures and multiple injuries), affecting, in nearly 2/3 of the cases, the trunk (mostly back) and lower extremities [5]. The severity of fall-related injuries is partly responsible for their high economical costs. An estimated 24% of the direct cost of all claims filed during 1989/1990 was attributed to falls [6].

Falls are often initiated by slip events. The US National Health Interview Survey questionnaire administered by the National Center for Health Statistics in 1997 revealed a clear majority (64%) of the work-related falls attributed to slipping, tripping or stumbling. Investigations of occupational falls occurring on the same level from 1992-1998 indicated that slipping was the most common triggering event (43% of the cases), followed by tripping (18%) and loss of balance (14%) (BLS, 1992-1998).

Existing approaches to reduce slips and falls are to: 1) control the environment to eliminate hazards through aggressive housekeeping, 2) increase awareness of workers in high risk areas, and 3) match shoes and floors to the environmental conditions and tasks that are required. This proposal addresses the third approach; namely, designing appropriate shoes and/or floors. Current methods include measuring the COF of the shoe-floor interface and determining if that measure is sufficient to resist slips. While valuable, this approach is limited by the fact that there is no consensus on the appropriate methods to measure slip resistance as relates to human slipping. In addition, slip resistance measurement can only be accomplished on existing shoes and floors. Thus, current methods cannot take a proactive approach to developing safe environments through design. We propose to take a new approach by developing a computational model that will predict the COF of a shoe-floor-contaminant. This model can then be used in the development and evaluation of shoes and floors under various conditions. In addition, the model will be able to evaluate the sensitivity of slip resistance to parameters (such as tread, materials, flooring, contaminant properties) that impact slips and falls. Thus, the significance of this project is the potential for reducing slip/fall injuries in the workplace using computational modeling. We believe that the computational models developed here will be used in the design and evaluation of work environments to reduce slip and fall injuries. In addition, the models will contribute to the fundamental knowledge of shoe-floor slipping that will then lead to improvements in slip testing and shoe design.

E.2. Current Methods and Models in Slip Resistance Evaluations

In this section, we briefly review current methods of evaluating the slip resistance of shoes and floors, and indicate the strengths and limitations of each method.

E.2.1. Slips Testing Devices

Slip resistance testing is a common empirical method for evaluating the slip resistance of the shoe-floor-contaminant interface. Given the theoretical complexity of the interface, slip resistance testing provides a straight-forward way to evaluate the potential for slips and falls for

existing environments. These measurements can be useful in getting a general sense of slip resistance of a particular environment; however, controversy exists regarding the quality of measures from the various devices that are used. Measures among the testing devices often disagree, depending upon the shoe, floor and contaminant involved. Experts have agreed that these tests should be performed under conditions that closely resemble what occurs during a human slip (ie biofidelic) [7]. Slip testers have used a variety of approaches to measure slip resistance including small portable devices for use in the field and large laboratory devices capable of exerting high loads and fast speeds. Many of the portable devices use a small amount of shoe material, while stationary lab devices often use the entire shoe. Chang et al. provides an overview of common used slipmeters [8].

The most common portable devices are the English XL and the Brungraber Mark II. Both of these devices allow for a collision between a shoe material and the floor at varying angles and the COF is determined by the maximum amount of angle that the shoe material is able to stick to the floor and not slip. The difference between these devices is the English XL is pneumatically driven and the Brungraber Mark II is gravity driven [9]. One major limitation of this method is that while studies have shown that the amount of tread has a significant effect on COF, there is often little or no tread on the pads [10].

Lab devices often test an entire shoe at higher loading levels under more controlled loading conditions with increased flexibility in shoe angle, loading levels, and sliding velocity. Numerous lab devices have been developed including the SATRA device (SATRA spec), the slip simulator [11], and the High Payload Precision Slipmeter [12]. While it is well-known that sliding velocity, shoe angle, and force are variable during a slip, none of these devices have attempted to reproduce these conditions during testing.

E.2.2. Human Centered Approaches

Because the primary goal of measuring friction is to reduce injuries that result from slipping, some human centered methods have been developed to evaluate shoes and floors. One approach for quantifying COF was developed by Skiba et al. having subjects walk on a surface with continuously increasing inclination until the subject fell or felt unsafe [13]. This angle is then used to determine the maximum available friction. This method was adopted as a German standard for determining slip resistance of a floor (DIN 51130, 1992). The use of inclination angle, while allowing for simple quantification of the COF from subject-based data, probably does not resemble a hazardous and dangerous slip precisely because of the anticipation factors that can affect gait [14]. In addition, the method is restricted to laboratory investigation and limited in its use for design.

Unexpected slips, which are more likely to lead to dangerous falls, can be produced in the laboratory by concealing the condition of the floor from the subject and determining the severity of the slip that incurs. The amount of friction required to prevent slipping is a relevant measure described by Redfern and colleagues as the Required COF (RCOF), and defined as the amount of shear force utilized per normal force. [15-17] This is often used as a threshold to determine whether a condition is likely to lead to a fall (i.e. when Required COF is greater than COF, a slip is likely). The difference between Required COF and measured COF has been used to determine the probability of a slip [15]; briefly described in Section C.1 and manuscript included in the Appendix). This method of evaluation has also been used by other with success [18].

E.2.3. Models of the Shoe-Floor-Contaminant Interface

The ability to model the shoe-floor-contaminant has been recognized by the research community as having great potential to assist in reducing slips and falls in the workplace. However, the problem is complex and requires collaborations across multiple fields. Shoe-floor-contaminant friction can be represented with the following equation:

$$\mathbf{COF} = \frac{\mathbf{COF_{asp}} * \mathbf{F_{N(asp)}} + \mathbf{F_{fr(fluid)}}}{\mathbf{F_{N(tot)}}} \quad \text{Eq. (1)}$$

Where COF_{asp} is the friction coefficient of the contacting asperities, $F_{N(asp)}$ is the normal load supported by the contacting asperities, $F_{fr(fluid)}$ is the friction force that occurs at the surface between the shoe and the fluid and $F_{N(tot)}$, which is the total normal force. Under the conditions relevant to slip and fall accidents, the frictional forces that occur between the shoe surface and the fluid are minimal and therefore the total friction coefficient is most dependent on the friction coefficient of the contacting asperities and the proportion of the total normal load supported by these asperities. Thus, maximizing the load supported by contacting asperities and minimizing the load supported by the fluid is critical to ensuring a safe friction coefficient.

One major difficulty in modeling friction is understanding the interaction of the sole and floor material with a fluid contaminant at the microscopic level. Most research that has been conducted approaches the relationship between surface roughness and COF empirically. Studies have shown that both floor surface roughness [19-21], floor surface waviness [21], and contaminant condition [19-22] significantly contribute to COF. Chang et al. showed that when viscosity is low, surface roughness affects friction coefficient but when viscosity is high, surface waviness dominates [21]. While these studies demonstrate that a relationship exists between roughness, waviness and wear on shoe-floor-contaminant friction, the mechanisms that cause these phenomena are still unknown, which limits the findings to just the materials and conditions that were tested. In addition, these purely experimental studies only provide information that is relevant to the exact experiments (i.e. similar forces, contaminants and materials) and do not contribute to a general understanding of shoe-floor-contaminant interface. Experimental results coupled with modeling data would shed light on the major lubrication mechanisms affecting shoe-floor-contaminant friction, which would be critical to designing slip resistant shoe and floor surfaces.

Macroscopic features of the sole surface have been initially investigated using the finite element method of modeling (FEM) with some success [23]. Sun et al. explored the effect of tread design on traction when interacting with soil using FEM to model the sole and the soil material. The results were promising, showing that certain tread designs were capable of providing larger traction forces than others.

E.3. Theoretical Modeling of Friction

Friction as a theoretical concept is complex. This is particularly true for human gait, with two disparate materials for shoes and floors, complex motions and forces of the shoe with respect to the surface, and a variety of potential contaminant conditions. In order to investigate this complex behavior, models will need to be developed initially from the microscopic level, building to the macroscopic level. There are some theoretical methods and knowledge from other fields that can be used as a starting point.

E.3.1. Microscopic Models of Friction

Very few studies of pedestrian slipping have attempted to investigate the nature of friction from a microscopic tribological perspective. In most slip studies, the friction between the shoe and floor has been characterized by a single value over the apparent shoe-floor contact area. Fundamentally, this is a gross approximation to the more complex phenomenon. During walking, contact between the shoe and floor actually occurs through the asperities (surface peaks) of the mating shoe and floor surfaces (Figure 2). In addition, the surface characteristics also have a significant effect on the lubricating fluid that separates the shoe and floor surface. Specifically, the fluid is incapable of flowing through asperities and thus fluid flow is altered by the shape and size of the asperities. Even though the shoe and floor surfaces appear to be flat on a millimeter scale, they are inherently rough and consist of micro and nano sized peaks and valleys. Therefore, when a shoe and a floor surface are brought into contact during walking, only the asperity peaks actually touch, making the real area of contact much smaller than the

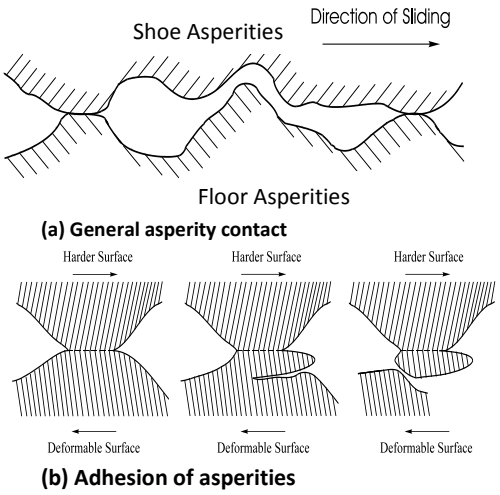

Figure 2: Diagram of Asperities

apparent area. In essence, friction is a highly localized phenomenon that is based on the interaction of individual asperities and the energy that is dissipation between them. The fluid flow is similarly a localized phenomenon such that there are regions where the two surfaces converge as asperities come into contact, which results in a peak in fluid pressure, and regions where the surfaces diverge, which results in a reduction in hydrodynamic pressure. Thus it is very important to consider the role of the surface structure modeling the friction during slip.

E.3.1.1.Microscopic Model for Dry Conditions

In the absence of a contaminant, the shoe-floor interfacial friction is characterized by the action of softer shoe asperities sliding over harder floor asperities in what is commonly referred to as the *Boundary Lubrication* (BL) regime. As discussed by Sayles and Poon [24, 25], the overall friction force in boundary lubrication can be attributed to the combined effects of adhesion, deformation and plowing. In the pioneering work on asperity interaction, Bowden and Tabor proposed that the interfacial friction between poorly lubricated surfaces is defined to be the minimum force, F, required to shear the welded junctions formed by adhesion bonds between contacting asperities [26]:

$$F = S_{eq} A, \qquad \text{Eq. (2)}$$

where S_{eq} is the equivalent shear strength of the shoe and floor materials and A is asperity contact area. In these conditions, most of the walking load is undertaken by the asperities on the interface and the interfacial friction is then controlled by the growth of the real contact areas. The resulting equation for the friction coefficient, COF, relating to the normal force (N) is given by:

$$F = COF^* F_{N(asp)} \qquad \text{Eq. (3)}$$

Closely examining the shear asperity model of Bowden and Tabor, the fracture of shoe asperities appears to be too severe, as shoe treads tend to have a fairly long life. Although some of the shoe asperities will weld to the floor asperities and be broken off during motion, it is more likely that the majority of them will elastically deform under load and return to their original shape.

E.3.1.2.Microscopic Model for Lubricated Surfaces

When analyzing the shoe-floor interface in the presence of a contaminant, it is critical to identify the type of lubrication that is occurring. The lubrication regimes can be best described by the Stribeck curve. The lubrication type of most interest for slips and fall is due to *Mixed Lubrication* (ML), as this represents the transition between high friction safe conditions and low-friction slippery conditions. Under non-slipping conditions, the total applied load between the shoe and the floor is predominantly carried out by asperity contacts with a minor contribution from the hydrodynamic action of the contaminant film, which is described by the boundary lubrication regime. In this situation, the overall friction coefficient for the interface will be close to dry conditions. As contaminant film begins to carry more of the load and there is less asperity interaction, the total friction force will become a combination of viscous friction and asperity interaction [27]. When the contaminant completely separates the shoe and floor asperities and carries the entire load, known as the Elastohydrodynamic Lubrication (EHL) regime, the friction coefficient will be extremely small and there will be substantial likelihood of slip.

Rheological properties of the contaminant (such as viscosity and extreme pressure) play an important role in defining the nature of the asperity interaction and the likelihood of slipping. Specifically, a contaminant with high viscosity can form a thicker film, enlarging the distance between the interacting asperities and reducing the amount of force supported by the contacting asperities, which results in a reduction of friction.

The role of the fluid in lubricating the shoe and floor surfaces can be evaluated at both the micro-level where the flow of fluid around asperities due to the shoe and floor roughness and material properties is evaluated and at the macro-level (i.e. whole shoe level) where the role of tread pattern, shoe and floor material and walking style (e.g. normal force, shoe-floor angle, heel velocity) can be evaluated. In each of these analyses, the hydrodynamics of the fluid can typically be described by the Reynolds equation.

$$\frac{\partial}{\partial x}\left[\frac{h^3}{12\eta}\frac{\partial p}{\partial x}\right]+\frac{\partial}{\partial y}\left[\frac{h^3}{12\eta}\frac{\partial p}{\partial y}\right]=\frac{v_{x(a)}+v_{x(b)}}{2}\frac{\partial h}{\partial x}+\frac{v_{y(a)}+v_{y(b)}}{2}\frac{\partial h}{\partial y}+\frac{\partial h}{\partial t} \quad \text{Eq. (4)}$$

This equation describes the relationship between the hydrodynamic pressures, the film thickness separating the fluids, the velocity of the shoe (a) and floor (b) surfaces, v_x and v_y, the viscosity of the fluid, η. The film thickness, h, can be represented as a function of the geometry of the shoe and floor surfaces (G(x,y)), the gap or overlap between the undeformed surfaces, d_0, and the deformation due to hydrodynamic and contact pressures (u(x,y)) [28].

$$h(x,y)=G(x,y)+u(x,y)+d_0 \quad \text{Eq. (5)}$$

The solution to this kind of equation requires numerical methods to be implemented such as a finite method approach coupled with iterative methods. The Reynolds equation in this general form (Eq. 7) can be applied at both the micro level to determine the hydrodynamic pressures caused by fluid that is wedged between two converging asperities and also at the macro level to demonstrate the effect of tread pattern on hydrodynamic pressures.

E.3.2. Macroscopic Models of the interface

Over the past several decades, the finite element method (FEM) has been used to provide valuable insight into the contact behavior of mating surfaces. For example, a finite element model of a tire contacting a road surface has been developed [29] where the tread pattern has been modeled without incorporating the tire or road asperities. This example demonstrated that FEM is capable of providing important information such as the interface contact pressure and the apparent contact area.

Another example that involves a rough soft surface against a hard surface that is thus applicable to shoe-floor-contaminant friction is chemical-mechanical polishing (CMP). CMP is a process to smooth silicon wafers using a soft rough polyurethane pad with a fluid slurry lubricating the surface. In order to better understand the hydrodynamics of the process, researchers have performed simulations to solve this mixed-lubrication problem [30]. In these simulations, the Reynolds equation with the flow factor adjustments is typically solved across the surface of the silicon wafer (Eq. 6). In order to adjust the film thickness for the roughness effects, the average film thickness is calculated from a method originally developed by Greenwood and Williamson which relates the average contact pressure (σ_x), distance between the mean lines of the two surfaces (h) and the distribution ($\Phi(z)$), material properties (E, v), shape (R) and density (η) of the asperities [31].

$$\sigma_x=\frac{4E}{3\left(1-\upsilon^2\right)}\eta R^{1/2}\int\left(z-h\right)^{3/2}\phi(z)dz \quad \text{(Eq. 6)}$$

In this analysis, researchers measured the inputs: E, v and Φ and calculated σ_x based on theoretical contact mechanics to solve for the film thickness, h. The film thickness was used to

solve for Reynolds equation and the resulting hydrodynamic pressure distribution was similar to experimentally recorded values

These simulations provide insight for how to model a soft material (polyurethane) against a hard material (silicon), while also considering the role of roughness. The CMP modeling is similar to the proposed shoe-floor models because each involves a soft material against a hard material, a lubricating fluid and the importance of surface roughness.

Following an analogous premise, analyses recently have been undertaken by Sun, et al to improve the understanding of how footwear performance is influenced by the tread pattern [23]. In their work, they developed finite element models to determine the traction performance of different macroscopic tread patterns in soil deformation around and below the boot. It is important to note that despite being macroscopic in nature, microscopic interaction between the contacting surfaces can be brought into FEM models through the definition of advanced friction models. As has been done previously by the investigators, these friction models are based on physical parameters that dominate the contact behavior such as interfacial velocity or material yield behavior.

F. Specific Aims

Specific Aim #1: Develop and validate a micro-level tribological model of the shoe-floor-contaminant interface based upon material properties, surface microstructure and contaminant characteristics. This model will be developed using concepts of lubrication, adhesiveness plowing, and deformation.

Specific Aim #2: Develop a macro-level model of the shoe-floor-contaminant interface that incorporates the micro-level model and macro-level shape and asperities (i.e. tread). This macro model will utilize the finite element method with critical input parameters derived from the micro-level model. Comparisons of the macro-level model COF predictions with slip resistance testing procedures will be made.

Specific Aim #3: Conduct human slipping experiments to validate the macro-model with actual slip/fall events. Slip prediction capabilities with the COF_{Macro} will be evaluated using a technique developed by the PI [15].

G.Methodology, Results and Discussion

G.1. Scientific Report #1: Micro-model of Shoe-Floor Friction (Aim 1) (Confidential)

G.1.1. Methods

Finite Element Model

Three dimensional shoe and floor models were created using eight-node solid hexahedron elements in explicit finite element analysis software (LS-Dyna®, Livermore Software Technology Corporation, Livermore, California, USA). This type of element is efficient and accurate in contact simulations and when exposed to severe deformations [33]. The materials simulated in the model were modeled based on the topography and material properties of two shoe materials and three ceramic tiles with different roughness levels, which were physically measured to ensure that the model inputs were relevant to actual shoe and floor samples. Roughness was applied to the interface side of the shoe and floor surfaces by raising and lowering nodes to achieve a checkerboard pattern (Figure 2). Asperity peaks and valleys were displaced from the mean line of the surface by half of the desired average peak to valley distance roughness (R_z) value. The microscopic shoe sample models were 0.8 mm in length, 0.5 mm in width and 0.5

mm in height. The floor models were 2.125 mm in length, 1 mm in width and 0.135 mm in height. The wavelengths of shoe and floor roughness patterns were 5 mm and 4 mm respectively (Figure 2). These wavelengths were taken from scans of shoe and floor surfaces. Mesh sizes for shoe samples elements ranged from 0.03125 mm to 0.125 mm while mesh size for floor elements was 0.0625 mm (Figure 2). In the preliminary modeling efforts, mesh refinement in the floor did not significantly impact the *von mises* stresses developed in the shoe, so all simulations were performed without mesh refinement of the floor elements. Shoe samples were meshed with a finer mesh for regions near the contact area.

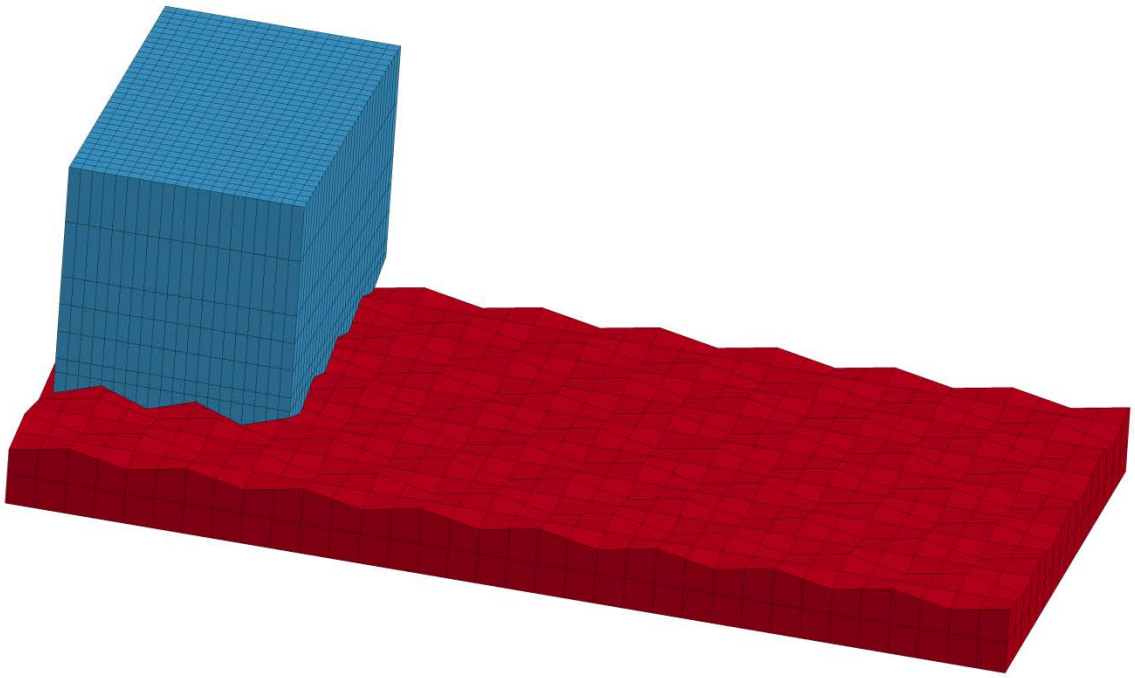

Figure 2. Shoe sample and floor with microscopic asperities created in LS-Dyna. (High shoe roughness and- medium floor roughness)

A viscoelastic material model was applied to the shoe elements (See Section 2.2 for material properties of the modeled materials) while a rigid material model was applied to the floor elements. A rigid material model was used for the floor because the modulus of ceramic floor material model was more than 20 times larger than the shoe materials' moduli. Initial models which applied linear elastic material properties to the flooring material with a modulus of elasticity of 20 times the shear modulus of the shoe material revealed highly similar results to simulations that used a rigid flooring material model. The viscoelastic material used for the shoe was chosen because time-dependent material properties are needed for simulating adhesion and hysteresis friction since both components are directly related to the viscoelastic properties of rubber [23]. The viscoelastic model describes shear stress relaxation of the material using a exponentially decaying function [34] (Equation 7).

$$G(t) = G_{\infty} + (G_0 - G_{\infty})\mathrm{e}^{-\beta \mathrm{t}}$$

Eq. 7

Boundary conditions were set to achieve pressures and sliding speeds relevant to walking and slipping. The contact pressure was controlled using the vertical displacement of the nodes on the top surface of the shoe. This downward movement occurred during the first 0.001 seconds of the simulation until an average normal contact pressure of 160 kPa was achieved. The contact pressure was set to this value to match the experimental conditions that were used in the validation (See Section 2.2). This pressure is of the same order of magnitude of under-shoe contact pressures during walking [35]. The second loading step moved the nodes on the top surface of the shoe to achieve the desired speed. Sliding speeds between 0.1 and 1 m/s were simulated to maintain consistency with the experimental validation research and because these speeds are relevant to slipping [36]. In all of the simulations, the bottom surface of the floor was constrained from both translation and rotation.

A segment based automatic surface to surface contact was used to achieve stability in the modeling efforts as recommended by Tokura to overcome the instabilities in simulating contact of rubberlike materials with rigid surfaces [32]. During model development, this contact algorithm was the only method capable of handling the large deformations of the soft rubber material and avoiding 'hourglassing' and 'checkerboarding' problems. The coefficient of friction for the contact was set to zero in order to isolate hysteresis friction from adhesion friction (i.e., the friction forces would only come from hysteresis friction and not due to friction from the contact algorithm). Lastly, the shoe sample was considered the slave material since it is softer and the floor sample was considered the master since it is harder.

Hysteresis coefficient of friction ($COF_{Hysteresis}$) was calculated by dividing average shear force due to hysteresis by the average normal force between the two surfaces (Equation 8). $COF_{Hysteresis}$ was averaged across the second loading step time period during sliding (Figure 3).

$$COF_{Hysteresis} = \frac{F_{Hysteresis}}{F_N} \quad \text{Eq. 8}$$

The ratio of real contact area to normal force was used as a measure of the adhesion coefficient of friction. Adhesion frictional force is commonly calculated as the product between the real area of contact, A_c, and the interfacial true shearing stress required to break the contact junctions, σ_s, [37] (Equation 9). Since the adhesion coefficient of friction ($COF_{Adhesion}$) is the ratio of adhesion friction force and the normal force (Equation 10), the ratio of real contact area to normal force (A_c/F_N) should be proportional to the adhesion friction (Equations 9-11.). The A_c/F_N was averaged across the second loading step to determine its average during sliding (Figure 3). This approach for quantifying adhesion friction is inappropriate for comparing adhesion across different materials since both the interfacial shearing strength and the real area of contact vary across material properties. Therefore, this ratio was only used to assess the effects of sliding speed, shoe roughness and floor roughness on adhesion friction.

$$F_{Adhesion} = \text{Seq} A_c \quad \text{Eq. 9}$$

$$COF_{Adhesion} = \frac{F_{Adhesion}}{F_{N(asp)}} \quad \text{Eq. 11}$$

$$COF_{Adhesion} \propto \frac{A_c}{F_{N(asp)}} \quad \text{Eq. 12}$$

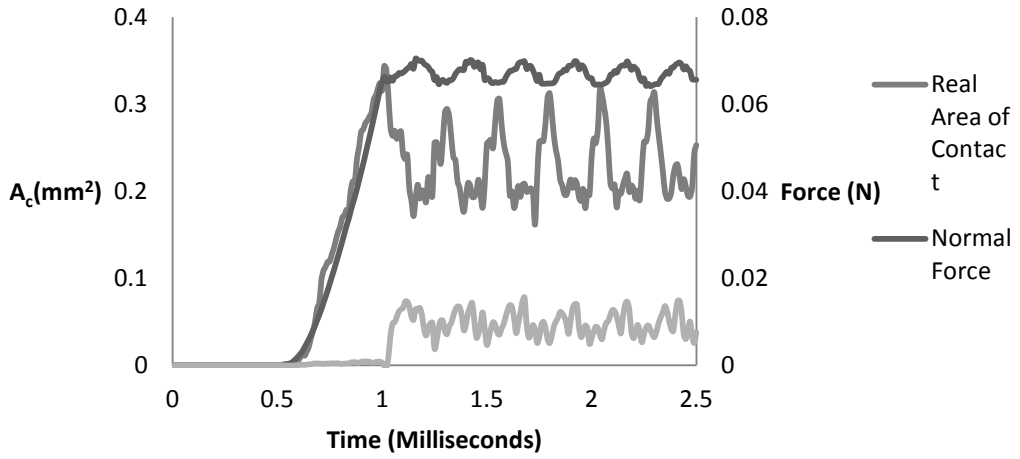

Figure 3. Real area of contact, normal and shear force generated between shoe sample and floor sample model with respect to time (Rubber material. High floor roughness. High shoe roughness.)

Experimental Validation

Two shoe materials (neolite and rubber) were modeled and tested experimentally. Neolite had a Shore A hardness of 95 measured using a durometer and it is considered a standard raw material in shoe-floor friction research [8]. The rubber sample, removed from a work shoe, had a Shore A hardness value of 50. Roughness parameters were measured using a two-dimensional contact type stylus profilometer. Eight roughness measurements were collected on each of the shoe samples and floorings using a scan length of 12.5 mm and a cutoff length of 0.80 mm. The roughness was described with the average peak-to-valley distance (R_z) averaged across the eight scans (Table 1) since this parameter has been reported to have a strong positive correlation with coefficient of friction [38]. Because the materials that were used in this study had different material properties and different roughness levels, simulations were conducted using both shoe roughness levels and both shoe material properties in order to isolate roughness vs. material effects. The wavelength that was used to define the spacing between asperity peaks was calculated from profilometer scans as length of the scan divided by the number of peaks.

Table 1. Average peak to valley distance parameter (R_z) for shoe samples and floors

Shoe/Floor	Materials	Average peak to valley distance (R_z)
Shoe Samples	Neolite (Low)	12.1 µm
	Rubber (High)	35.1 µm
Floors	Low Roughness	16.6 µm
	Medium Roughness	24.3 µm
	High Roughness	35.1 µm

The material parameters for the shoe material were defined by experimentally-measured values when possible or from reference data. Density of the shoe samples was measured based on the volume and mass of the samples. The two shear moduli, bulk modulus and the exponential decay constant were measured with compression stress relaxation tests using MTS machine (MTS Systems Corporation, Eden Prairie, Minnesota, USA), according to the methods recommended for testing of elastomeric bearings [39]. Two rectangular blocks of neolite (average thickness of 5.5 mm, average area of 612 mm^2) and rubber (average thickness of 6.1 mm, average area of 552 mm^2) shoe samples with approximately equal and uniform thickness were adhered to two steel plates. For each of the shoe materials, the compression test was done three times and the results were averaged. The testing method compresses the materials by 10% of the total thickness of elastomers, then applies this constant displacement level for 240 seconds and finally unloads the samples.

Typical plot of force curve with respect to time is shown in Figure 4. According to [39], the slope of the loading portion of the force-displacement curve between compression of 2 percent of thickness ($F_{0.02}$ in Figure 4) and the maximum force (F_0 in Figure 4) can be used for calculating the short time compressive modulus, K_0 (Equations 13 and 14).The slope of the straight line connecting the force in 2 percent of thickness ($F_{0.02}$ in Figure 3.) and the asymptotic force (F_∞ in Figure 4) can also be used for calculating long time compressive modulus, K_∞ (Equations 15 and 16).

$$K_0 = \frac{F_0 - F_{0.02}}{0.18T} \quad \text{Eq. 13}$$

$$E_0 = K_0 \frac{2T}{A} \quad \text{Eq. 14}$$

$$K_\infty = \frac{F_\infty - F_{0.02}}{0.18T} \quad \text{Eq. 15}$$

$$E_\infty = K_\infty \frac{2T}{A} \quad \text{Eq. 16}$$

Poisson's ratio was set to 0.499 for the shoe sample since rubber is usually categorized as a nearly incompressible material and is reported to have a Poisson's ratio of 0.49-0.499 [40].

Table 2. Viscoelastic material parameters used for modeling neolite and rubber

Material	G_0 (MPa)	G_∞ (MPa)	K (MPa)	β (1/s)
Neolite	30.24	18.66	9324	0.013
Rubber	0.59	0.44	2180	0.025

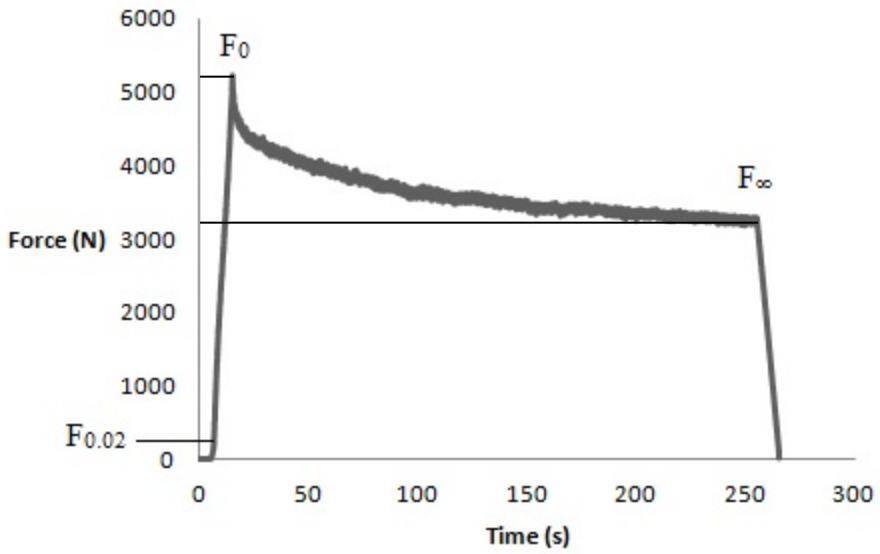

Figure 4. Variation of force with respect to time in stress relaxation test for Neolite

Model output was compared with experimental data collected with a pin-on-disk tribometer on ceramic tiles with three different roughness levels using the same two materials (neolite and rubber) at six sliding speeds [42]. The simulated speeds included 0.1, 0.25, 0.5, 0.75, and 1 m/s to match speeds used in the experimental study. The experimental study, quantified hysteresis using a lubricant (SAE 75W140) that blocks adhesion for both shoe and floor materials at each of the speeds. The study also quantified fluid lubricated adhesion friction at each of the speeds by subtracting the hysteresis friction (measured with SAE 75W140) from the wet coefficient of friction when using different lubricants. Dry adhesion from the experimental study (at speed of 0.01 m/s) was compared with lowest simulated speed (0.1 m/s) to assess validity of the model in simulating the effects of shoe and floor roughness on dry adhesion because the experimental study did not measure dry adhesion for higher speeds. To examine the effects of speed on adhesion, the wet adhesion data from the lowest viscosity fluid, 25% glycerol/75% water lubricant were compared with the model output as part of the validation for the effects of speed on adhesion.

G.1.2. Results

Hysteresis

Increased shoe and floor roughness generated large increases in $COF_{Hysteresis}$ for both materials (Figure 5). A 161-169% increase in hysteresis coefficient of friction was observed with increasing neolite shoe roughness and a 10-35% increase in hysteresis coefficient of friction was observed with increasing rubber shoe roughness. Increasing floor roughness caused a 42-45% increase in hysteresis coefficient of friction of the neolite material and a 164-170% increase in hysteresis coefficient of friction of the rubber material. The connection between hysteresis friction and shoe roughness was stronger for the neolite shoe material, while the connection between hysteresis friction and floor roughness was stronger for the rubber material.

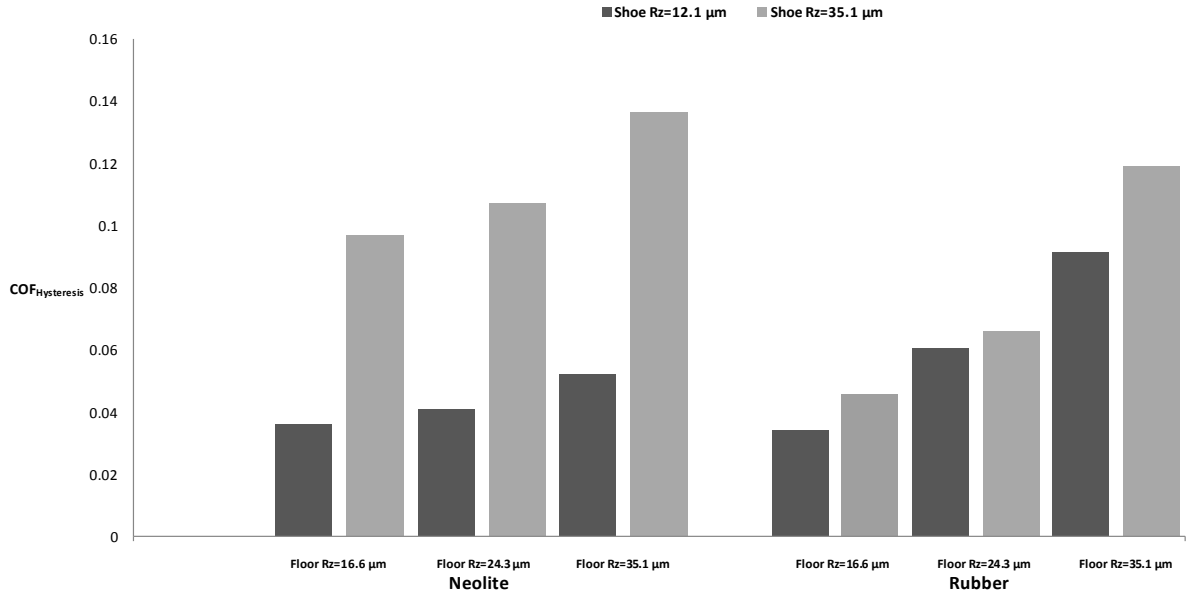

Figure 5: Variation of $COF_{Hysteresis}$ with shoe/floor roughness for 0.1 m/s speed.

Sliding speed had a minor and inconsistent effect on hysteresis friction depending on the shoe material and shoe/floor roughness levels (Figure 6). The majority of shoe/floor combinations showed a slight increase (7-27 %) in hysteresis friction with sliding speed although the high roughness neolite demonstrated a negative (18% decrease) trend when sliding against low roughness flooring.

A)

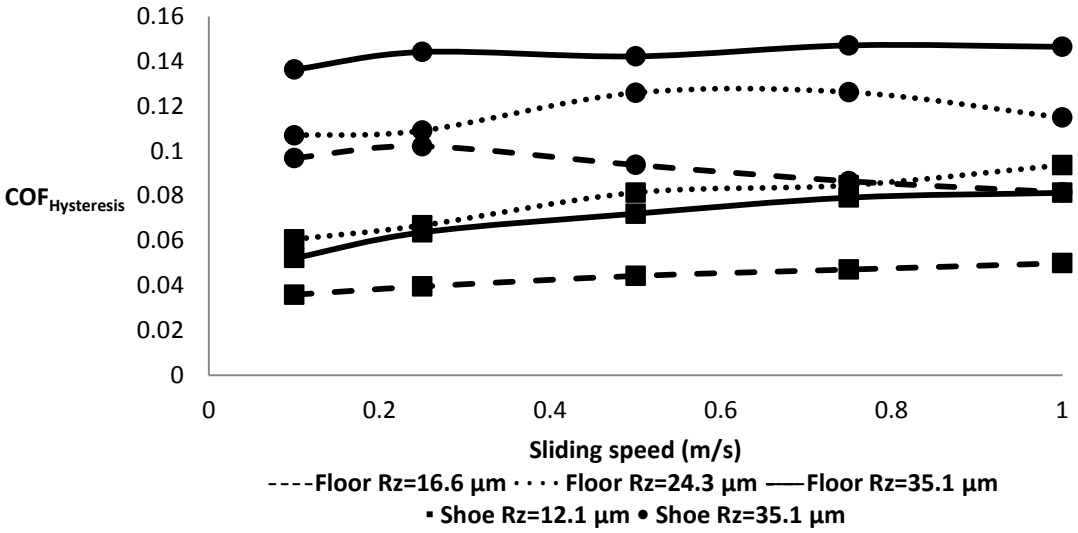

B)

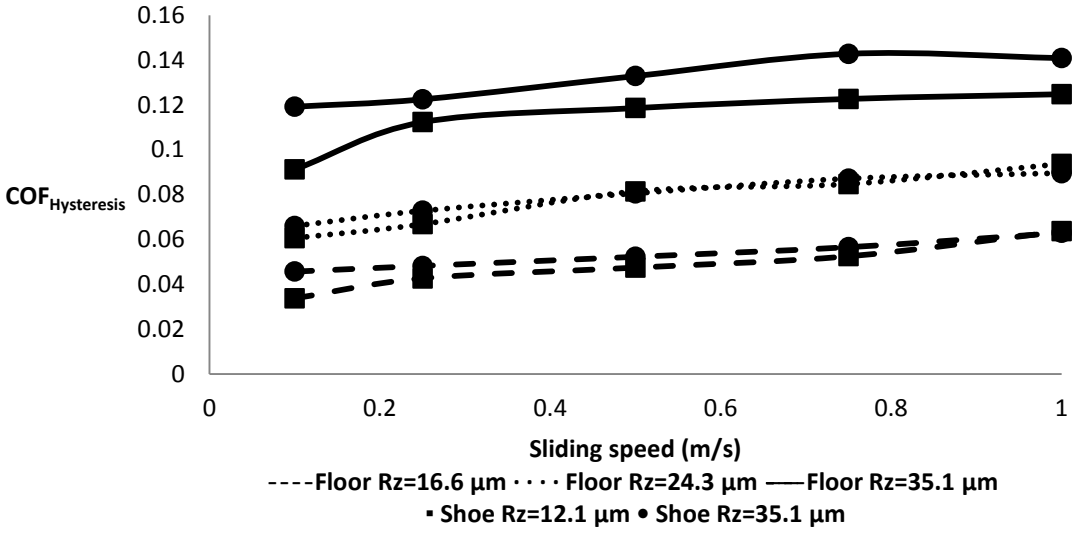

Figure 6: Variation of $COF_{Hysteresis}$ of neolite (A) and rubber (B) sample for different speeds and combinations of shoe-floor roughness.

Adhesion

The model indicated that sliding speed had a strong effect on A_c/F_N, indicating that the adhesion friction is highly dependent on sliding speed. With increasing sliding speed from 0.1 m/s to 1 m/s, a decrease in ratio of real contact area to normal force was observed in both materials at all shoe and floor roughness levels (Figure 7). Neolite simulations showed a 16-29% decrease in ratio of real area of contact to normal force with increasing sliding speed from 0.1 to 1 m/s for different combinations of shoe-floor roughnesses and rubber simulations had a 12-25% decrease in adhesion friction with increasing sliding speed for different models with different shoe-floor roughness levels.

A)

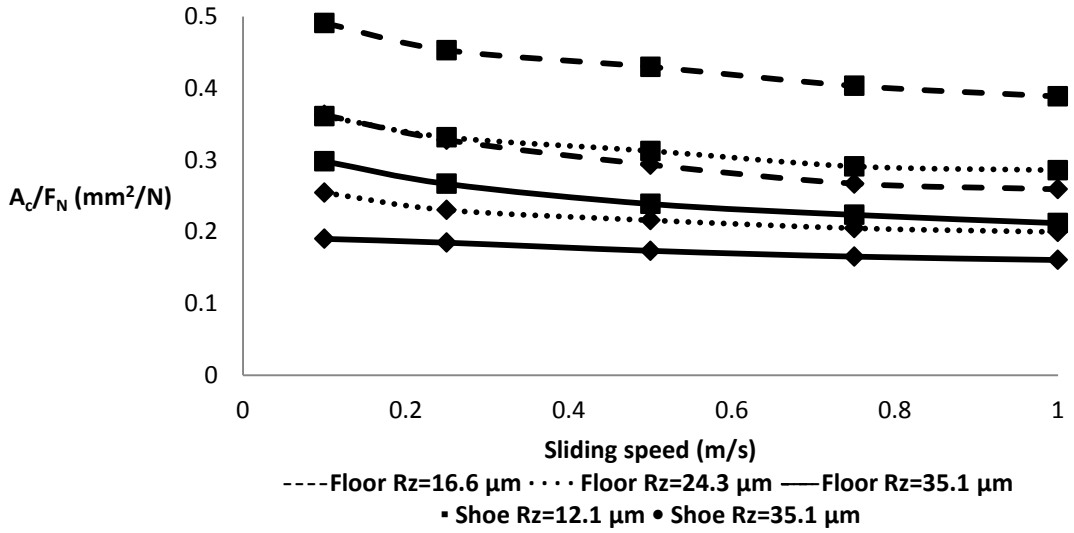

B)

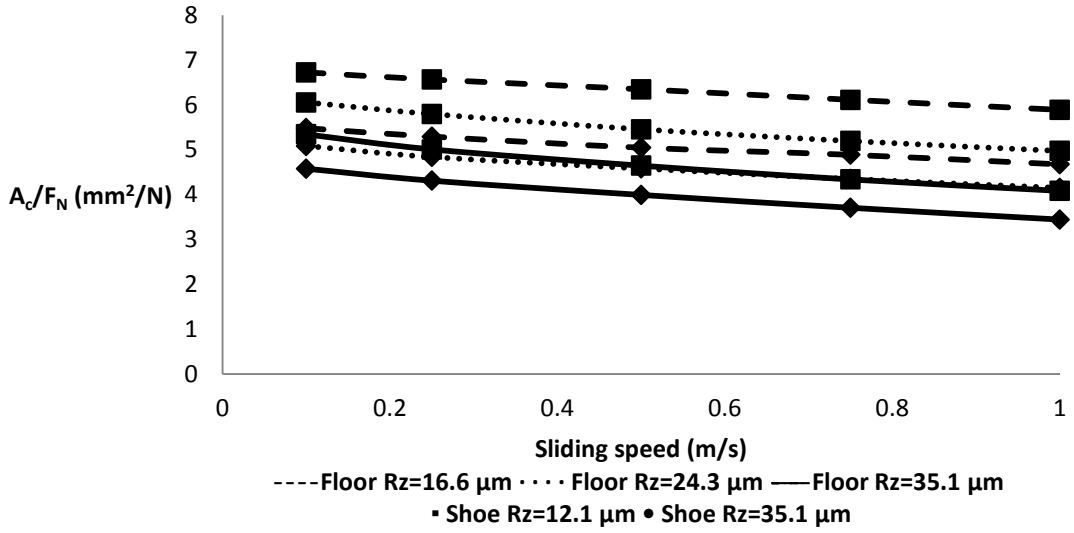

Figure 7. Variation of ratio of A_c/F_N of neolite (A) and rubber (B) sample for different speeds and combinations of shoe-floor roughness

Increasing shoe or floor roughness led to a reduced A_c/F_N (Figure 8). A 26-36% reduction in A_c/F_N was observed with increasing neolite shoe roughness while increasing rubber shoe roughness caused a 14-18% decrease in ratio of real area of contact to normal force. Increasing floor roughness caused a 39-47% reduction in ratio of real area of contact to normal load in the neolite material and a 17-21% decrease in adhesion was observed in rubber with increasing floor roughness.

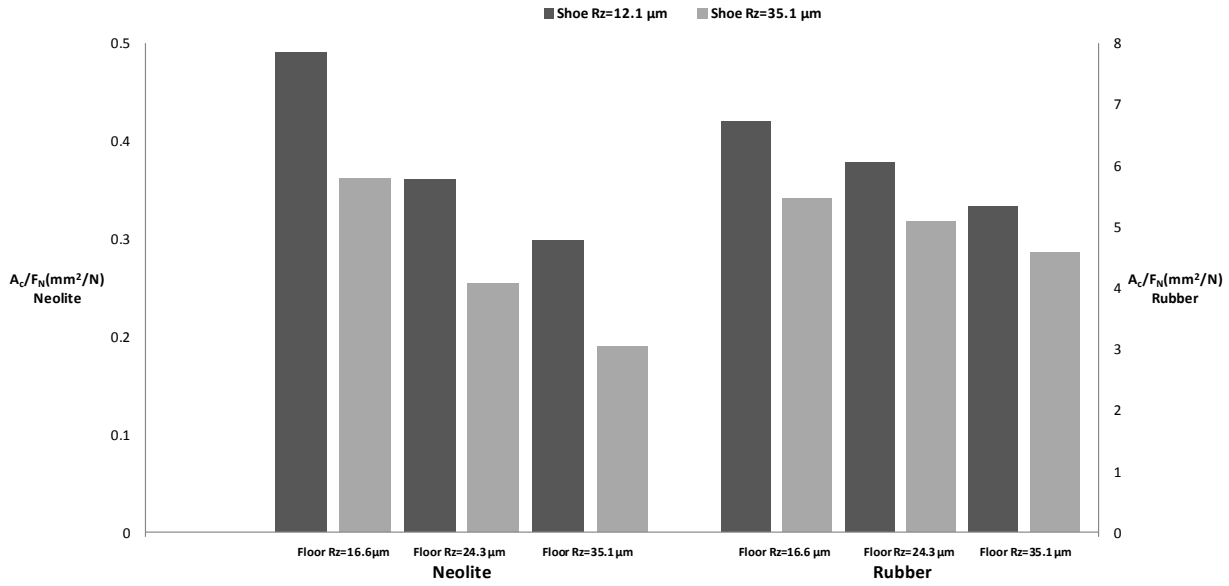

Figure 8. Effects of shoe and floor roughness on the ratio of A_c/F_N.

Experimental Validation of Model

The effects of shoe material and floor roughness on hysteresis friction were consistent between the model and the experimental studies (Figure 9). Increasing floor roughness led to larger hysteresis friction values in both studies. Also, the rougher but softer rubber material had greater hysteresis friction in both the experimental and modeling study. Speed had an opposite effect on the finite element model than the experimental study. The model predicted an increase in hysteresis friction with increasing sliding speed while the experimental studies demonstrated a reduction in hysteresis friction with increasing sliding speeds (Figure 6).

A)

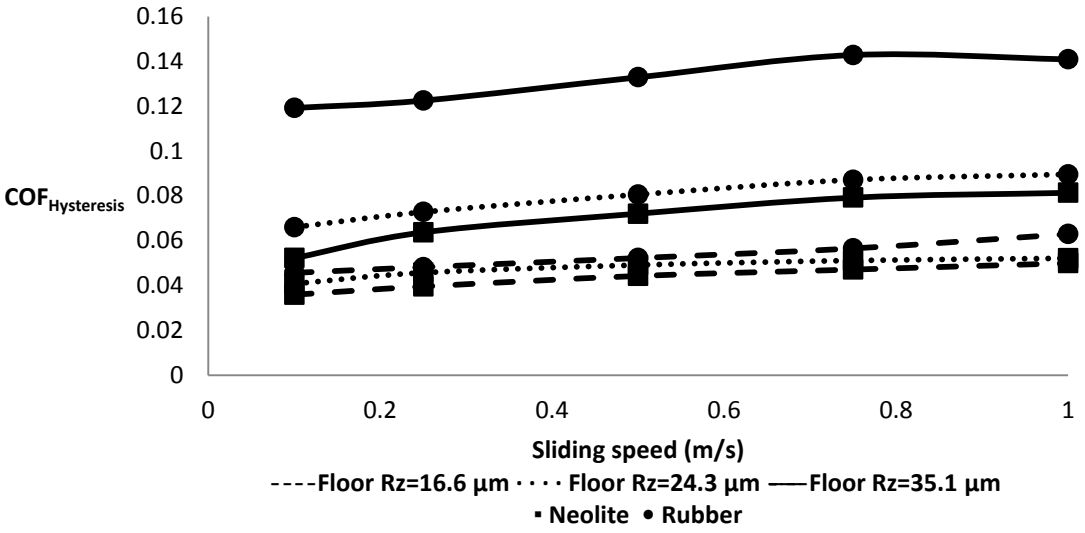

B)

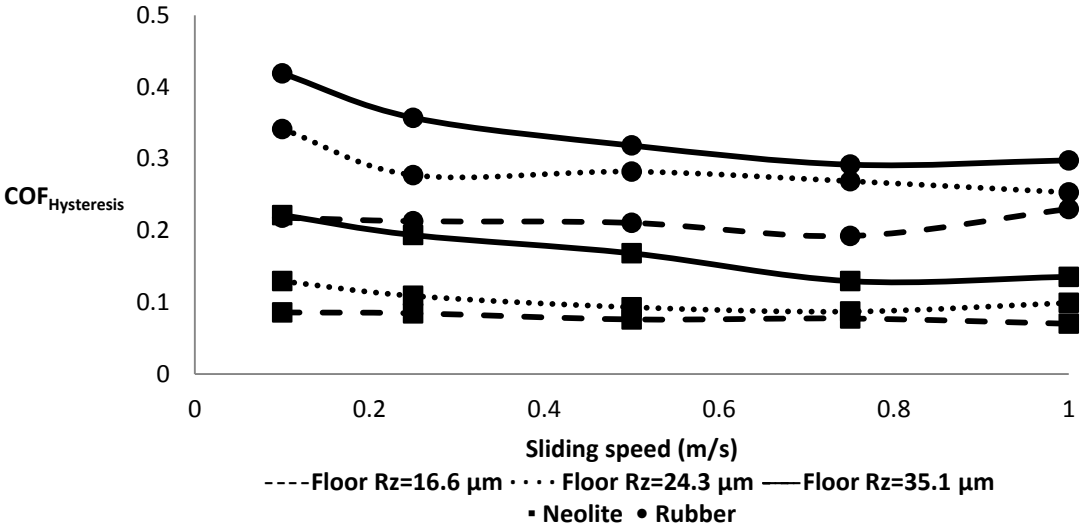

Figure 9. Variation of $COF_{Hysteresis}$ for the two shoe materials with different floor roughness in different sliding speeds from model (A) and experimental study (B)

The model and experiments were consistent in reproducing the effects of speed on adhesion but were only moderately consistent in reproducing the effects of roughness on adhesion. Both the model and experiments demonstrated an exponential decay trend in adhesion friction as sliding speed increased (Figure 10). The reduction in adhesion friction due to increasing sliding speed ranged from 30% to 76% in the experiments, while the model predicted a reduction of 12% to 29%. The model consistently demonstrated a reduction in adhesion friction with increasing roughness although this trend was only observed experimentally for the rubber material (Figure 11).

A)

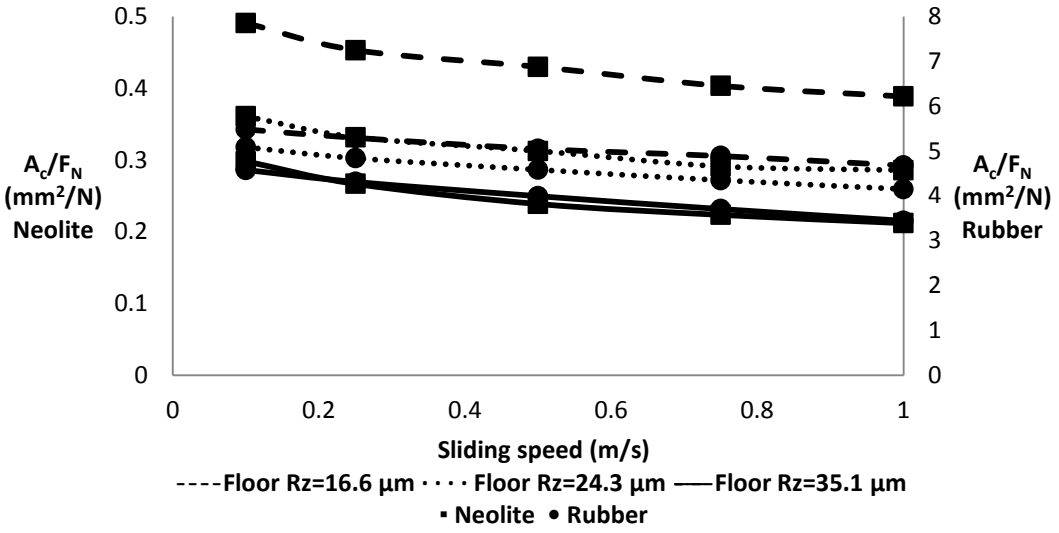

B)

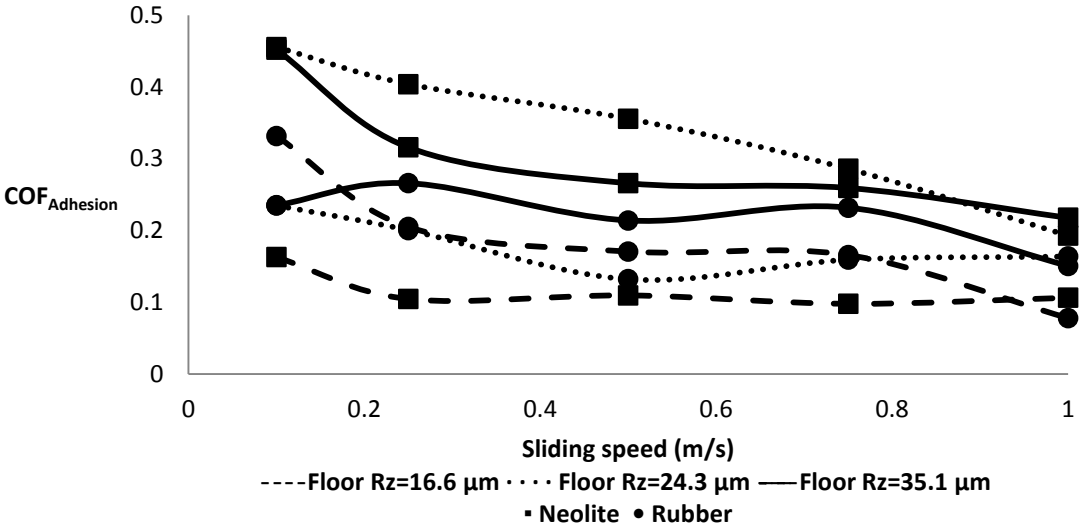

Figure 10. Variation of A_c/F_N from model (A) and $COF_{Adhesion}$ from experimental study (B) for the two shoe materials with different floor roughness in different sliding speeds.

A)

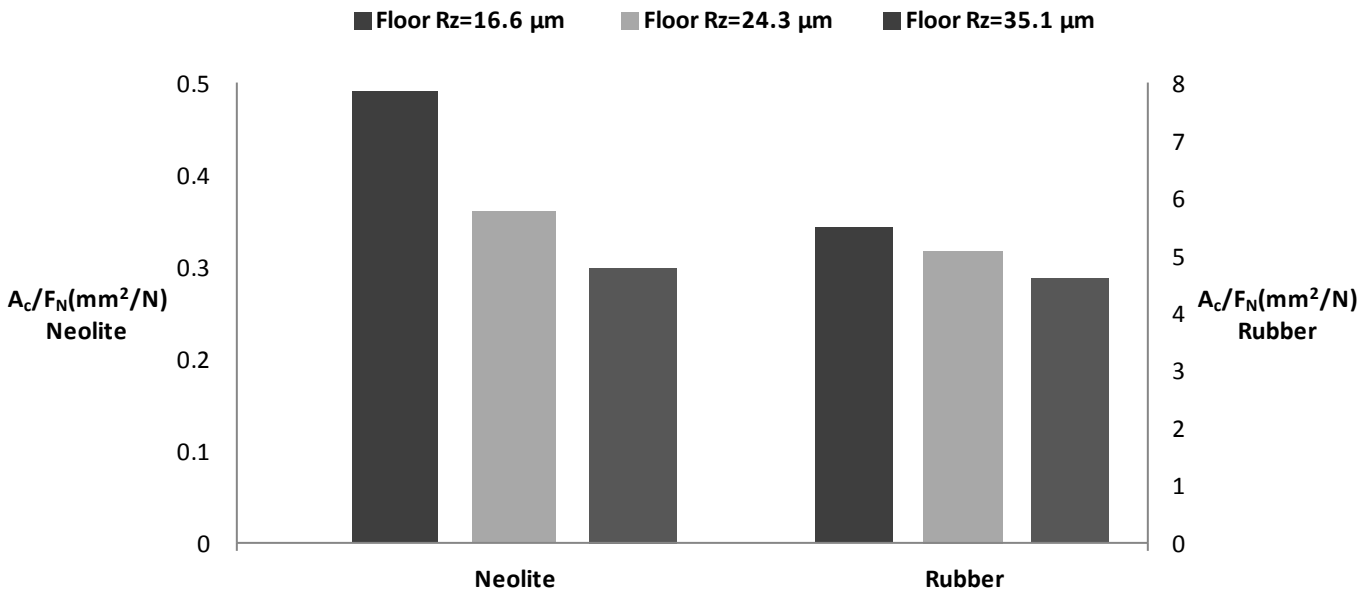

B)

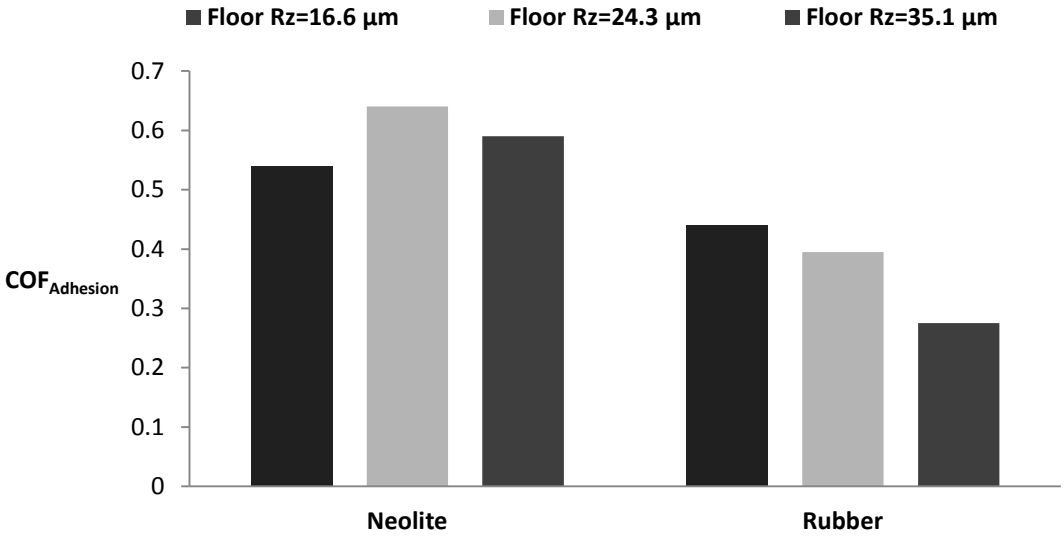

Figure 11. Variation of A_c/F_N for lowest speed model with different floor roughness (A) compared to $COF_{Adhesion}$ in low speed from experimental study (B)

G.1.3. Discussion

The finite element model reproduced the effects of shoe material and floor roughness on hysteresis friction and the effects of speed on adhesion friction. Increased shoe/floor roughness resulted in elevated hysteresis coefficient of friction for both of the materials. Increasing the shear moduli of the shoe material led to an increase in hysteresis friction. The model was not particularly effective at predicting the effects of speed on lubricated hysteresis friction as hysteresis friction in the model was not sensitive to sliding speed and the experiments showed a negative correlation between speed and friction. The model predicted a negative correlation between floor roughness

and adhesion friction, consistent with the experimental results for one material but not for the other material. Increased sliding speed led to a lower ratio of real area of contact to normal force, which was consistent with the experimental data.

The predicted effects of shoe and floor roughness on adhesion and hysteresis friction are consistent with previous modeling studies and tribological theory. The model predicted a consistent positive correlation between roughness of the shoe or floor material and hysteresis friction. Typically, higher levels of roughness will result in higher deformation in contacting asperities [23-25], which results in additional energy lost in the viscoelastic material as it was observed in finite element model of Bui et al. [43] , experimental study of [23] and theoretical studies of [24,25]. The model predicted a lower adhesion friction with increasing shoe/floor roughness due to a reduction in the real area of contact. The decrease in the ratio of real contact area to normal force with increasing shoe/floor roughness suggests that increased asperity height reduces the amount that the soft shoe material conforms around the floor surface asperities in agreement with tribological theory [27,44] and experimental study of [13].

The model predictions for the effects of sliding speed on adhesion are largely supported by tribological theory, while the validity of the model's ability to predict the effects of speed on hysteresis friction cannot be confirmed. The model, in agreement with the experimental studies on wet adhesion, demonstrated a reduction in real area of contact with increasing sliding speed. At higher sliding velocities, asperities of the soft shoe surface will have less time to viscoelastically conform around the harder floor asperities to form adhesional bonds, which reduces the real area of contact and decreases adhesion. [36,45]. The results of the simulations indicated that speed does not have a dramatic effect on the hysteresis friction and that the trend between sliding speed and hysteresis friction changes with different materials and roughness levels, while the experimental studies indicate that increasing sliding speed consistently reduced the hysteresis coefficient of friction. The lack of agreement between the simulations and experimental results may be due to limitations in the experimental studies to isolate hysteresis from hydrodynamic effects. Those experiments used a high viscosity oil to block adhesion and isolate hysteresis friction. However, these high viscosity fluids also increase hydrodynamic pressures and reduce interaction by causing separation between the surfaces [46,47]. To conclusively test the ability of the model to simulate the effects of speed on hysteresis friction, novel experiments that isolate hysteresis friction without viscous fluid would need to be developed. Alternatively, the model developed in this paper would need to simulate the hydrodynamic effects of the fluid [22]

One strength of the model is its ability to evaluate the net change in hysteresis friction across shoe materials that have different material properties and roughness. Nosonovsky et al. [48] explained that materials self-organize to different steady-state roughness values dependent on their material properties and the counter surface that is causing the wear. Previous work has attempted to describe the effects of shoe material properties on shoe-floor friction, which has led to conclusions that softer shoe materials lead to larger lubricated or hysteresis friction [13,49-51]. The model used in this study reveals that the increased hysteresis friction for softer shoe materials is likely due to the fact that softer shoe materials experience more adhesional wear [48,52-54], which increases their roughness. Thus, the increased lubricated friction that has been

observed with the soft shoe is not directly caused by the softer material but rather its higher roughness. The model used in this study was able to successfully determine that the soft rougher shoe material had a net increase in the hysteresis friction. Therefore, this model may have benefits in identifying shoe materials with high hysteresis friction by considering both their material properties and steady-state roughness.

Future developments of the model may improve its utility in enhancing slip-resistant shoe and floor designs. To improve the ability of the model to reproduce experimental trends between hysteresis friction and sliding speed, a hybrid model capable of considering the effects of both fluid and solid may need to be developed. The fluid component of this model would need to model the hydrodynamic effects of the model and its impact on the separation and deformation of the shoe material similar to [22]. Findings of this study suggests that shoe and floor roughness, sliding speed and material properties are the most important parameters for understanding the hysteresis and adhesion friction in shoe-floor slip events and controlling these parameters can be useful in designing slip-resistant shoe and flooring surfaces. The modeling study presented in this paper could be used as a basic framework for more advanced models of complex multi-factorial shoe-floor-contaminant friction by also considering the macroscopic features of shoes such as tread.

G.2. Scientific Report #2: Microscopic models of fluid hydrodynamics and its impact on COF [32] (Aim 1)

G.2.1. Methods

Experiments were conducted using a pin-on-disk type tribometer, the photograph and schematic views of which are shown in Fig. 12(a) and 1(b), respectively. The pin-on-disk type tribometer was custom developed by instrumenting a rate table (disk) on which the floor material is mounted. A normal load is applied to the shaft directly above the shoe material (pin). When the rate table rotates relative to the fixed shoe material the frictional (or shear) force is recorded by load cells. The coefficient of friction was measured as the ratio between the measured shear (frictional) force and the applied normal force.

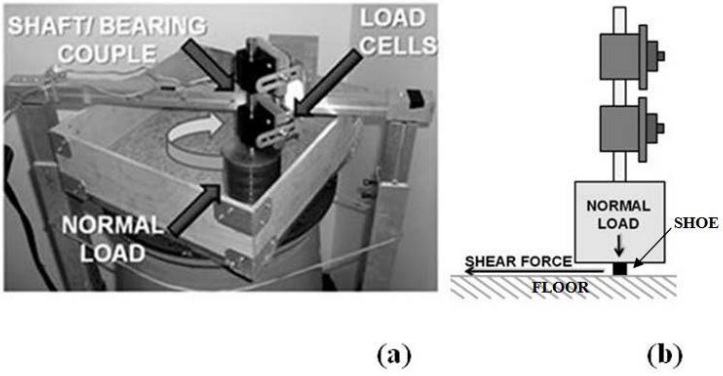

Figure 12. Custom pin-on-disk tribometer used to measure shoe-floor-contaminant coefficient of friction (a) photograph, (b) schematic showing floor material (disk), shoe material (pin), and direction of shear and normal forces used to calculate the coefficient of friction.

A pin-on-disk tribometer was used in this study because of its flexibility to easily modify testing conditions and to understand fundamentally the interactions of the shoe and floor surfaces. It is expected that shoe tread pattern and loading conditions that exist during actual slipping accidents may affect the exact coefficient of friction measurements. Yet, because

previous research by one of the present authors [33] has shown a similar Stribeck effect with entire shoes, it is anticipated that the general trends that are identified in this study are applicable to whole-shoe testing. Using the pin-on-disk type apparatus, the sliding speed can be varied over a range of speeds that are relevant to walking. Previously publications have described the requirements for biomechanically relevant, 'biofidelic', slip resistance testing and recommended a sliding velocity at the shoe-floor interface between 0-1.0 m sec^{-1} [22]. In the present study, experiments were conducted for 11 defined, biologically relevant sliding speeds, namely 0.05, 0.1, 0.2, 0.3, 0.4, 0.5, 0.6, 0.7, 0.8, 0.9 and 1.0 m sec^{-1}. In addition, all tests were carried out for a constant normal load of 20.9 N in ambient conditions, resulting in a contact pressure of approximately 266.1 kPa. The normal load was selected to achieve a contact pressure between 200 and 1000 kPa, which has been identified as a biomechanically-relevant range of pressures [22]. In order to isolate boundary lubrication and wedge term effects specific to the shoe and floor materials rather than the performance of a whole shoe design against a floor surface, other biologically relevant parameters (i.e. shoe angle, tread, normal force build-up rate) were not incorporated into the experimental design. A typical variation in the coefficient of friction values recorded over a 10 second period is presented in Figure 13. As part of the protocol, five experiments were recorded for each testing condition. The order of each set of experiments was randomized.

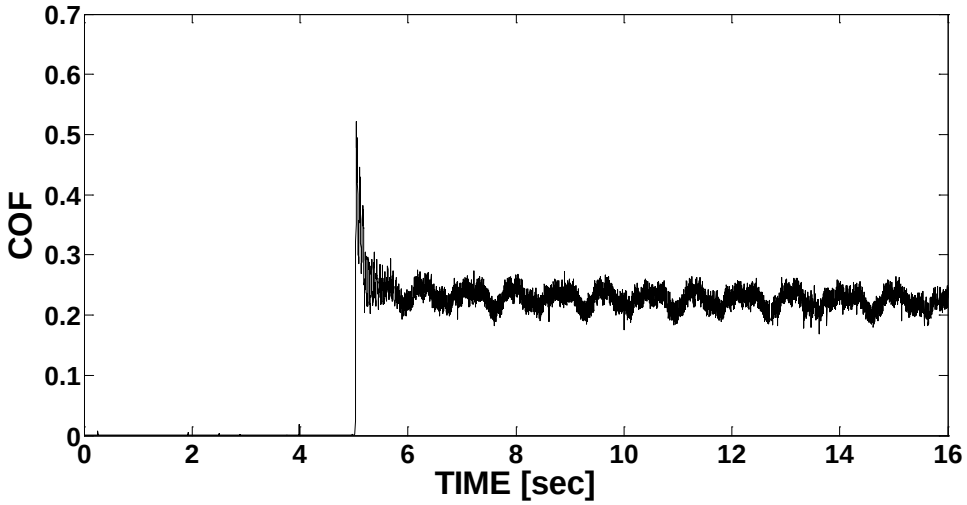

Figure 13. Typical time-history of coefficient of friction

In the presented experiments, materials and contaminants relevant to shoe-floor friction were examined. The pins were made of untreaded polyurethane and the counterpart, floor material, was made of commercially available vinyl tile. The pins were 10 mm in diameter with a reduced radius of curvature of approximately 23.3 μm. The floor material for all experiments was standard 305 mm × 305 mm, 35 mm thick vinyl floor tiles with a track radius of 80 mm. The surface roughness parameter, RMS of roughness (R_q), of the shoe and floor materials was measured using a 2D contact type stylus profilometer with a cutoff filter length of 0.8 mm. A single floor material was used for all testing with a roughness value of R_q = 1.34 ± 0.2 µm. The roughness of the polyurethane shoe material was controlled by abrading the shoe material with 220 grit silicon carbide paper for each experiment, resulting in a roughness of approximately 8.2µm. The fluid contaminants examined are water, 1.5% detergent, 25% water-75% glycerol concentration, 50% water-50% glycerol concentration, 75 % water-25% glycerol concentration, and canola oil with corresponding viscosities of 0.52 cP, 1.8 cP, 1.9 cP, 5.54 cP, 41 cP, and 74.6 cP, respectively. The viscosity of the fluids was measured at ambient conditions (approximately 20-25°C) using a viscometer. The detergent-water concentration was selected to follow the manufacturer's instructions of approximately 1.5% detergent for normal cleaning.

Canola oil was selected since it is commonly present in a restaurant setting. Glycerol was chosen because the fluid concentrations and viscosity can be easily varied to study the viscosity effects.

In another set of experiments, the ability to vary frictional effects by varying shoe roughness was explored. To vary the polyurethane shoe roughness, the shoe material was abraded with varying grades of silicon carbide paper which resulted in a limited range of achievable variation in RMS roughness, 9.3 µm, 8.2 µm, and 7.3 µm corresponding to 100 grit, 220 grit, and 400 grit silicon carbide paper, respectively. For these experiments, three combinations of glycerol and water, namely 25% water - 75% glycerol, 50% water - 50% glycerol, and 75% water - 25% glycerol that were used in the previously described set of experiments were applied to the shoe-floor contact.

Consistent with previous research, lubricated shoe-floor friction decayed with increasing speed following the Stribeck effect [33, 34]. An exponential decay fit was used to quantify the change (resistance to decay) in the coefficient of friction with increasing speed. A regression analysis was performed using the following equation calculating variables relevant to quantifying boundary lubrication friction and friction decay with speed.

$$COF = COF_{asymptote} + (COF_{BL} - COF_{asymptote})\, e^{-v/\tau_{hydro}} \quad (17)$$

Equation (17) tracks the change in the coefficient of friction with speed and quantifies boundary lubrication and hydrodynamic effects. COF_{BL} is indicative of the coefficient of friction under boundary lubrication, which occurs at very low speeds before hydrodynamic effects cause a dramatic decrease in friction, and was calculated for the coefficient of friction value as velocity approaches zero. The variable τ_{hydro} represents the resistance to decay of the coefficient of friction due to fluid pressure or hydrodynamic lubrication effects which cause the coefficient of friction to decrease. τ_{hydro} is a measure most closely related to the hydrodynamic fluid effects which causes the coefficient of friction to decay under the mixed-lubrication regime. As velocity increases to high sliding speeds, the coefficient of friction approaches an asymptote which is quantified by the variable $COF_{asymptote}$.

An optimization method, the Nelder-Mead Simplex method [35], was used to fit the above model, i.e. Equation (17), to the collected coefficient of friction data. Figure 14 shows an example dataset fit with the regression equation, Eq. (17), resulting in a calculated boundary coefficient of friction (COF_{BL}) of 0.83, calculated hydrodynamic effect (τ_{hydro}) of 0.18, and an asymptote ($COF_{asymptote}$) of 0.16. The Nelder-Mead Simplex method is a direct search method of nonlinear, unconstrained optimization and was applied to minimize the Euclidean distance between the predictive exponential function and the collected coefficient of friction data, resulting in a best fit equation [35, 36]. $COF_{asymptote}$ and COF_{BL} were bounded using MATLAB [37] so that the resulting best fit does not include coefficient of friction values less than zero.

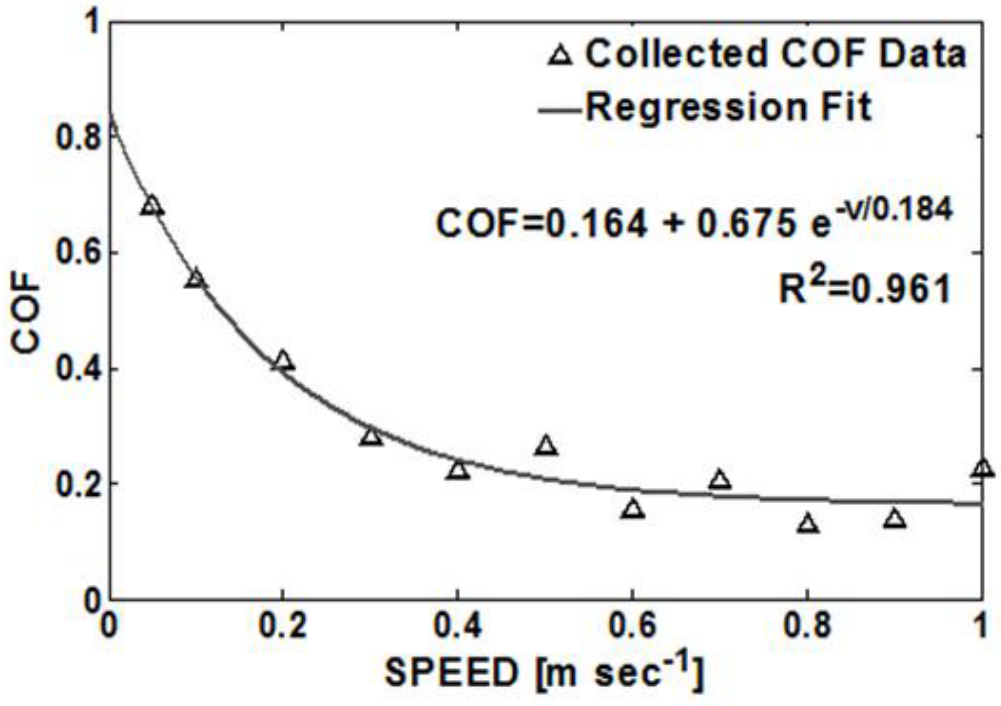

Figure 14. Variation of coefficient of friction with speed (triangles) for 25% glycerol-75% water lubrication and 8.2μm shoe roughness; the solid line represents the exponential regression fit. The values obtained for the variables of Equation (1) are COF_{BL}= 0.839, τ_{hydro} = 0.184, and $COF_{ASYMPTOTE}$=0.164.

In addition to quantifying the boundary and hydrodynamic effects of empirical data, the theoretical non-dimensional film thickness of each shoe-floor-contaminant combination was calculated. Based on maps of lubrication regimes developed by Esfahanian and Hamrock [38], shoe-floor-lubricant contact was identified to function under the isoviscous-elastic regime, also known as soft-EHL. In the isoviscous-elastic regime, the fluid pressures are relatively low and elastic deformation of material relative to the film thickness is relatively high [39]. This regime is commonly encountered in scenarios such as seals and tires [39]. Hamrock and Dowson developed the non-dimensional film thickness equation under soft-EHL by least-square fitting data based on soft-EHL conditions [33]. Under soft-EHL contact the non-dimensional film thickness is calculated from the following equation [39].

$$\tilde{H}_{e,min} = 7.43U^{0.65}W^{-0.21}\left(1 - 0.85e^{-0.31k}\right) \quad (18)$$

where

$$\tilde{H}_{e,min} = \frac{\tilde{h}_{min}}{R'}$$

$$U = \frac{\eta v}{E'R'}$$

$$W = \frac{w}{E'R'}$$

The parameters (velocity (v), reduced radius of curvature (R'), viscosity (η), effective elastic modulus (E'), and normal load (w)) which were used to calculate the film thickness were measured or calculated. The velocity, viscosity, and normal load were measured as testing parameters. The effective elastic modulus was assumed to be approximately equivalent to the

elastic modulus of the much softer material, polyurethane, and measured to be approximately 2.0MPa [34]. Table 3 summarizes all relevant parameters used to calculate the non-dimensional film thickness. The reduced radius of curvature was calculated by measuring the 2D surface profile of the shoe pin and fitting a second-order polynomial, Eq. (3) [34], to the profile of the shoe material to determine the curvature of the material.

$$h(r) = B * r^2 \tag{19}$$

Table 3. Results of regression variables (COF_{BL}, τ_{hydro}, and $COF_{asymptote}$) for varying shoe material roughness

Viscosity(composition)	**Roughness**	**COF_{BL}**	**τ_{hydro} [m sec^{-1}]**	**$COF_{asymptote}$**
1.9cP (25%-75% glycerol-water)	9.3μm	0.817 (0.049)	0.235 (0.086)	0.134 (0.033)
	8.2μm	0.656 (0.049)	0.500 (0.086)	0.099 (0.033)
	7.3μm	0.648 (0.049)	0.467 (0.086)	0.112 (0.033)
5.54cP (50%-50% glycerol-water)	9.3μm	0.431 (0.049)	0.260 (0.086)	0.128 (0.033)
	8.2μm	0.470 (0.049)	0.193 (0.086)	0.111 (0.033)
	7.3μm	0.485 (0.054)	0.252 (0.097)	0.098 (0.037)

The reduced radius of curvature is then calculated from Equation (20). Figure 15 shows an example of a surface profile fit with the second-order polynomial. The regression variable indicative of curvature, B, was determined by regression fitting.

$$R' = \frac{1}{2 * B} \tag{20}$$

The assumption that the shoe sample was symmetric was made based on similar profile scans in perpendicular directions, resulting in k=1. The ratio of the film thickness to roughness (λ) is related to the transition between boundary lubrication, mixed lubrication, and full-film lubrication. The ratio relates to asperity contact available. When λ is less than 1, the contact is defined to be in the boundary lubrication regime. When λ is between 1 an 3, the contact is defined to be within the mixed lubrication regime. When λ is greater than 3, the contact is defined to be in the full-film lubrication regime. The variable is calculated from the following equation [39]

$$\lambda = \frac{\tilde{H}_{e,min} * R'}{\sigma^*} \tag{21}$$

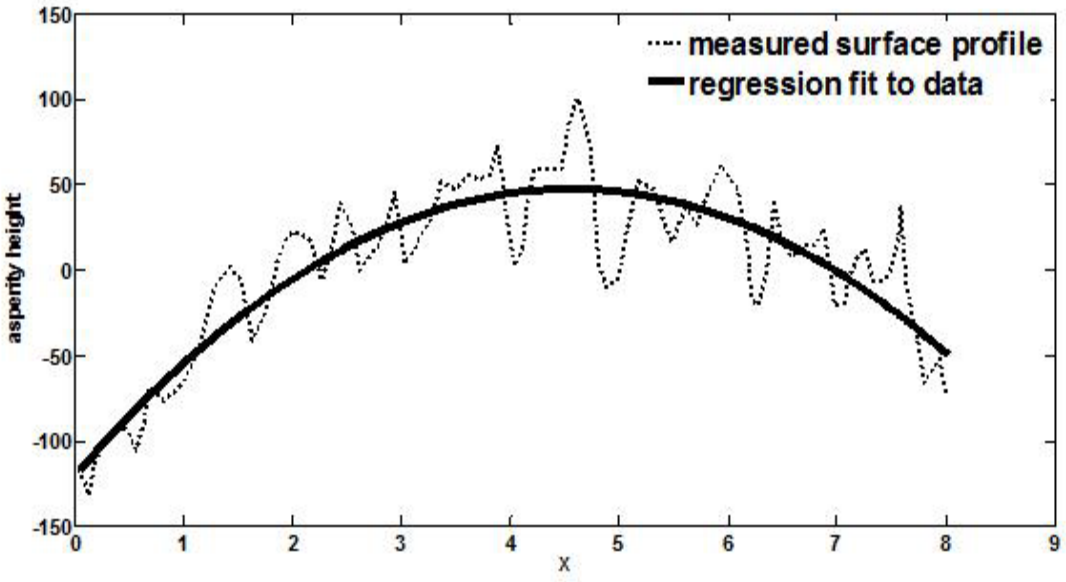

Figure 15. Example of surface profile fit with a second-order polynomial to calculate the reduced radius of curvature (R'); the dotted line shows the measured surface profile and the solid line is the second-order polynomial regression fit to the data

Statistical Analysis

ANOVA analyses were conducted to determine the effects of fluid composition and fluid viscosity on the lubrication parameters, COF_{BL}, τ_{hydro} and $COF_{asymptote}$. In the study, fluid composition was treated as a nominal variable, while fluid viscosity was treated as a continuous variable. The effect of common liquid contaminants on boundary lubrication was evaluated with liquid contaminant composition (viscosity) as the fixed-effect independent variable and $COF_{BL,}$ $\tau_{hydro,}$ and $COF_{asymptote}$ as the dependent variables. An alpha (α) value of 0.05 was used for all analyses, based on a 95% confidence interval. Statistical analysis software, JMP 8 (SAS ®, Cary, NC), was used for all statistical analysis. Only data sets with good regression fits (R^2>0.8, n=29) or moderately good fits (R^2>0.5, n=6) were used in this study.

G.2.2. Results & Discussion

Figure 16 shows the results of all data collection. All coefficient of friction values were found to compress to a single master curve when the coefficient of friction was plotted with respect to viscosity*speed. While not all testing conditions resulted in a decaying COF with speed over the range of 0.05-1.0 m sec^{-1}, it is expected that over a greater range of speeds all conditions tested in this study would follow the trend since all data was found to compress onto a single master curve. The testing speed range of 0.05-1.0 m sec^{-1} was selected to follow recommendations for biofidelic testing conditions [22].

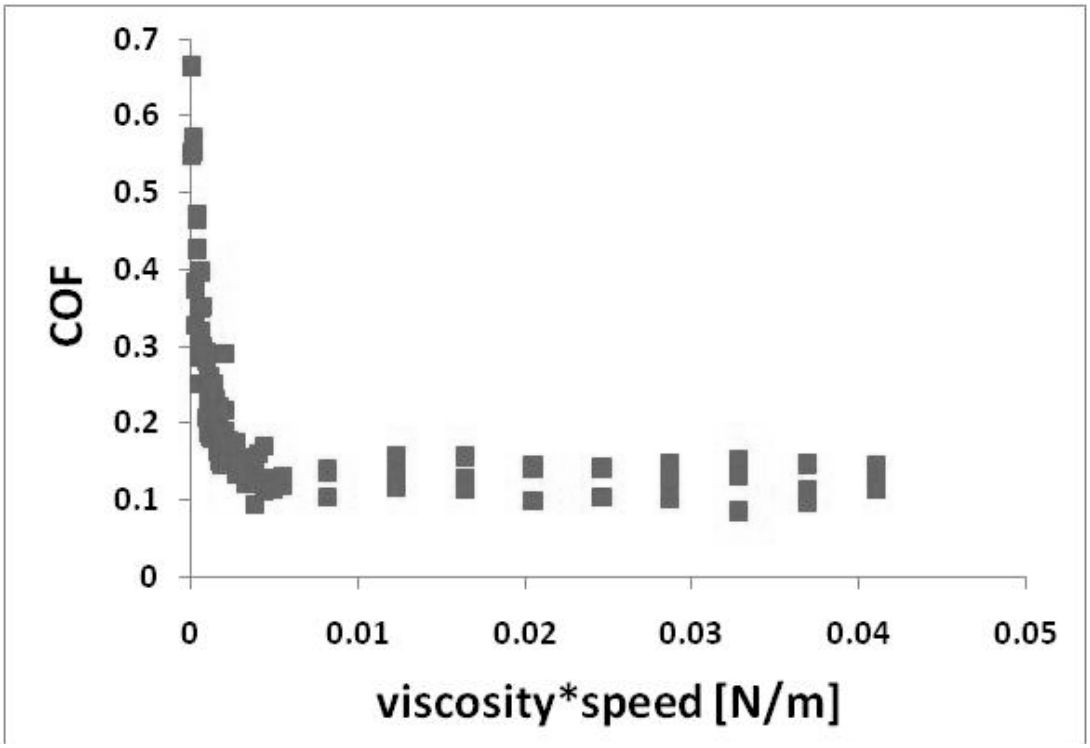

Figure 16. Master curve of all COF data collected across all experiments plotted with respect to viscosity*speed.

Figure 17 shows the variation of the regression fit of the coefficient of friction with varying speed for various lubricants. Good exponential fits (R^2>0.8) were achieved for the fluids: 25% glycerol - 75% water, detergent, and 50% glycerol -50% water. A moderately good fit (R^2>0.5) was achieved for water. Good exponential regression fits could not be made for experimental conditions lubricated with 75% glycerol – 25% water and canola oil (R^2<0.5). The COF_{BL} for canola oil and 75% glycerol - 25% water was estimated by the mean coefficient of friction for the experiment. Since both lubricants' coefficient of friction values did not vary considerably with speed (i.e. standard deviation is less than 0.05), COF_{BL} was set to the average coefficient of friction. However, since the experiments collected under 75% glycerol – 25% water and canola oil lubricated conditions could not be fit with an exponential regression τ_{hydro} and $COF_{asymptote}$ could not be calculated.

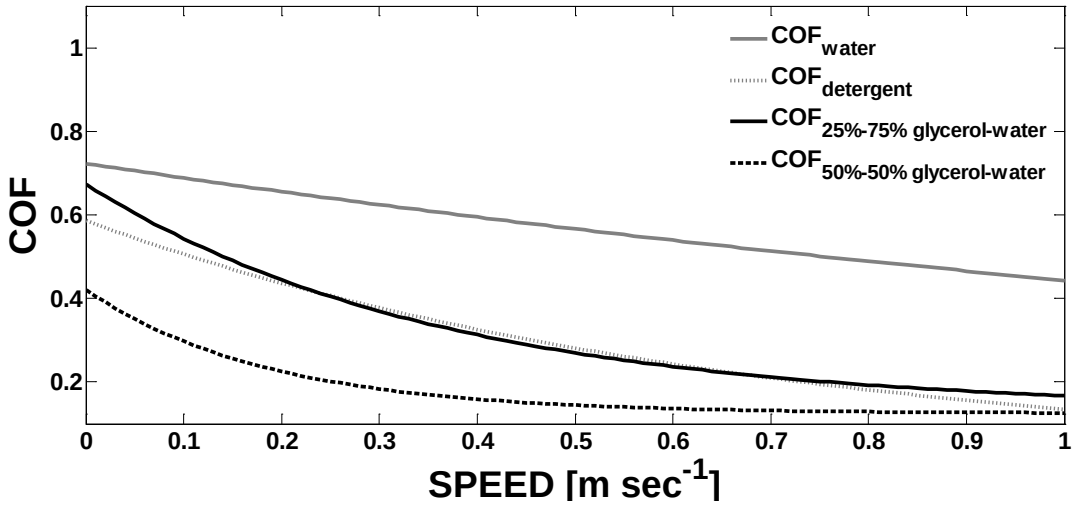

Figure 17. Average exponential regression fits of average COF data under water, detergent , 25% glycerol – 75% water, and 50% glycerol – 50% water lubrication.

Boundary Lubrication Effects

Figure 18 shows the variation of COF_{BL} for varying lubricants. COF_{BL} was found to be significantly affected by varying fluid lubrication as indicated by ANOVA analysis ($p_{fluid}<0.01$). The mean boundary lubrication coefficient of friction, COF_{BL}, was highest for water ($COF_{BL}=0.69(0.04)$), followed by 25% glycerol - 75% water ($COF_{BL}=0.65(0.03)$), 1.5% detergent ($COF_{BL}=0.58(0.03)$), 50% glycerol - 50% water (0.47(0.03)), 75% glycerol - 25% water ($COF_{BL}=0.16(0.05)$), and then canola oil ($COF_{BL}=0.10(0.02)$), Fig. 7. Post-hoc analysis revealed a significant difference between COF_{BL} under water and 50% glycerol- 50% water lubricated conditions. COF_{BL} under 25% glycerol – 75% water lubrication was significantly higher than COF_{BL} under 50%-50% glycerol-water lubrication. The COF_{BL} under canola oil and the COF_{BL} under 75% glycerol – 25% water lubrication were not significantly different between the two lubrication conditions. However, the COF_{BL} of canola oil and 75% glycerol – 25% water lubricated conditions were both significantly lower when compared to water, 25% glycerol – 75% water, 1.5% detergent, and 50% glycerol – 50% water lubricated conditions.

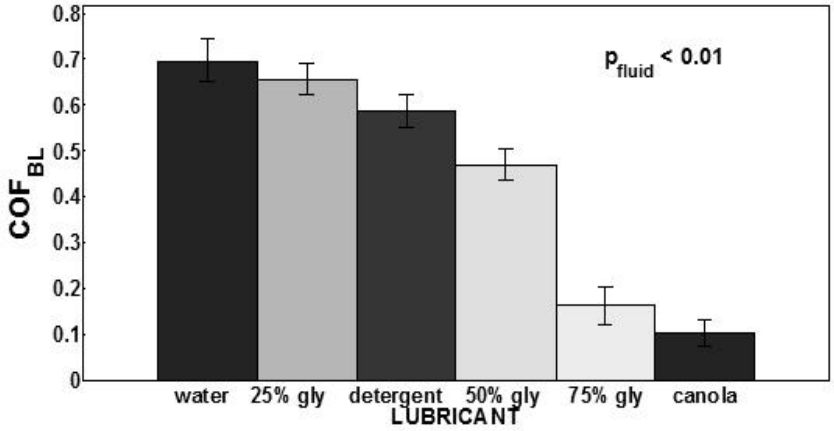

Figure 18. Average COF_{BL} with standard deviations for water, detergent, 25% glycerol – 75% water, 50% glycerol – 50% water, 75% glycerol – 25% water, and canola oil.

Boundary lubrication friction is significantly affected by the molecular structure of the liquid lubricant, with long chains and polar molecules providing the best liquid lubrication [40]. These long polar chains form bonds with materials creating a molecular-scale lubricating film between asperities [41]. These results are consistent with boundary lubrication theory since water is composed of the shortest molecules used in this experiment with a chemical formula of H_2O, followed by glycerol with a chemical formula of $C_3H_5(OH)_3$, and canola oil has the longest chain composed of a glycerin group with long carbon chains bonded to the glycerin's hydroxyl groups [42]. It is noteworthy that as the ratio of glycerol to water molecules increased, which would subsequently increase the average chain length, the coefficient of friction consistently decreased. The effect of chain length of detergent is unclear since the full composition of the industrially available detergent was not available. However, most detergents are composed of multiple components including surfactants [43] which can be used as wetting agents. Surfaces that are wetted more easily typically result in better boundary lubrication [41].

Non-dimensional film thickness calculations provided insight into the lubrication regimes in which each testing shoe-floor-lubricant condition operated. Figure (19) shows the calculated

non-dimensional film thickness for each testing condition. The calculated non-dimensional film thickness of water is lowest throughout all conditions, corresponding to the highest level of material contact and therefore presumably the highest coefficient of friction under boundary conditions, COF_{BL}. As predicted by the film thickness, the water lubricated contacts should never transition out of boundary lubrication under the conditions tested. Contacts lubricated with detergent and 25% glycerol - 75% water are also predicted to function only under boundary lubrication. Under 75% glycerol - 25% water lubrication and canola oil lubrication the contacts are predicted to transition into mixed lubrication with increased speed. It is important to note that the non-dimensional film thickness parameter lambda (λ) calculated in the present investigation is contradictory with other shoe-floor-contaminant friction results, which report shoe-floor-contaminant friction functioning heavily in mixed lubrication [33, 34]. The lubrication regimes were previously [33, 34] identified by visual inspection. However, the calculation of non-dimensional film thickness suggests that the contact is primarily in boundary lubrication (λ<1), transitioning into mixed lubrication at relatively high speeds. These results suggest a speed effect within boundary lubrication.

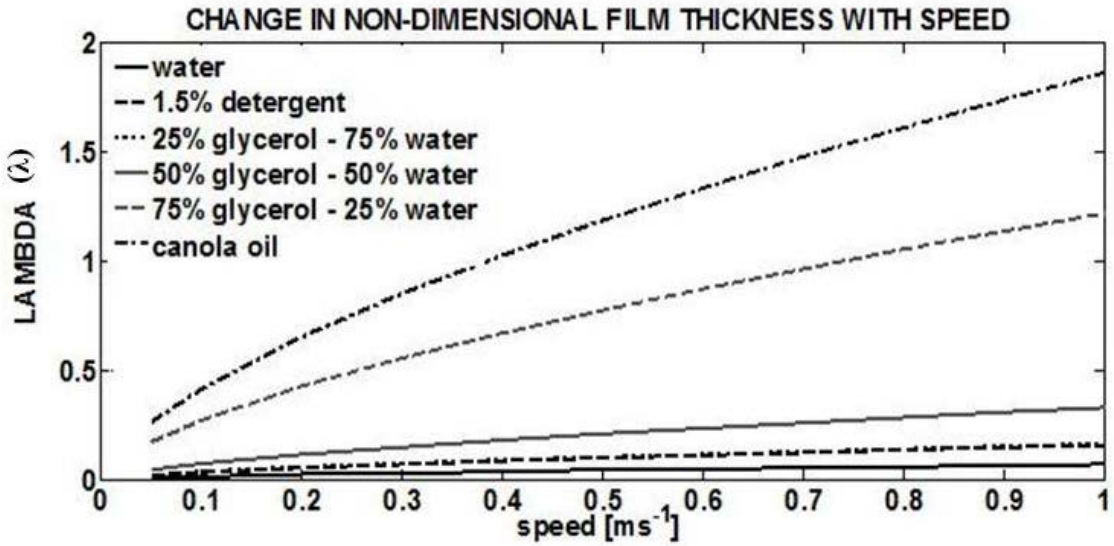

Figure 19. Calculated non-dimensional film thickness with increasing speed for water, detergent, 25% glycerol – 75% water, 50% glycerol – 50% water, 75% glycerol – 25% water, and canola oil lubricants (NOTE: the non-dimensional film thickness of detergent and 25% glycerol – 75% water are very close and therefore appear merged)

Additional testing was performed to determine the effect of changes in shoe material roughness on the coefficient of friction. Within the achievable range the polyurethane shoe material roughness (R_q) was 7.3μm, 8.2μm, and 9.3μm. Roughness (p=0.3951) and roughness-viscosity (p=0.0677) interaction did not have a significant effect on COF_{BL}. Table 3 summarizes the results of curve fitting the collected coefficient of friction data to calculate the regression variables indicative of boundary lubrication and hydrodynamic effects. Previous researchers have found that roughness (R_{tm}=4.4μm-51.9μm) across different shoe materials is correlated with coefficient of friction [37, 38]. Yet it is unclear if the shoe roughness or the shoe material properties cause the improved friction performance. Compared to the wide range of shoe material roughnesses that typically occur across different shoe surfaces, the range examined in this study was limited which may explain the lack of a roughness effect. Additionally, the roughness of the less elastic material of a tribo-couple tends to have a significant influence on friction, whereas the asperities of the softer material tend to deform resulting in minimal influence on friction [39]. Moreover, using silicon carbide paper may not be an effective way to

modify shoe roughness to achieve improved slip-performance. In this study, there was no significant difference or trend observed in COF_{BL} due to order.

Hydrodynamic Effects

Figure 20 shows the variation of τ_{hydro} with viscosity for various lubricants. Varying fluid contaminant significantly affected τ_{hydro} as indicated by ANOVA analysis ($p_{fluid}<0.001$). The fluid viscosity had a prominent affect on the hydrodynamic lubrication variable, τ_{hydro}. Higher fluid viscosity resulted in less resistance to coefficient of friction decay with increasing speed. Mean τ_{hydro} was 2.09(0.27), 0.68(0.17), 0.50(0.17), and 0.19(0.17) m sec^{-1} for water (0.52cP), 1.5% detergent (1.8cP), 25% glycerol - 75% water (1.9cP), and 50% glycerol – 50% water (5.54cP), respectively. When lubricated with water, the value of τ_{hydro} was very high indicating a low sensitivity of the coefficient of friction to increasing speed, whereas τ_{hydro} was low for 50% glycerol -50% water lubrication indicating low resistance of coefficient of friction to decay with increasing speed. The effect of fluid viscosity on hydrodynamic lubrication is consistent with previous research [33, 34, 44, 45]. Higher fluid viscosity resulted in a high rate of coefficient of friction decay with increasing speed as a result of fluid pressure build-up due to the wedge effect [34, 45].

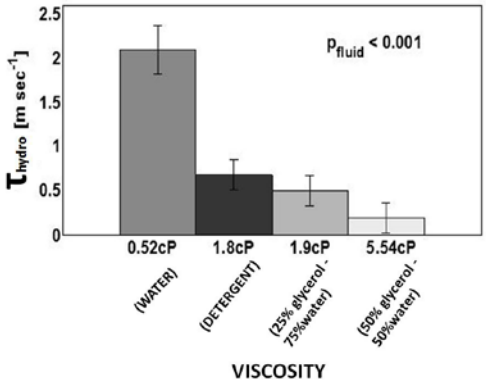

Figure 20. Average τ_{hydro} with standard deviations for water, detergent, 25% glycerol – 75% water, and 50% glycerol – 50% water lubrication.

$COF_{asymptote}$ was significantly affected by fluid contaminant composition ($p<0.05$). $COF_{asymptote}$ was 0.001(0.000), 0.001(0.000), 0.099(0.027), and 0.111(0.027) when the shoe-floor material was lubricated with water, 1.5% detergent, 25% glycerol -75% water, and 50% glycerol -50% water, respectively. It should be noted that the two lowest viscosity fluids (water and 1.5% detergent), which never fully achieved their lower asymptote, had the lowest values of $COF_{asymptote}$. Because these fluids did not approach an asymptote in the tested range of speeds, the estimate of $COF_{asymptote}$ is not as reliable for water and detergent as it would be for the other fluids. Lubricated engineering materials typically have a coefficient of friction that approaches values as low as 0.001 with increasing speed [41]. In this study, as well as other studies that have looked at lubricated shoe-floor friction over speed [33, 34], it has been found that values of shoe-floor-contaminant coefficient of friction often have much higher asymptotic values closer to 0.1 under the examined conditions. The calculations of non-dimensional film thickness suggest that the shoe-floor-lubricant contact never reaches full hydrodynamic lubrication which may explain the higher than expected asymptote. With increased speed, the contact may transition into full hydrodynamic lubrication, however it is predicted that these speeds would be outside of the range expected for human ambulation.

Additional measurements examining the effect of achievable variations in shoe roughness under varying concentrations of glycerol identified no roughness effect (Table 3). τ_{hydro} was not significantly affected by roughness ($p=0.395$) or viscosity-roughness ($p=0.167$) interaction and no trends were observed. The asymptote that COF approaches, $COF_{asymptote}$,

was not found to be significantly affected by fluid viscosity (p=0.919), shoe material roughness (p=0.673), or the combined viscosity-roughness effect (p=0.925). In this study, there was no significant difference or trend observed in τ_{hydro}, or $COF_{asymptote}$ due to order.

The purpose of this study was to evaluate the effects of varying liquid lubricant and achievable shoe material roughness on the coefficient of friction between a single shoe (polyurethane) and a single floor material (vinyl tile). Understanding the lubrication regime that is relevant to a fluid might be critical to identifying shoe and floor surfaces that should be used in environments where specific fluids are present. A combination of understanding the boundary lubrication and hydrodynamic effects may allow for improved selection of shoe-floor combinations in expectation of the presence of a lubricant. For example, when a relatively good boundary lubricant is present, shoe and floor materials should be selected that are able to penetrate the boundary lubrication layer and make material contact. Whereas when a fluid is present that produces significant hydrodynamic effects, improved shoe tread might be additionally necessary to reduce hydrodynamic pressures and subsequently improve frictional properties.

Limitations

A limitation of the regression model is that it did not effectively describe all experimental conditions. Not all testing conditions resulted in a decaying COF within the examined range of speeds, 0.05-1.0 m sec^{-1}. It is expected that if the testing speeds were extended, the model would have fit the water and 1.5% detergent, which is supported by the fact that all data was found to compress onto a master curve (Fig. 16) when COF was plotted with respect to viscosity*speed. The model may be less appropriate for long molecular length, high viscous fluids including canola oil and high concentration glycerol.

Lubrication regimes were identified quantitatively by employing Hamrock and Dowson's dimensionless film thickness equation for soft-EHL. In this study, the equation was used to approximate the film thickness and identify lubrication regime. However, a limitation of the equation is that it was derived from limited testing and therefore was only used to approximate shoe-floor-lubricant lubrication regimes.

G.3. Scientific Report #3: Microscopic models of fluid in boundary lubrication and its impact on COF [46] (Aim 1)

G.3.1. Methods

Apparatus and Materials:

Experiments were conducted using a custom developed pin-on-disk type tribometer as presented in Fig. 12 (a) and 1(b). The floor material (disk) was mounted on a rate table and the shoe material (pin) was mounted on a shaft and bearing couple. A normal load is applied to a shaft directly above the pin. When the rate table rotates relative to the fixed shoe material (pin) the frictional force is recorded by load cells.

Three shoe materials, polyurethane (40 Shore A hardness) and two rubber materials (60 and 70 Shore A hardness) were examined. Shoe material specimens were all 10 mm diameter circular samples and untreaded. Commercially available vinyl tile (99 Shore A hardness) and marble tile (>>100 Shore A hardness) samples (304.8mm x 304.8mm x 35 mm in dimensions) were tested. A durometer was used to measure the hardness of each shoe and floor sample on a Shore A scale of 1 to 100. The hardness of the marble sample greatly exceeded the Shore A scale. Therefore, the effect of varying the ratio of shoe to floor hardness is discussed qualitatively. The ratio of shoe hardness to floor hardness would be greatest for 70 Shore A hardness rubber to vinyl tile contact and smallest for polyurethane to marble tile contact.

In addition to material hardness, the roughness of the shoe and floor material samples was measured. Preliminary experiments revealed that material properties and surface structure could not be varied independently and the harder shoe materials tended to be less rough than the softer shoe materials. In order to quantify material roughness, a 2D contact type stylus

profilometer was used to measure surface roughness parameters of all materials. The variables presented are the arithmetic mean (R_a), the maximum peak to valley height (R_z), the maximum profile peak height (R_p), and the total height of the profile (R_t) using a cutoff length of 0.8 mm.

Eight lubrication conditions were examined: dry (unlubricated), water (0.52 cP), 1.5% diluted detergent (1.8 cP), 25% glycerol–75% water (1.9 cP), 50% glycerol–50% water (5.54 cP), 75% glycerol–25% water (41 cP), canola oil (74.6 cP) and SAE 75W-140 gear oil (376.5 cP). Some lubricants were selected based on their relevance to a slip and fall accident (water, detergent, vegetable oil). Other lubricants were chosen so that their fluid properties could be easily controlled (diluted glycerol concentrations). The dry and SAE gear oil were used to quantify the amount of friction due to hysteresis and adhesion as described in Section 3.3 (Data Analysis).

Experiments:

Tests were carried out under a normal load of 20.9 N in ambient conditions, resulting in a biofidelic contact pressure of approximately 266.1 kPa [8], and at a single sliding speed of 0.01 m sec^{-1} selected to be low enough to ensure boundary lubrication. Shoes were conditioned with 220 grit sand paper between each measurement to ensure that the shoe roughness was consistent across trials. Each trial consisted of 10 seconds and the frictional force was recorded once steady state friction force was achieved (Fig. 21). Between trials, fluids were completely cleaned from the surface with detergent and water and then were rinsed with water. Under the testing conditions, the soft-EHL equations for determining film thickness were found to be most appropriate [38]. These soft-EHL equations were applied to estimate the film thickness in order to verify the lubrication regime [47]. The equivalent modulus was assumed to be equal to the softer shoe materials, which were polyurethane and rubber (approximate elastic modulus of 10-50 MPa [48, 49]). These equations indicated that the film thickness was much less than the RMS roughness for all conditions, thus confirming the boundary lubrication assumption.

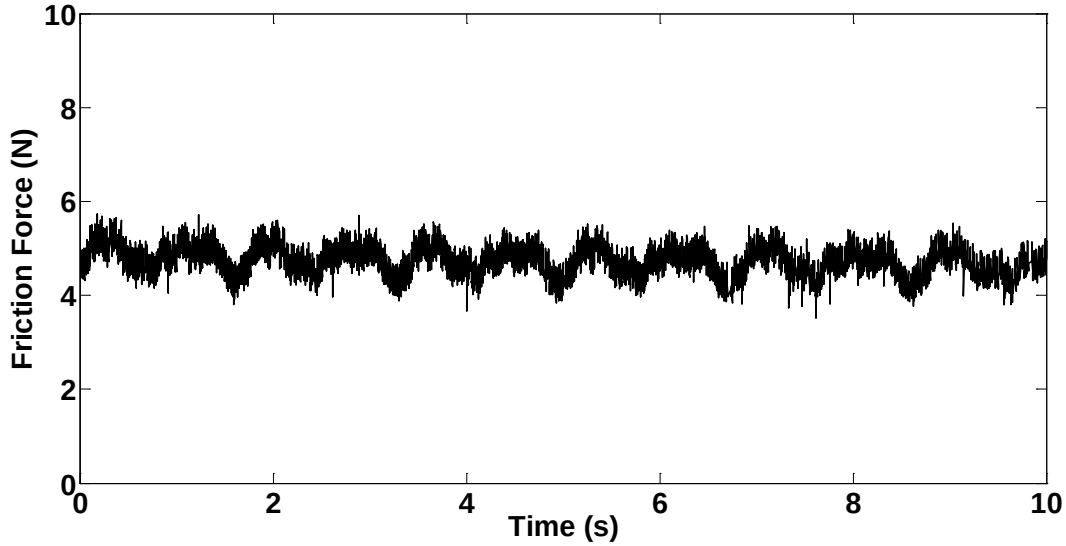

Fig. 21. Typical time-history of friction force during experiment.

Data Analysis:

The contributions of adhesion and hysteresis to the overall dry friction were quantified by considering both dry conditions and conditions where an excellent boundary lubricant was assumed to block all adhesion. This method has been used to isolate the relative contributions of adhesion and ploughing during metal friction [50, 51]. The dry friction force (F) was assumed to include friction due to the adhesion and hysteresis contributions, Eq. (22).

$$F_{dry} = F_{adhesion} + F_{\ hysteresis} \tag{22}$$

The lubricant, SAE 75W-140 gear oil (376.5 cP), was used to block most of the adhesion and to isolate the friction due to hysteresis [52]. The difference between the dry and SAE 75W-140 lubricated, $F_{SAE\ 75W\text{-}140}$, friction represents the friction due to adhesion, Eq. (24) [52].

$$F_{hysteresis} = F_{SAE\ 75W-140} \quad (23)$$

$$F_{adhesion} = F_{dry} - F_{\ hysteresis} \quad (24)$$

The amount of boundary lubrication adhesion in the presence of fluid contaminants was then quantified. The friction force due to adhesion was calculated for each lubricant by subtracting the hysteresis friction (Eq. 25) from the friction for a given lubricant.

$$F_{adhesion(lubricated)} = F_{lubricated} - F_{hysteresis} \quad (25)$$

Statistical Analysis:

Statistical analyses were performed to identify significant effects of shoe material and flooring on dry adhesion and hysteresis friction and to identify significant effects of shoe material, flooring and fluid on the lubricated adhesion. An ANOVA analysis was conducted with $F_{adhesion}$ and $F_{hysteresis}$ as the dependent variables and shoe material and flooring as the independent variables. The lubricated friction due to adhesion ($F_{Adhesion(lubricated)}$) was analyzed using two ANOVA models. The first model was meant to determine the contributions from the shoe, flooring and lubricant on adhesion friction. Independent variables for this analysis included the shoe material, floor material, lubricant and all interaction effects. The second model was a simplified model to determine the predictive ability of just the fluid and dry adhesion friction based on the principle that a fluid blocks a portion but not all adhesion friction. $F_{adhesion(lubricated)}$ was the dependent variable and the fluid, $F_{Adhesion(dry)}$ and their interaction were the independent variables. If these variables were found to be statistically significant, a regression model using the parameter estimates would be generated (Eq. (26)) with α and β as fluid properties and $F_{adhesion(dry)}$ being a property of the combined shoe and floor combination. The fluid parameter, α, represents how much adhesion friction the fluid has while the parameter, β, represents the dependence of the adhesion friction on the dry friction.

$$F_{adhesion(lubricated)} = \alpha + \beta * F_{adhesion(dry)} \quad (26)$$

G.3.2. Results & Discussion

Adhesion

Dry adhesion friction was significantly affected by the shoe material and shoe-material-flooring interaction ($p<0.01$). For both flooring conditions, adhesion was highest with the hardest rubber shoe material and lowest for the relatively soft polyurethane shoe material (Fig. 22). The marble flooring was found to have higher adhesion than the vinyl flooring with the hard rubber shoe surface but this effect was reversed for the soft rubber and polyurethane shoe materials.

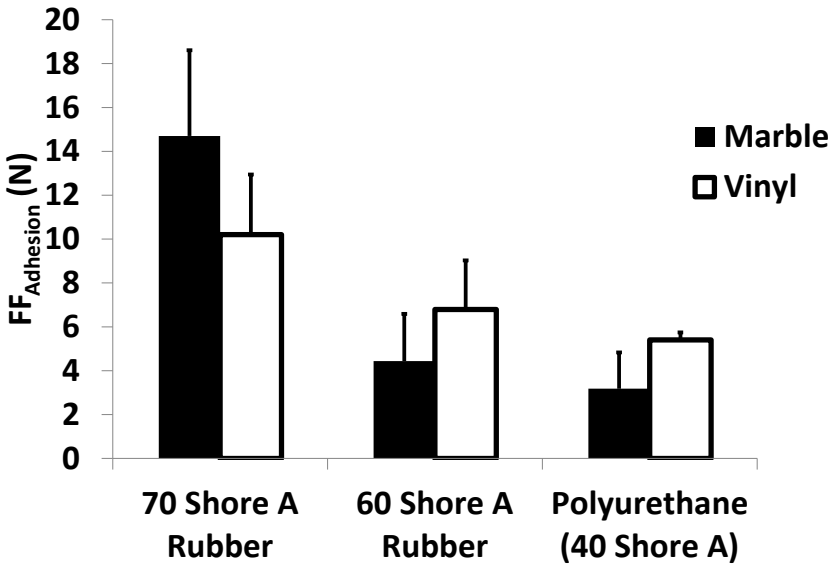

Fig. 22. Change in adhesion friction (FFadhesion) with respect to varying shoe and floor materials

The result that harder materials resulted in higher adhesion friction initially seems to contradict adhesion theory. Typically, softer and more compliant materials are associated with higher adhesion due to an increase in the real area of contact between materials [41]. The results of this study, however, may be explained by the inverse relationship between shoe hardness and roughness (Table 4). Material properties and roughness are both contributing factors to the real area of contact [53]. Thus the low roughness of the hard material may have actually resulted in a higher real area of contact than the soft but high roughness polyurethane. Another explanation for this effect may be that the hard material formed stronger adhesional junctions with the floor surface that may have required higher shear forces to break due to an increased level of fracture toughness [54].

Table 4: Surface profile parameters for all shoe and floor samples, average of 5 measurements ± standard deviation

Material	Ra(μm)	Rz(μm)	Rp(μm)	Rr(μm)
polyurethane (40 Shore A)	6.46 ±0.78	31.32±4.95	16.74±3.00	36.22±6.60
Rubber (60 Shore A)	5.23±0.50	29.26±2.59	13.66±1.11	35.10±4.95
Rubber (70 Shore A)	3.39±0.38	19.98±2.77	8.94±1.09	23.98±4.46
Vinyl (99 Shore A)	1.89±0.19	12.42±2.00	4.92±0.66	30.54±9.84
Marble (>100 Shore A)	0.17±0.05	1.86±0.48	0.40±0.25	11.50±3.18

Hysteresis:

Hysteresis friction was found to be affected by both the shoe and the floor materials (Fig. 23). Hysteresis friction tended to be highest for the softest material and lowest for the hardest material. In addition, the greatest hysteresis occurred when the hard marble was combined with the soft polyurethane while the smallest hysteresis was found when the hard rubber was

combined with the softer floor material, vinyl. These results are consistent with hysteresis theory that states hysteresis friction is proportional to the penetration depth of the hard asperity into the softer elastomer [55]. A softer shoe material would allow the floor asperities to achieve greater penetration depth.

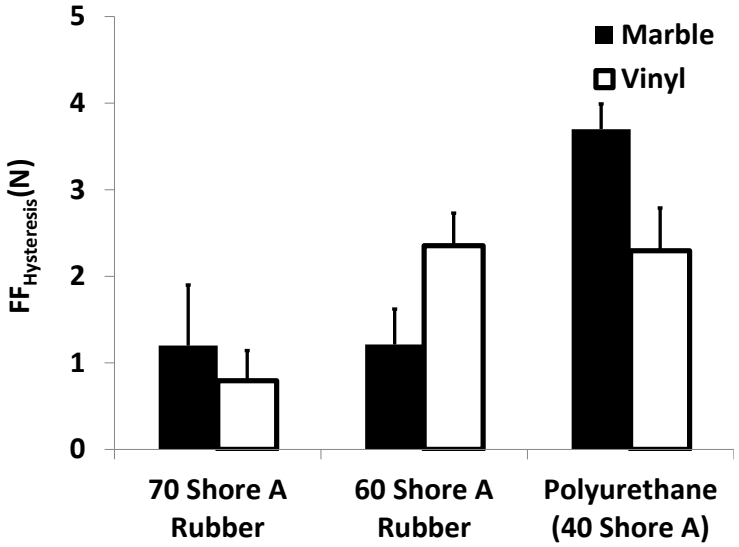

Fig. 23 Change in hysteresis friction (FFhysteresis) with respect to varying shoe and floor materials

Effect of Lubricants on Adhesion

The $FF_{adhesion}$ was found to be significantly affected by shoe material ($p<0.001$), lubricant ($p<0.001$), shoe-floor interaction ($p<0.05$), shoe-lubricant interaction ($p<0.001$), and floor-lubricant interaction ($p<0.001$). Adhesion in the presence of a fluid, therefore, is a complex and multifactorial parameter that is influenced by the shoe material, floor material and fluid. For the case of polyurethane, the amount of adhesion was highest for the water, followed by a statistical tie between the 25% and 50% diluted glycerol, then detergent and 75% glycerol and then canola oil (Fig. 5). The soft rubber shoe material had, on average, more adhesion friction than the polyurethane and hard rubber, which were similar (Fig. 5). The addition of a liquid lubricant typically results in decreased surface energy and thereby decreased adhesion [41]. Adhesion was blocked least in the water and most in the high-viscous canola oil. While there were not significant differences across the different concentrations of glycerol, the boundary lubrication friction force tended to have an inverse relationship with both the viscosity of the fluid or the length of the molecules [41]. Water is composed of the shortest chain molecules and therefore only formed a small monolayer, whereas canola oil is composed of the longest chain molecules and therefore was able to block more adhesion by generating a larger monolayer.

Further exploration of the lubricant-shoe material interaction revealed that the friction variation across the fluids was just 0.89N (range from 1.87 to 2.76N) for polyurethane shoe material but was 4.61N (range from 0.45 to 5.06N) and 3.88N (1.25 to 5.02N) for the hard rubber and soft rubber, respectively (Fig. 24). The shoe-lubricant effect may be explained by elastomer tribology theory that has examined the friction and wear of elastomers in the presences of fluids. Polyurethane materials have been shown to resist polishing [56], have a higher friction coefficient in the presence of oil contaminants [57] and wear at a slower rate than rubber during sliding in the presence of a fluid [58]. Therefore, rubber is more prone to react with lubricants during sliding. This may explain why the variation in frictional force across the different fluids was so much higher for rubber than it was for the polyurethane material. These

results identify that some shoe materials (i.e. polyurethane) have adhesion friction that is largely independent of the fluid that is present. This may provide guidance to identify the best shoes for resisting low boundary lubrication friction in environments where excellent lubricants (i.e. oils) are found.

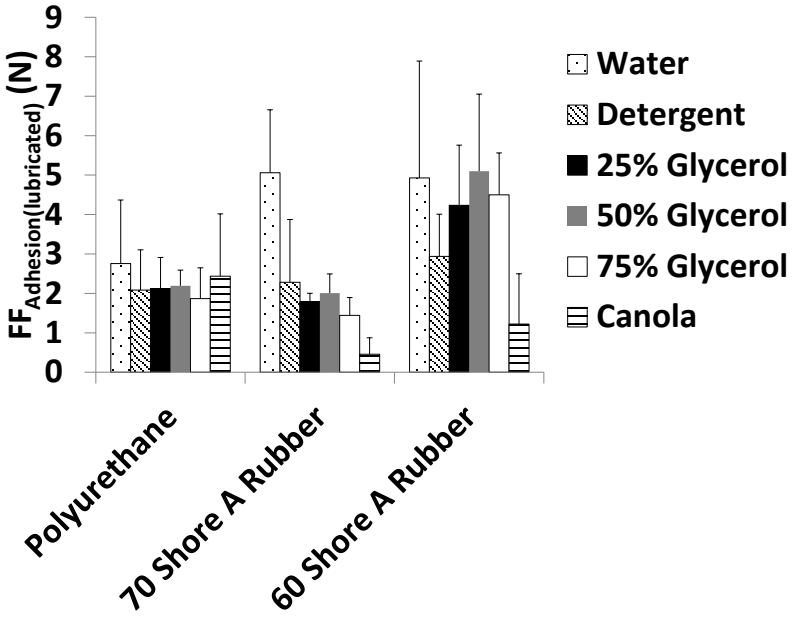

Fig. 24: Adhesion friction force (FFadhesion(lubricated)) with respect to varying lubricants and shoe materials

Further exploration of the shoe-floor interaction indicated that the vinyl flooring had more friction than the marble flooring although this relationship was reversed when tested against the soft rubber shoe material (Fig. 25). The floor-lubricant interaction was driven by the lower marble adhesion friction than vinyl adhesion friction for all fluids except the low-concentration glycerol fluids. The R^2 of the ANOVA model considering shoe, flooring, lubricant and first order interactions was 0.66 indicating that 66% of the friction variation could be explained by considering the primary and first interaction effects.

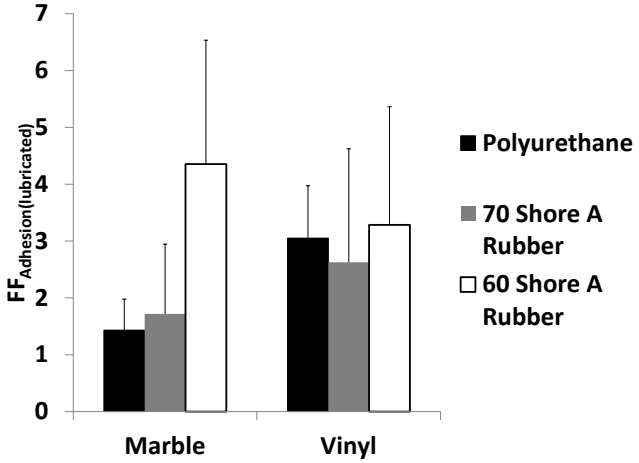

Fig. 25: Adhesion friction force ($FF_{adhesion(lubricated)}$) across the different shoe and floor surfaces

The second model (Eq. 5) revealed that the lubricant ($p<0.001$), dry adhesion friction ($p<0.001$) and their interaction ($p<0.01$) were statistically significant. This model had an R^2 of 0.49 indicating that fluid and dry adhesion friction alone were capable of predicting 49% of the total adhesion friction. The α fluid estimate, which indicates adhesion friction independent of the shoe-floor combination, was found to be highest for water, lowest for canola oil and similar for detergent and glycerol combinations. The β parameter, which indicates the dependence of lubricated adhesion friction on dry adhesion friction, was found to be highest among the glycerol fluids, moderate for the water and detergent contaminants and low for the canola oil contaminant (Table 5). Therefore, some fluids (i.e. water) have high adhesion friction but are not strongly linked with the dry adhesion friction, while the glycerol contaminants have lower adhesion friction intercept but the lubricated adhesion has strong dependence on dry adhesion friction. Canola oil has low adhesion friction and the lubricated adhesion has a low dependence on the dry adhesion. The average error between the predicted values and the actual friction values was 1.05N, which was only slightly higher than the average standard deviation for each shoe-floor-fluid combination (0.82N). These experimental results demonstrate the potential for an adhesion friction model, which is based on just two fluid parameters and the dry adhesion friction, to predict lubricated adhesion friction. This regression model may be incorporated to improve existing shoe-floor-contaminant friction models that have considered the hydrodynamics between shoe and floor materials but have not considered the boundary lubrication effects [59].

Table 5: Parameter estimates (α and β) for predicting lubricated adhesion

Fluid	α (N)	β
Water	4.3263	0.0531
1.5% Detergent	2.6125	0.0399
25% Glycerol	2.5707	0.0822
50% Glycerol	2.8006	0.1027
75% Glycerol	2.3826	0.0927
Canola oil	1.7556	0.0106

Limitations/Assumptions

1. This study only considered a single normal load and sliding speed. Coefficient of friction for shoe and floor materials has been shown to have some dependence on the normal force [60]. Therefore, the friction values and the trends observed in this study may vary with normal force. The adhesion friction regression equation also may have minimal relevance as the normal loading approaches 0 [61]. The normal force was selected so that it resulted in contact pressures similar to walking (See Section 3.2), to ensure relevance to human slipping events. In addition, sliding speeds were relatively low (0.01 m sec^{-1}) compared to slipping events (up to 1 m) [62] in order to isolate the effects of boundary lubrication. Slipping events occurring at higher speeds may include hydrodynamic effects due to the wedge term [59, 60]. Friction measurements were conducted at steady state, which may ignore transitional squeeze film effects [63].
2. While adhesion was assumed to be mostly blocked by SAE 75W-140 oil, it is likely that a very small amount of adhesion could have still occurred at the interface, which was included in the hysteresis portion of friction.

3. Experiments were conducted using a pin-on-disk apparatus, which did not include many of the dynamic effects of slipping or the hydrodynamic effects in the shoe-floor surface during slipping. These results, however, are expected to be relevant to slips that occur in the absence of hydrodynamic effects. The fact that boundary lubrication friction forces were frequently under 20% of the normal load (i.e. under an available coefficient of friction value of 0.20) threshold needed to support ambulation [64] indicates that slips may occur in the absence of hydrodynamic effects.

G.4. Scientific Report #4: Under-Shoe Fluid Pressures During Slip-Testing: Effects of Fluid and Shoe Tread [65] (Aim 2)

G.4.1. Methods

Apparatus, Experiments and Materials

The experimental apparatus consisted of a robotic device that reproduced forces and sliding speeds similar to a human slip, a force plate and a fluid pressure sensor embedded in the floor that measured hydrodynamic pressures. The robotic device was similar to the Portable Slip Simulator, which is a portable adaptation of the Slip Simulator and was developed by researchers at the Finnish Institute of Occupational Health [66]. The device consists of three linear motors installed vertically to generate vertical forces and a horizontal motor that moved the shoe anteriorly during the slip (Figure 26). Vertical forces of approximately 250 or 500 N were built up over a 30 ms time period with higher forces being used for lower friction values [66] (Figure 27). The lower vertical forces were used when the coefficient of friction exceeded 0.11 because of a limited force production capacity in the horizontal motor. The selection of the vertical force level has previously been shown to not affect results of this device between 250 or 500 N [66]. The magnitude of the vertical force was selected so that it produces about 40-85% of the body weight for a 60 kg adult, which is in the approximate range of the peak force typically generated during unexpected slips [64]. The sliding velocity was held at approximately 0.7 m/s during the simulated slip similar to sliding velocities that have been previously demonstrated in human slipping studies (Figure 27) [14]. Shoe angle was set to 10 degrees, which is similar to shoe angles that are observed during slipping [67, 68]. These testing conditions were consistent with a set of testing recommendations that have been set by a group of slip-testing experts [8]. All data was collected at room temperature (20°C) and the fluid contaminants were given adequate time to reach room temperature before tests were conducted. The robotic device was operated over a force platform in order to ensure the correct normal forces during the simulated slip were achieved (Figure 27). A fluid pressure sensor (Setra 209, inlet diameter: 10 mm) was embedded into the floor surface to measure hydrodynamic pressures in the shoe-floor interface. The top of the pressure sensor was slightly recessed below the top of the floor surface to prevent it from interfering with the shoe. This method has been used in other tribological applications such as chemical mechanical polishing to measure thin-film fluid pressures [69]. Pressure data were sampled at 1000 Hz.

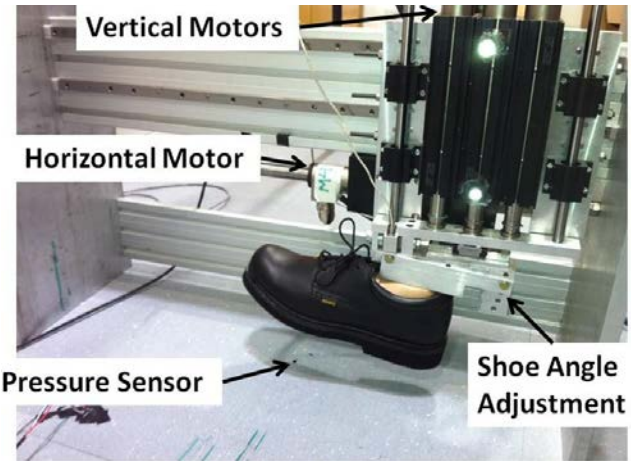

Figure 26: Slip-testing apparatus including the device and the pressure sensor.

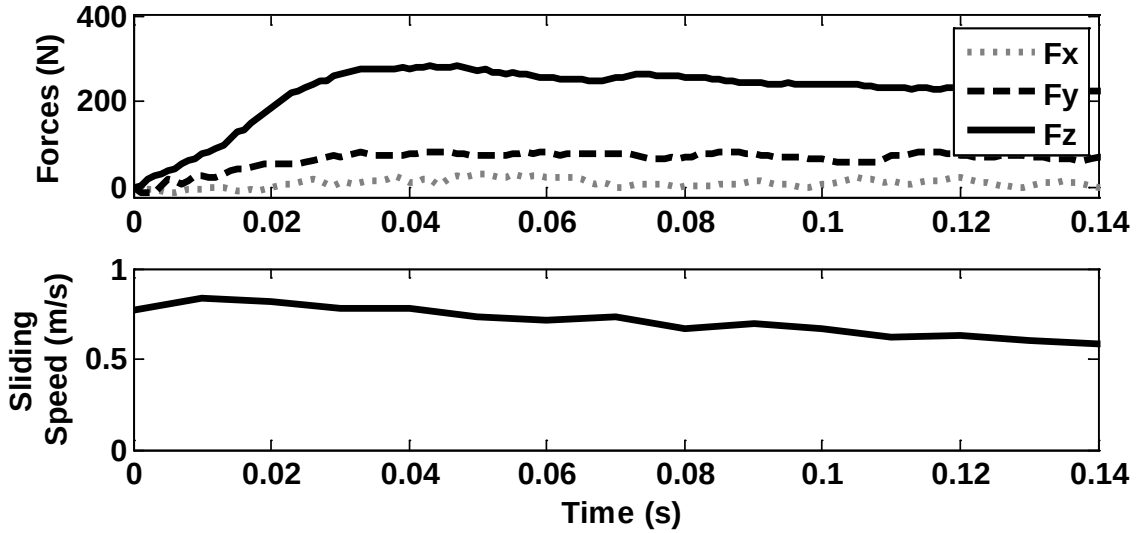

Figure 27: Representative forces and sliding speeds from a slip test. In the top graph, Fz is the normal force, Fy is the shear force in the slipping direction, and Fx is the shear force perpendicular to the slipping direction.

For each shoe-floor-fluid condition, seven trials were collected to characterize the fluid pressures across the shoe surface. The shoe was placed in a different location relative to the pressure sensor for each of the seven fluid pressure trials so that a different part of the shoe was measured with each trial. Between each of the fluid pressure trials, the shoe was moved 10 mm laterally. A reflective marker was attached to the shoe and tracked with motion capture system (Motion Analysis Corporation, Santa Rosa, CA) in order to determine the position of the shoe relative to the pressure sensor. Floor surfaces were flooded with the fluid contaminant to the point where adding additional liquid did not increase the thickness of the fluid film. The inlet of the pressure sensor was fully filled with the fluid to prevent air, which is compressible, from affecting the measurements. Fluid contaminants were reapplied to the floor surfaces between each trial. The shoe surface was pre-wetted with the contaminant before the start of data collection and the shoe surface was thoroughly cleaned before a new fluid was tested to ensure no contamination across fluids.

The testing materials included two shoe types, which were abraded to three different tread depth levels, one floor material and two fluid contaminants. The shoe designs included an

athletic shoe and a work shoe (Figure 28), the flooring was a vinyl tile and the fluids included a diluted glycerol solution (90% glycerol and 10% water by volume, 219 cP) and a detergent solution (Pledge Commercial Line Multi Surface Floor Cleaner ®) (1.5% detergent, 98.5% water by volume, 1.89 cP). Shoe heels were abraded in order to systematically remove tread, similar to methods developed by the International Standards Organization for evaluating the abrasion resistance of shoe materials [70]. The three different tread depth levels included full tread, where the shoes were just lightly abraded to remove the outermost layer; half tread, where tread was removed until the tread depth was approximately half of its original level; and no tread, where most of the tread was removed (Figure 28). During the abrading process, the material removal process was periodically paused to ensure that heat generation was not causing a chemical change in the shoe material. Because of the complex shape of the athletic shoe's tread, some minor tread features were not fully removed in order to prevent exposing the midsole material. Shoe hardness was measured using Shore A hardness scale, tread was measured using calipers and shoe roughness was measured using a 2D profilometer (see Table 6 for measurements). Hardness, tread and roughness measurements were taken from the back section of the heel. The floor hardness was measured to be 99 on a Shore A scale. The floor roughness had an average roughness (Ra) of 0.33 μm, an RMS roughness of 0.45 μm and an average peak to valley height (Rz) of 1.00 μm. Roughness and waviness quantities were measured at 4 different orientations over an evaluation length of 8mm with a stylus profilometer (Taylor Hobson Surtronic 25), calculated using a cutoff length of 0.8 mm and averaged.

Figure 28: Shoes tested in this study from left to right are: full tread athletic, half tread athletic, no tread athletic, full tread work, half tread work, and no tread work shoe. Tread was only removed from the heel of the shoe as that was the contact region during slipping.

Table 6: Tread width, tread depth, shoe hardness, and shoe roughness for all of the shoes considered in this study.

	Work Shoe			**Athletic Shoe**		
	Full Tread	**Half Tread**	**No Tread**	**Full Tread**	**Half Tread**	**No Tread**
Tread channel width (mm)	2.5	2.4	N/A	5.5	3.5	N/A
Tread depth (mm)	3.0	1.5	0	4.0	2.0	0.0

Shoe Hardness (Shore A)	58	71	68	85	83	79
Roughness (Ra) (μm)	7.24	5.74	4.44	5.05	5.24	4.43

Data Analysis

A map of the fluid pressures across the shoe surface was developed by combining multiple fluid pressure scans. The location of the shoe relative to the pressure sensor was calculated for each time point for each of the seven scans in order to generate a 2D map of hydrodynamic pressures. The total load supported by the fluid was calculated by integrating the fluid pressures over the shoe sole surface. A numerical integration technique was applied to calculate the load supported by the fluid. Specifically, each pressure value was multiplied by the distance between scans, Δx (10 mm), and the displacement between each time series sample, Δy (Eq. 27). The displacement between each time series sample is the product of the sliding velocity (0.7 m/s) and the time between samples (0.001s). This analysis relied on the assumption that the fluid pressures were in steady state since the different time points were used to calculate fluid pressures at different locations. High load support by the fluid is indicative that a fluid film is separating the surfaces [59]. The effects of tread depth and fluid viscosity on the fluid pressure support were tested using an ANOVA where the total load supported by the fluid was the dependent variable. Fluid, tread depth and their interaction were the independent variables.

$$NF_{fluid} = \sum p\Delta x\Delta y = \sum p\Delta x * v\Delta t \qquad \text{Eq. (27)}$$

G.4.2. Results

Substantial hydrodynamic pressures were observed in conditions where the high viscosity fluid was combined with untreaded shoes (Figure 29). Peak hydrodynamic pressures were located centrally on the posterior portion of the heel for the work shoe and were distributed across the posterior portion of the untreaded athletic shoe. The fluid pressures of the athletic shoe were divided into two regions on either side of a tread channel that ran in an arc across the posterior portion shoe (Figure 28). The largest fluid pressures were identified on the medial side of the shoe just anterior to this tread channel (Figure 29). The peak hydrodynamic pressure was 234 kPa and 214 kPa for the work shoe and athletic shoe, respectively. Tread depth ($p<0.01$), fluid ($p<0.01$) and the interaction between fluid and tread depth ($p<0.01$) all significantly influenced the load supported by the fluid. The load supported by the fluid was 201 N of the 500 N vertical force for the untreaded work shoe and 83 N of the 500 N vertical force for the untreaded athletic shoe when the glycerol was present (Figure 30). The load supported by the fluid was negligible (i.e., was less than 5N or 1% of the total normal load) with medium or full tread shoes or with a low viscosity fluids.

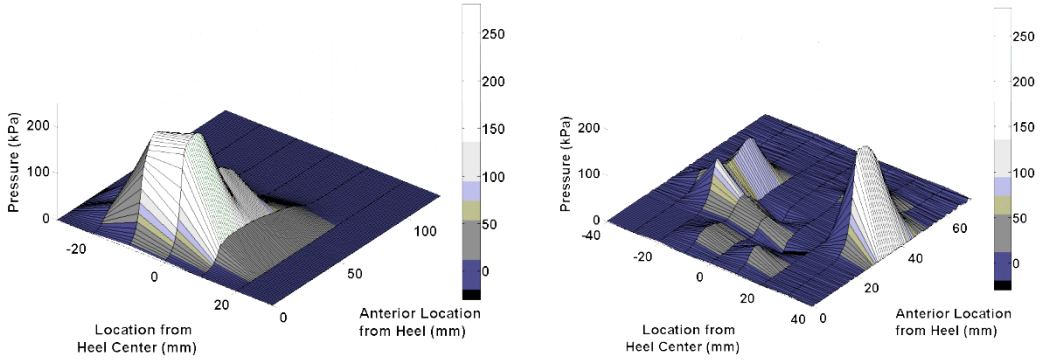

Figure 29: Hydrodynamic pressure profile of the work shoe (left) and the athletic shoe (right). The axis on the left represents the position relative to the center of the heel (lateral is positive) and the axis on the right represents the anterior position from the heel.

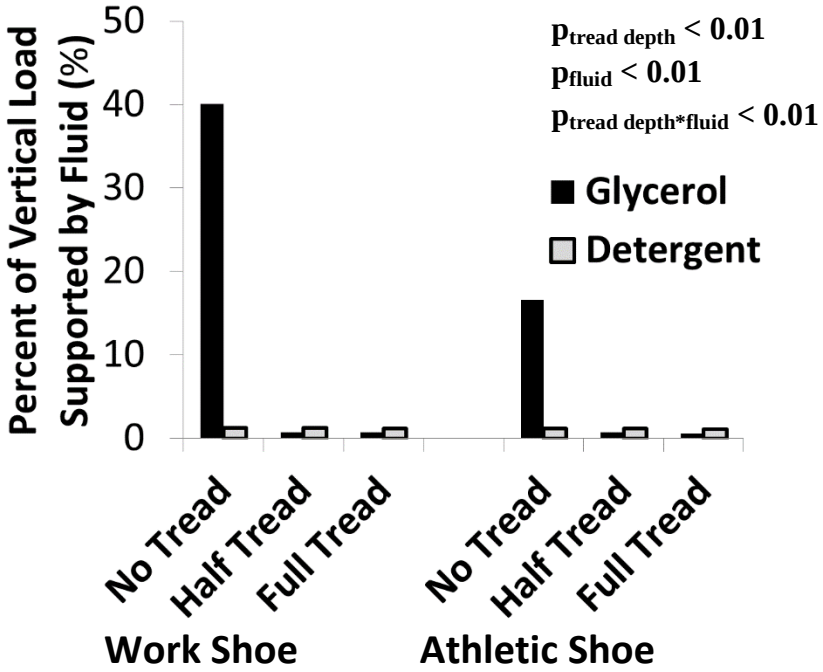

Figure 30: Effects of tread depth on the load supported by the fluid for the work shoe (left) and the athletic shoe (right) in the presence of glycerol (black bars) and detergent (gray bars).

G.4.3. Discussion

This study aimed to introduce an approach for measuring fluid pressures in the shoe-floor interface and demonstrate its utility by evaluating different tread depths and fluids for two different shoes. The methodology successfully measured hydrodynamic pressures, which were mapped across the shoe surface. Hydrodynamic pressures were observed when a high viscosity fluid was combined with an untreaded shoe. Hydrodynamic pressures were not present for treaded shoes and when a low viscosity fluid was present.

The empirical relationships between fluid pressures, tread depth and fluid are consistent with tribological theory and human-based slipping studies. The absence of shoe tread led to the development of fluid pressures as has been hypothesized by other researchers [71-74] and confirmed in unexpected slips of human subjects [3]. Since the film thickness (h), a function of the shoe geometry [59], has an inverse relationship with fluid pressures (p) according to the Reynolds equation (Eq. 1a), the finding that tread channels reduce fluid pressures is consistent with this theory. Also, the absence of hydrodynamic pressures for the low-viscosity fluid is consistent with the Reynolds equation. Since viscosity, η, is in the denominator of the left-hand terms that include pressure, p, as a numerator; a positive association between fluid pressure and fluid viscosity is expected.

Measuring hydrodynamic pressures may serve as a tool for designing shoe tread and developing shoe replacement guidelines. For example, the peak pressures were found near the centerline of the shoe approximately 20 mm anterior of the heel, suggesting that tread is most critical in this region of the shoe. Furthermore, a tread depth of 1.5 mm and 2.0 mm was sufficient to eliminate fluid pressures in the work and athletic shoes, respectively. Interestingly, the relationship between fluid pressures and tread depth were not linear. Fluid pressures dramatically decreased from no tread to half tread and then did not change between half tread and full tread. This suggests that shoe wear may have little effect on the slip-resistance of shoe

tread until a threshold is reached. Once the wear threshold is reached, a dramatic reduction in slip-resistance can be expected when stepping on high viscosity fluids. The threshold at which fluid pressures begin to develop may provide a basis for developing shoe replacement guidelines. Lastly, the finding that fluid pressures were only observed for the high viscosity fluid suggests that tread becomes particularly important in environments where high viscosity fluids (i.e., vegetable oils, machining oils, etc.) are common.

Future experimental studies should focus on expanding the number of conditions that were considered including additional tread designs, flooring and fluids. In addition, the effects of testing parameters such as shoe angle, slipping speed and vertical forces on hydrodynamic effects are not yet known. The method of artificially wearing the shoes using abrasion should be validated by comparing the results of this study with fluid pressures from naturally worn shoes. Since shoe roughness changed as the shoe wore down, additional studies should be conducted to determine if fluid pressures are more dependent on the macroscopic-scale features (tread) or the microscopic-scale features (roughness) of the shoe outsole. Lastly, a sensitivity study should be conducted to determine whether the load supported by the fluid is sensitive to the distance between scans and to determine if a gap of 10 mm is accurate for characterizing fluid pressures across the entire shoe surface.

G.5. Scientific Report #5: Under-Shoe Fluid Pressures During Unexpected Slipping [75] (Aims 2 and 3)

G.5.1. Methods

Eighteen subjects between the ages of 20 and 33 years old were recruited to participate in the study (10 female, mean ± standard deviation: age 23.5 ± 4.0 years, height 1.71 ± 0.072m, weight 70.0 ± 11.8 kg), which was approved by the University of Pittsburgh Institutional Review Board. Only healthy subjects without significant musculoskeletal or neurological disorders were included. All subjects provided informed consent prior to data collection.

Participants performed two sets of walking trials, both of which concluded with an unexpected slip. Participants wore fully treaded shoes during one slip and untreaded shoes during the other slip. The shoes were made of a rubber compound (Shore A Hardness: 58) and were advertised as being slip-resistant (Figure 31). The treaded shoes had a tread depth of 2.4 mm, a tread width of 5 mm and a tread channel width of 2.4 mm, while the untreaded shoes had the tread completely removed from the shoe sole (Figure 31). An abrasion process was used to remove the tread using 80 grit sand paper similar to standard testing methods for shoe wear [70]. The order in which the shoes were introduced was randomized. Slips were induced with a 90%:10% glycerol:water solution (viscosity: 219 cP) that was spread evenly across a 610x610mm floor surface. Prior to each slip, participants performed 5-8 baseline dry trials. During the baseline dry trials, the participants' starting position was adjusted so that their heel hit directly behind an array of fluid pressure sensors. Participants listened to music and faced the wall between each trial to reduce their awareness that a fluid contaminant had been placed on the floor, similar to previous studies that have achieved unexpected slips [76-79]. The lights were dimmed to obscure the condition of the floor. Subjects were made aware during the informed consent process that they might experience a slippery floor at some point but were not informed of the location, nature or timing of the slippery surface. Subjects' pressure data were analyzed only if they either stepped directly on the fluid pressure sensor array or if they slipped across the array. A subject was considered to have stepped or slid on a fluid pressure sensor if a marker placed on the subject's heel passed within the boundaries of the sensor array during the slip. The heel marker was used instead of other foot markers because previous studies have indicated that the foot is inclined at the start of an unexpected slip and that the heel portion of the shoe is in contact with the floor throughout the slip [14, 67]. Eleven of eighteen slips with untreaded shoes and six of eighteen slips with treaded shoes met these qualifications and were

included in the analysis. Peak slipping speed was only calculated when the subject stepped cleanly on the glycerol-covered area.

Figure 31: Picture of the fully treaded shoes (left) and the untreaded shoes that had the tread fully removed (right)

The instrumentation included an array of fluid pressure sensors and a reflective marker placed posteriorly and inferiorly on the heel. A 3x3 array of fluid pressure sensors were embedded beneath the floor surface to measure hydrodynamic pressures as the participants slipped across the floor surface (Figure 32). The fluid pressure sensors were spaced 30 mm apart from each other in both directions. The pressure sensors (Gems ® 3100-R-150PG-08-F-X-3) had an inlet diameter of 4 mm, accuracy of 2.5 kPa and range of 1000 kPa. When the fluid contaminant was applied to the floor, the inlet of each pressure sensor was filled completely with fluid to ensure continuous fluid from the transducer to the top of the floor surface. Similar methods have been used to evaluate shoes using a slip-tester [80] and in evaluating the tribology of chemical mechanical polishing [69]. A marker was place on the inferior portion of the heel in order to track the slipping kinematics. Marker position was tracked with a 14 camera motion capture system (Vicon MX). The system was calibrated to achieve an accuracy of within 1mm.

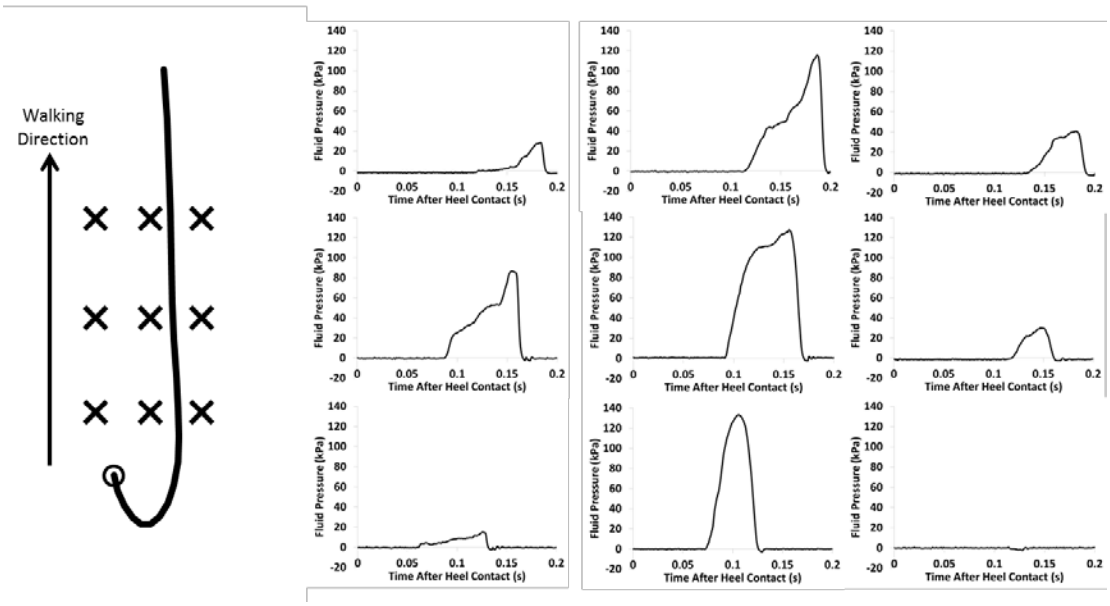

Figure 32: Representative heel trajectory (left) and time-series fluid pressures (right) during a single subject's unexpected slip with untreaded shoes. The thick solid line represents the heel trajectory, the circle is the location of the heel at heel contact and each of the fluid pressure sensors is marked with an X. The fluid pressure graphs are positioned according to their location in the pressure sensor array (i.e., the top left graph corresponds to the top left sensor).

The fluid pressures were characterized using the magnitude of the fluid pressures and the duration in which the pressures exceeded baseline levels. Fluid pressures were typically characterized by a single peak (Figure 32) and the maximum of that peak was identified. Fluid pressure duration was defined as the time between the first and last moment that fluid pressures exceeded 5 standard deviations of baseline levels. Typical baseline standard deviation pressures were around 0.24 kPa. The severity of the slip was characterized using peak slipping speed (PSS), which was defined as the peak resultant speed during the slip [79]. In order to accomplish the secondary objective of determining the effects of the instantaneous slipping speed and the medial/lateral position relative to the shoe, the spatiotemporal variables of the foot relative to each individual fluid sensor were calculated. The instantaneous resultant slipping speed (IRSS) was calculated at the time that the heel passed each of the fluid pressure sensors. IRSS was used for this analysis instead of the peak sliding speed because IRSS relates to the state of the shoe when the heel was over the sensor and is therefore more relevant to how shoe kinematics influence the fluid pressures observed in a given sensor. The medial-lateral distance between the heel marker and the fluid pressure sensor was also calculated at the time when the heel marker passed by the pressure sensor in the anterior-posterior direction to determine if hydrodynamic pressures varied across the shoe surface. In addition to IRSS and the medial-lateral position, the sensor position relative to walking direction (SPRWD) was analyzed to determine how fluid pressures varied as the slip progressed. SPRWD was an ordinal variable with three different levels based on their location relative to the direction of walking (i.e., the foot slipped over the first row, second row and third row of sensors sequentially).

ANOVA methods were used to test the effects of shoe tread on fluid pressures and peak slipping speed (PSS) as well as to determine the effects of the instantaneous resultant slipping speed (IRSS), medial-lateral position and sensor position relative to walking direction (SPRWD) on fluid pressures. The fluid pressures were characterized using the peak pressure across the entire fluid pressure sensor array and the pressure duration time. Differences in the peak fluid

pressure, fluid pressure distance and peak slipping speed (PSS) across the two tread conditions were analyzed using a t-test. A regression analysis was performed between PSS and maximum hydrodynamic pressures across all of the sensors to determine if fluid pressures were predictive of the slip severity. An ANOVA procedure was performed to determine the effects of foot position, IRSS and SPRWD on peak hydrodynamic pressures for each individual sensor. Peak hydrodynamic pressure for each fluid sensor was the dependent variable; while IRSS (continuous), medial-lateral distance from the heel to the pressure sensor (continuous) and the sensor's anterior/posterior position in the array (ordinal) as the independent variables.

G.5.2. Results

The subjects' heel landed on or slipped across the fluid pressure sensors in eleven of the untreaded conditions (61%) and six of the treaded conditions (33%). Maximum fluid pressures ($p<0.01$) and peak slip velocities ($p<0.01$) were higher in the untreaded condition compared with the treaded condition. The mean (standard deviation) maximum fluid pressures across all of the sensors were 124 kPa (75 kPa) for the untreaded shoe condition and 1.1 kPa (0.29 kPa) for the treaded shoes. In the trials where subjects cleanly hit the contaminant, peak slipping speeds were 2.03 m/s (1.09 m/s) for untreaded shoes and 0.08 m/s (0.02 m/s) for treaded shoes. In the trials where subjects slipped over the fluid pressure sensors, peak slipping speeds (PSS) were 1.57 m/s (0.80 m/s) for the untreaded shoes and 0.063 (0.017 m/s) for the treaded shoes. PSS was significantly positively correlated with the maximum fluid pressure measurements ($r=.87$) (Figure 33).

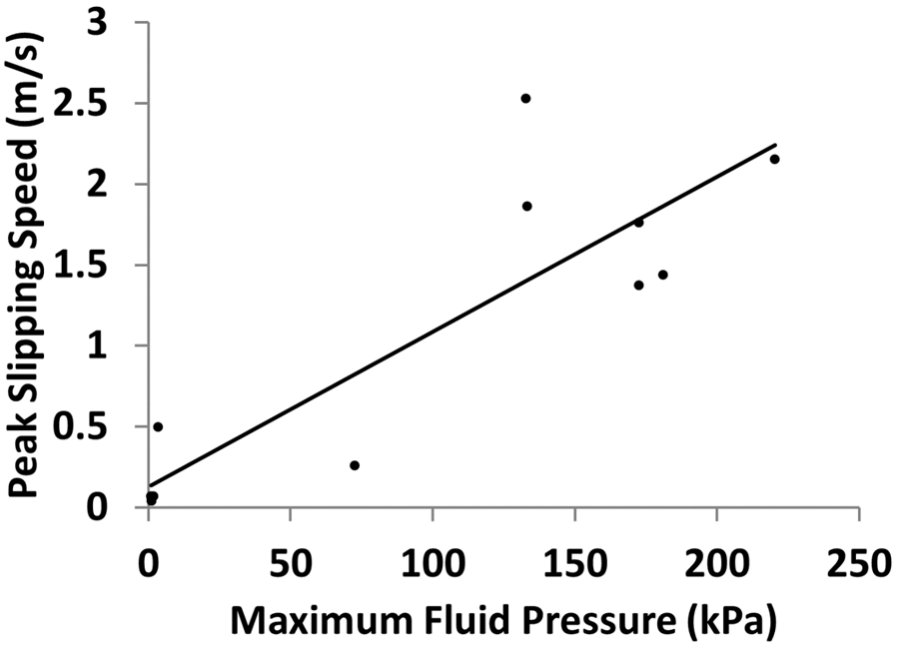

Figure 33: Peak slipping speed for each subject plotted against the peak hydrodynamic fluid pressures.

The effects of the sensor position relative to walking direction (SPRWD), medial-lateral position and instantaneous resultant slipping speed (IRSS) on fluid pressures were only analyzed using the untreaded conditions since fluid pressures exceeded baseline levels for just one of the treaded condition trials. The peak fluid pressures for the individual pressure sensors were dependent on the SPRWD ($p<0.01$), on the IRSS ($p<0.001$) during slipping, and the medial-lateral distance ($p<0.001$) of the sensor relative to the heel (Figure 34). Fluid pressures

were highest at the first row of sensors and progressively decreased for the second and third row (Figure 34C). IRSS was positively correlated with fluid pressures (Figure 34A). Fluid pressures were highest at the center of the heel and decreased toward the sides of the heel (Figure 34B). The mean (standard deviation) pressure duration was 75 ms (50 ms) and was not significantly affected by any of the examined variables.

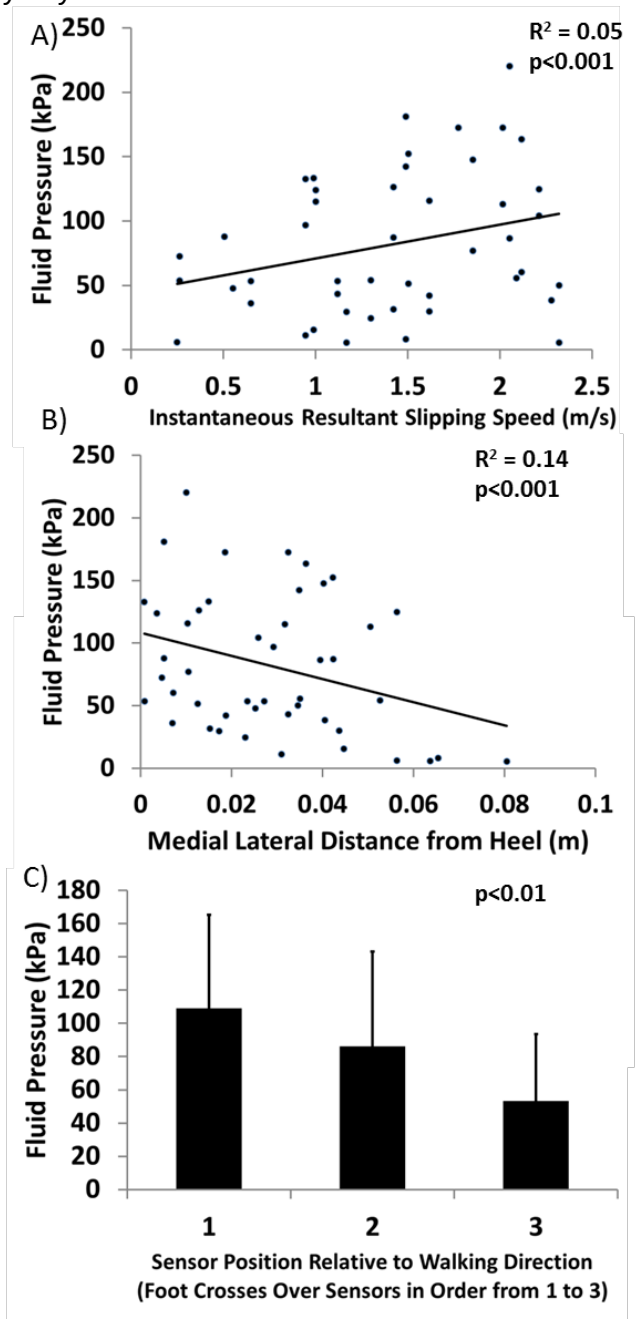

Figure 34: Effects of instantaneous resultant slipping speed (A), medial-lateral position of the sensor relative to the heel (B) and the sensor position relative to walking direction (C) on the peak fluid pressure for each individual sensor.

IRSS, the medial-lateral distance between the heel and the sensor, and the SPRWD seemed to all contribute independently to the overall fluid pressure values (Table 7). When regressed by themselves, each of the variables was only able to describe between 5% and 14%

of the total variability. When two of the three variables were considered, between 20% and 26% of the variability was described. When all three variables were included in the regression analysis, 41% of the variability was described.

Table 7: Adjusted R2 values to describe the amount of fluid pressure variability that was described by sensor position relative to walking distance (SPRWD), medial-lateral distance (ML Distance) and instantaneous resultant slipping speed (IRSS).

Variables	R2
SPRWD	0.11
ML Distance	0.14
IRSS	0.05
SPRWD & ML Distance	0.24
SPRWD & IRSS	0.20
ML Distance & IRSS	0.26
SPRWD, ML Distance & IRSS	0.41

G.5.3. Discussion

The primary finding in this study was the dramatic effect tread had on the reduction of hydrodynamic pressures during a slip. This effect, in turn, was shown to significantly reduce the slip severity (Figure 33). It was also found that hydrodynamic pressures were affected by the instantaneous resultant slipping speed (IRSS) (Figure 34A), the medial-lateral location relative to the heel (Figure 34B) and were reduced later in the slip (Figure 34C). Finally, the results were consistent with tribology theory, particularly the wedge and squeeze film effects of the Reynolds equation.

The findings are consistent with fundamental tribological theory, and suggest the existence of wedge and squeeze-film effects during slipping (Figure 35). The correlations found between fluid pressures and slipping speed, fluid pressure positioning relative to the walking direction and medial/lateral position are also consistent with this view. The squeeze film effect is influenced by dwell time, fluid viscosity, distance from the center of the shoe, while the wedge effect is influenced by fluid viscosity, distance from the center of the shoe and and slipping speed [47] (Figure 35). For example, increased slipping speed is known to increase fluid pressures [59]and decrease available friction due to the wedge term effect [22, 59, 81]. The positive correlation identified between peak fluid pressure and IRSS (Figure 34A) indicates that the increased slipping speed causes an increase in hydrodynamic pressures during real slip events, again predicted by the wedge term. The wedge term effect acts as a positive feedback system where IRSS leads to higher fluid pressures (Figure 34A); those higher fluid pressures reduce the available friction; and the resulting lower friction values allow the foot to accelerate, which could lead to further increases in the instantaneous slipping speed and eventually a higher peak slipping speed (Figure 33). The reduction in hydrodynamic pressures as the heel slips across the fluid pressure sensor array indicates that squeeze-film effects are also present during human slipping events. According to squeeze film theory, the lubricating ability of the fluid decreases over time [47]. Fluid pressures were reduced by approximately 50% when the foot reached the third row of sensors compared with the first row of sensors (Figure 34C). This reduction in fluid pressures during the progression of the slip indicates that dwell time had a decreasing effect. The finding that fluid pressures are largest near the center of the shoe and decrease towards the edges is consistent with previous studies that modeled the wedge effect [59]. Up to 41% of the variability in fluid pressures was described when including all three of these effects, indicating that fluid pressure has a dependence on location, time and IRSS (Table

7). Lastly, this study confirmed that the drainage channels provided by tread are capable of reducing hydrodynamic effects, which is consistent with a previous study by our group that showed this effect using a mechanical slip-tester [80]. For the conditions tested in this study, 2.5 mm of tread was sufficient for eliminating fluid pressure and reducing the severity of slips. Because only two tread depths were tested in this experiment, additional experiments would be needed to identify the minimum amount of tread that is required to prevent under-shoe fluid pressures.

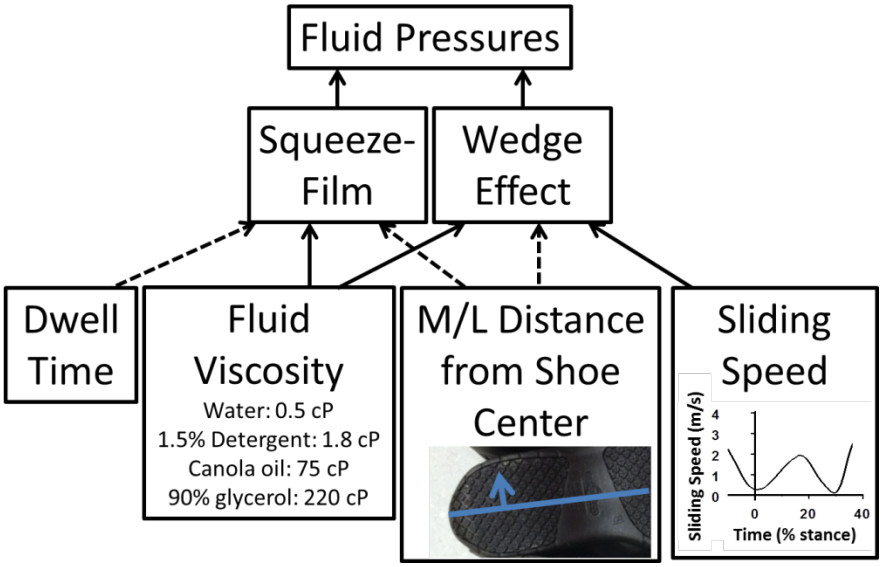

Figure 35: Conceptual model for the effects of dwell time, fluid viscosity, medial/lateral (M/L) distance from the center of the shoe and sliding speed on the wedge and squeeze-film effects of the Reynolds equation [47]. Solid lines represent factors that would increase fluid pressures while dashed lines represent factors that would decrease fluid pressures. Viscosity values from water, detergent, canola oil [32] and 90% glycerol [80] viscosity values were taken by previous tribology research. The plot within the “Sliding Speed” box is a representative time-series slipping speed profile where 0% time is heel contact.

The measurement of hydrodynamic pressures may be appropriate for evaluating the ability of mechanical slip-testers to mimic the under-shoe tribology of human slips. In 2001, a panel of slip-testing experts determined that slip-testing devices should be tribologically fidelic (i.e., mimic the tribological interaction of a human slip) [82]. The results from this study can be used as reference data to evaluate the ability of slip-testing devices to mimic a real slip. Our previous research using a slip-tester had identified peak fluid pressures of 240 kPa when testing the same untreaded shoes with the same fluid and similar vinyl composition flooring [80], which is similar to the maximum fluid pressure observed in this study (220 kPa) and was on the same order of magnitude for the average peak fluid pressure (124 kPa). Future research could systematically modify the slip-testing parameters of this device (vertical force, slipping speed and shoe angle) to achieve fluid pressures similar to the fluid pressures observed during actual slip events.

The technique introduced in this manuscript has potential for evaluating shoe tread design and wear. The shoe that was used in this study was advertised as slip-resistant and appeared to be effective when the tread was present. Other shoe tread designs may be less effective at eliminating hydrodynamic pressures and slip severity. Repeating these experiments across different tread patterns may provide insight into how the design of the tread affects both the hydrodynamics in the shoe-floor interface and the slip outcomes. Our testing revealed that a loss of tread can negatively affect the slip-resistance of the shoe. Testing shoes with varying

levels of wear may provide additional insights into the amount of tread required to sustain slip-resistance. Knowing the tread thresholds required to sustain slip resistance will be beneficial for developing shoe-replacement guidelines.

G.6. Scientific Report #4: Impact of Boundary Lubrication COF on Slip Risk (Aim 3) (Confidential)

G.6.1. Methods

Subjects

Thirty-one subjects were recruited to participate in the study including 13 female subjects (mean age: 23.9 +/- 5.02 years; mean height: 171 +/-5.68 cm; mean mass: 77.2 +/- 23.2 kg; mean shoe size: 7.5 +/- 0.78 US Men's Shoe Size) and 17 male subjects (age: 24.0 +/- 4.19 years; height: 177 cm +/- 7.89 cm; mean mass: 76.3 +/- 17.1 kg; mean shoe size: 9.6 +/- 1.2 US Men's Shoe Size). Subjects were screened to ensure that they did not have any musculoskeletal or neurological problem that would negatively impact their gait. Two subjects were removed from the analysis because they were frequently looking down and it was determined that they were anticipating a slip throughout testing.

Materials

Three different shoe materials were tested against a vinyl tile floor with a 50% glycerol/50% water contaminant. The three shoe materials were selected with a high hardness level, a medium hardness level and a low hardness level. All of the shoes had an identical tread pattern, which included a non-treaded slight bevel on the posterior/lateral and then 10 lugs across the heel section. The outsole also had a cross-hatch texturing to it on the heel region. The fluid contaminant was selected based on preliminary research that identified that the available coefficient of friction for the shoe-floor-fluid interface was between 0.15 and 0.2 for all of the shoes when using this fluid and floor.

Slip-Testing Approach

The coefficient of friction and the under-shoe fluid pressures were measured, while a slip-testing device applied a normal force to each of the shoe and traversed it across the floor surface. The slip-testing device consists of three vertical motors that apply the vertical force and one horizontal motor that applies the horizontal force to overcome friction similar to the Portable Slip Simulator [66]. The vertical force used during testing was 250 N, the horizontal sliding speed was 0.3 m/s and the shoe-floor angle was seven degrees. Coefficient of friction values measured using a 250 N vertical force has previously been shown to provide very close results to those measured using a 500 N vertical force for this device [66]. These testing conditions were selected because they are similar to those specified in whole shoe testing standards [83, 84]. The 250 N force was reached in approximately 200 ms. Four repeated trials of each shoe material (for a Men US Size 9 shoe) were performed. Forces were measured using a 6DOF force plate. In addition to the COF testing, a fluid pressure scan was collected for each of the boots similar to methods outlined in Singh and Beschorner [65].

Human Slipping Approach

Participants performed four blocks of walking trials and the final two blocks of walking trials concluded with a slip event. For each of the three first blocks of trials, the subjects wore shoes with a different outsole material in randomized order. The fourth block of trials was performed using the same pair of shoes as the second block of trials. The baseline trials during

the first three blocks of trials were intended to determine if differences in RCOF existed across the different shoe outsoles during baseline walking, while the unexpected slip in the third and fourth block of trials were intended to determine the risk of slipping from each of the shoe materials. After the first slip, subjects performed an additional 5-20 unperturbed walking trials to allow them to return to baseline walking before the second slip was induced. During the unexpected slipping trial, 150 ml was spread evenly across the 0.4 m x 0.6 m force plate to achieve a fluid thickness of 0.6 mm. Both subjects and the research team that was interacting with the subjects were blinded to the shoe outsole materials making this a double-blind study.

Data Analysis

Force plate data was used to calculate the available and required coefficient of friction, while foot kinematic data was used to calculate slip severity. The slip-resistance of each shoe outsole material was assessed based on the average coefficient of friction. Coefficient of friction was calculated as the average ratio of resultant shear force to normal force over the 200 ms immediately following when the vertical force reached 250N. Required coefficient of friction (RCOF) was calculated from the five trials immediately preceding the slip where the subject cleanly hit the force plate with the same foot that experienced the slip. RCOF was measured as the peak ratio of shear to vertical force once the vertical force was over 100 N, the RCOF was increasing and in the anterior direction [85]. The ground reaction forces were filtered using a fourth-order low-pass Butterworth filter with a cutoff frequency of 36 Hz [85]. The occurrence of a slip was categorized based on the peak slipping speed after the subject's foot came in contact with the fluid contaminant. The peak resultant speed of a virtual marker placed at the base of the subject's heel was determined by identifying the peak slipping speed between the first and second local minimum after heel contact or when the subject's foot slipped off of the force plate. Subjects were considered to have experienced a slip if the peak resultant slipping speed exceeded 0.2 m/s. Slipping trials where the subjects did not hit cleanly on the force plate (n=6) were excluded from the analysis.

Statistical analyses were implemented to determine whether the risk of slipping varied across the outsole materials, whether the available and required coefficient of friction was different across the outsole materials and whether required coefficient of friction, available coefficient of friction or the difference between the two predicted slip risk. To determine whether slipping rate varied across the outsole materials, a Fisher's Exact test was performed with a binary variable denoting slip outcome as the dependent variable and the shoe outsole material as the dependent variable. To determine if the available and required coefficient of friction varied across shoe material, an ANOVA was performed with coefficient of friction as the dependent variable, the shoe material, slip order (first or second) and the interaction as the independent variables. A post-hoc Tukey HSD test was used in case shoe material was found to be significant to determine which shoe materials were different than the other shoe materials. Lastly, three logistic regression models were tested where slip outcome was the dependent variable and the independent variable was available coefficient of friction (model 1), required coefficient of friction (model 2) or the difference between available and required coefficient of friction (model 3).

G.6.2. Results

Twenty-nine percent of slip trials resulted in a slip. The outsole shoe material significantly influenced the risk of slipping ($p<0.05$) with fewer slips observed for the soft outsole

material than the medium or hard outsole materials (Figure 36). The slip risk was not distinguishable between the medium hardness and hardest materials. Also, fewer slips were observed during the second slip ($p<0.05$) than the first slip. The available friction was significantly higher for the soft outsole material than the medium and hard outsole materials, which were statistically indistinguishable (Figure 37). Under-shoe fluid pressures (<10 kPa) were very small for all of the shoe materials when measured for the slip-tester and when measured during human slips. Neither the outsole material nor the slip order influenced the amount of required coefficient of friction.

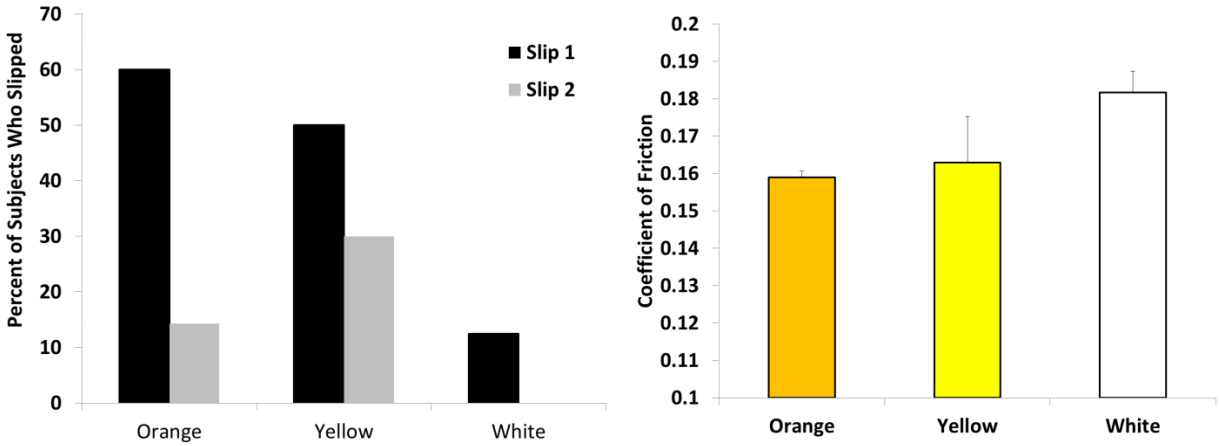

Figure 36: Effect of shoe material on slip risk (left) and available coefficient of friction (right). Error bars on the right figure are standard deviations. Color codes refer to the hardness of materials (orange is the hardest, yellow is the medium hardness and white is the least hard.

A)

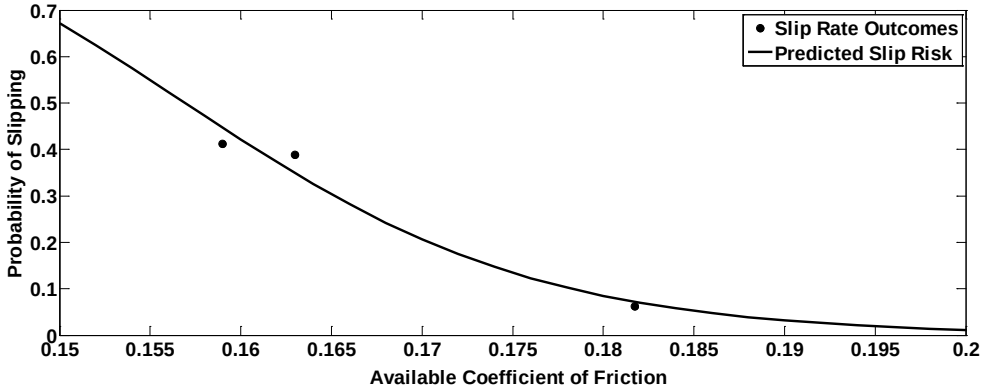

B)

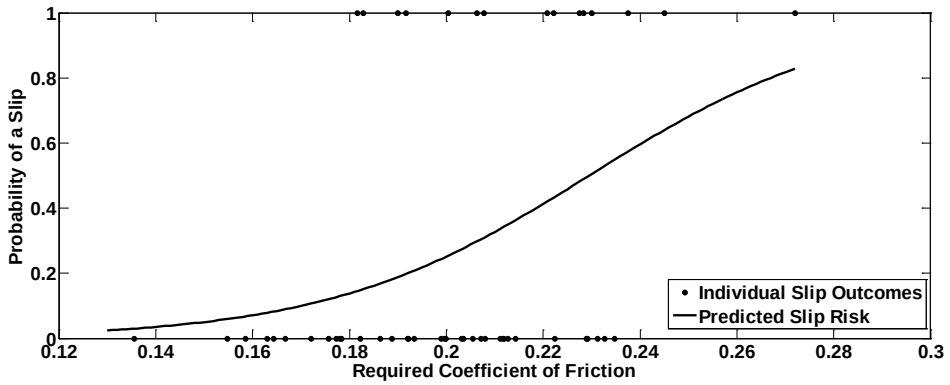

C)

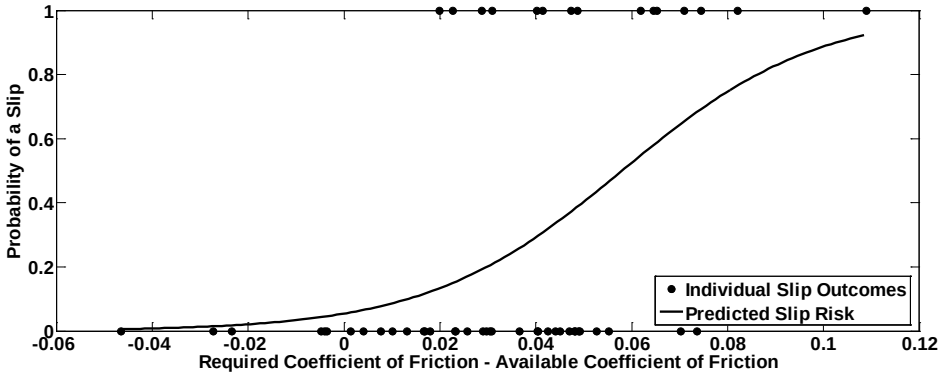

Figure 37: Slip outcomes and logistic fit curves for available coefficient of friction (A), required coefficient of friction (B) and the difference between available and required coefficient of friction (C).

The dependent variable was statistically significant in all three logistic regression models. Specifically, larger available coefficient of friction was found to reduce slip risk ($p<0.01$),

increased required coefficient of friction was found to increase slip risk ($p<0.01$), and a larger difference between required coefficient of friction and available coefficient of friction was found to increase slip risk ($p<0.001$). The predicted risk for the three materials was 54% for the hardest material, 42% for the medium hardness and 7.7% for the softest. The model predicted that the subject with the lowest RCOF had just a 3% chance of slipping, while the subject with the highest RCOF had a 83% chance of slipping. The subject with the median RCOF had just a 26% risk of slipping. The subject-outsole material pair with the lowest RCOF-ACOF had a projected slip risk of just 0.6%, while the subject-outsole material pair with the highest RCOF-ACOF had a projected slip risk of 92.5%. The projected slip risk for the RCOF-ACOF was 21%.

G.6.3. Discussion

This study demonstrated that even modest changes in available coefficient of friction can result in dramatic changes in slip risk. Specifically an increase in friction from 0.159 to 0.182 changed the slip rate from 41% to 6%. Furthermore, a wide range of slip risk between 3% and 83% is predicted by an individual's required coefficient of friction. A slip-resistant outsole material combined with low required friction generated a slip risk of less than 1%, whereas when a slippery outsole material is combined with a high required coefficient of friction, the risk increases to 92%.

This study confirms that modest changes in the boundary lubrication coefficient of friction caused by different outsole materials can dramatically alter slip risk. Finite element models of shoe-floor friction reveal that softer shoe materials allow for better conformance of the shoe asperities to the floor topography, which increases adhesion friction. Softer shoe materials also were found to slightly reduce the amount of hysteresis friction. Since this study used a relatively low viscosity fluid (50% glycerol), which only blocks about 50% of 60% of dry adhesion in boundary lubrication [86], it is likely that the hardest material experienced increases in adhesion friction due to increased contact area that exceeded the losses in hysteresis friction due to reduced energy loss during load cycling.

The findings that ACOF and the difference between RCOF and ACOF predicted slip risk were largely consistent with other research. Increases in ACOF and the difference between ACOF and RCOF were found to increase slip risk as suggested in previous research [15, 87-89]. The model that considered both RCOF and ACOF also predicted slips with more certainty than either variable on its own given that it had a larger $\beta 1$ coefficient. The ACOF-RCOF value that predicted a 50% slip rate was -0.06, which is within the range suggested by other studies that used full-shoe slip-testers (0.16 [15] and -0.11 [89]). Furthermore, the $\beta 1$ for the ACOF-RCOF model (-49.2) was similar to other studies (-41.2 to -45.1 [88]; -54.7 [87]).

The findings that individual RCOF is predictive of slip risk supports the relevance of a large body of research that has assumed that individual RCOF is related to slip risk. For example, Burnfield and Powers concluded that center of mass dynamics influenced slip risk based on the finding that center of mass dynamics influenced slipping risk [18]. The finding that RCOF on its own was predictive of slip risk supports the underlying assumption of this paper that RCOF was related to slip risk. The wide range in predicted slip risk across the subjects in this study (3-83%) suggests that interventions that reduce RCOF may have potential for reducing individual slip risk.

H.References for Scientific Report

1. Moore, C.T., et al., *Analysis of shoe friction during sliding against floor material: role of fluid contaminant.* Journal of Tribology, 2012. **134**(4): p. 041104.
2. Singh, G. and K.E. Beschorner, *A Method for Measuring Fluid Pressures in the Shoe-Floor-Fluid Interface: Application to Shoe Tread Evaluation.* IIE Transactions on Occupational Ergonomics and Human Factors, 2014(just-accepted): p. 00-00.
3. Beschorner, K.E., et al., *Fluid Pressures at the Shoe-Floor-Contaminant Interface During Slips: Effects of Tread & Implications on Slip Severity.* Journal of Biomechanics, 2014. **47**(2): p. 458-463.
4. Mirhassani Moghaddam, S.R., *Finite Element Analysis of Contribution of Adhesion and Hysteresis to Shoe-floor Friction*, in *Industrial Engineering*. 2013, University of Wisconsin-Milwaukee: Milwaukee, WI.
5. Ruser, J.W., *Nonfatal workplace injuries to older workers: evidence from the BLS Survey of Occupational Injuries and Illnesses*, in *National Occupation Injury Research Symposium (NOIRS)*. 2000.
6. Leamon, T.B. and P.L. Murphy, *Occupational slips and falls: more than a trivial problem.* Ergonomics, 1995. **38**(3): p. 487-498.
7. Courtney, T.K., et al., *Occupational slip, trip, and fall-related injuries--can the contribution of slipperiness be isolated?* Ergonomics, 2001. **44**(13): p. 1118-1137.
8. Chang, W.R., et al., *The role of friction in the measurement of slipperiness, Part 2: survey of friction measurement devices.* Ergonomics, 2001. **44**(13): p. 1233-1261.
9. Chang, W.R. and S. Matz, *The slip resistance of common footwear materials measured with two slipmeters.* Appl Ergon, 2001. **32**(6): p. 549-58.
10. Liberty Mutual Research Institute, *Preventing Slips and Falls- Slip-Resistant Footwear*. 2004: Hopkinton, MA. p. LP 5407.
11. Gronqvist, R., et al., *An apparatus and a method for determining the slip resistance of shoes and floors by simulation of human foot motions.* Ergonomics, 1989. **32**(8): p. 979-95.
12. Beschorner, K.E., et al., *Effects of slip testing parameters on measured coefficient of friction.* Applied ergonomics, 2007. **38**(6): p. 773-780.
13. Skiba, R., A. Kuschefski, and N. Cziuk, *Entwicklung eines normgerechten Prufverfahrens zur Ermittlung der Gleitsicherheit von Schuhsohlen, Forschung Fb 526.* Schriftenreihe der Bundesanstalt fur Arbeitsschutz, 1987.
14. Cham, R. and M.S. Redfern, *Heel contact dynamics during slip events on level and inclined surfaces.* Safety Science, 2002. **40**(7-8): p. 559-576.
15. Hanson, J.P., M.S. Redfern, and M. Mazumdar, *Predicting slips and falls considering required and available friction.* Ergonomics, 1999. **42**(12): p. 1619-1633.
16. McVay, E.J. and M.S. Redfern, *Rampway safety: foot forces as a function of rampway angle.* American Industrial Hygiene Association, 1994. **55**(7): p. 626-634.
17. Redfern, M.S. and J. DiPasquale, *Biomechanics of descending ramps.* Gait & posture, 1997. **6**(2): p. 119-125.
18. Burnfield, J.M. and C.M. Powers, *The Role of Center of Mass Kinematics in Predicting Peak Utilized Coefficient of Friction During Walking*.* Journal of forensic sciences, 2007. **52**(6): p. 1328-1333.
19. Chang, W.-R., *The effect of surface roughness on the measurement of slip resistance.* International Journal of Industrial Ergonomics, 1999. **24**(3): p. 299-313.

20. Chang, W.-R., *Preferred surface microscopic geometric features on floors as potential interventions for slip and fall accidents on liquid contaminated surfaces.* Journal of safety research, 2004. **35**(1): p. 71-79.
21. Chang, W.-R., et al., *The effect of surface waviness on friction between Neolite and quarry tiles.* Ergonomics, 2004. **47**(8): p. 890-906.
22. Beschorner, K.E., et al., *Effects of slip testing parameters or measured coefficient of friction.* Applied Ergonomics, 2007. **38**(6): p. 773-780.
23. Sun, Z., D. Howard, and M. Moatamedi, *Finite element analysis of footwear and ground interaction.* Strain, 2005. **41**(3): p. 113-117.
24. Poon, C. and R. Sayles. *Frictional transition in boundary lubrication sliding*. in *2nd Int. Conf. on Combustion Engines-Reduction of Friction and Wear, IMechE, London*. 1989.
25. Poon, C. and R. Sayles, *The classification of rough surfce contacts in relation to tribology.* Journal of Physics D: Applied Physics, 1992. **25**(1A): p. A249.
26. Bowden, F. and D. Tabor, *Mechanism of metallic friction.* Nature, 1942. **150**(3798): p. 197-199.
27. Moore, D.F., *Principles and applications of tribology*. Vol. 1. 1975: Pergamon Press Oxford.
28. Hu, Y.-Z. and D. Zhu, *A full numerical solution to the mixed lubrication in point contacts.* Journal of Tribology, 2000. **122**(1): p. 1-9.
29. Zhang, H., et al., *A new algorithm for numerical solution of 3D elastoplastic contact problems with orthotropic friction law.* Computational mechanics, 2004. **34**(1): p. 1-14.
30. Ng, S.H., et al., *An analysis of mixed lubrication in chemical mechanical polishing.* Journal of tribology, 2005. **127**(2): p. 287-292.
31. Greenwood, J. and J. Williamson, *Contact of nominally flat surfaces.* Proceedings of the Royal Society of London. Series A. Mathematical and Physical Sciences, 1966. **295**(1442): p. 300-319.
32. Moore, C.T., et al., *Analysis of Shoe Friction During Sliding Against Floor Material: Role of Fluid Contaminant.* Journal of Tribology, 2012. **134**: p. 041104.
33. Beschorner, K.E., M.S. Redfern, W.L. Porter, and R.E. Debski, *Effects of slip testing parameters on measured coefficient of friction.* Applied Ergonomics, 2007. **38**(773-780).
34. Beschorner, K., Michael Lovell, C. Fred Higgs III, and Mark S. Redfern, *Modeling mixed-lubrication of a shoe-floor interface applied to a pin-on-disk apparatus.* Tribology Transactions, 2009. **52**: p. 560-568.
35. Nelder, J.A., and R. Mead, *A simplex method for function mimimization.* The Computer Journal, 1965. **7**: p. 308-313.
36. Lagarias, J.C., J.A. Reeds, M.H. Wright, and P.E. Wright, *Convergence properties of the Nelder-Mead Simplex Method in low dimensions.* SIAM Journal of Optimization, 1998. **9**(1): p. 112-147.
37. D'Errico, J. *MATLAB Central - File Detail - Fminsearchbnd. MathWorks - MATLAB and Simulink for Technical Computing. MATLAB*. 2006 [cited 2010 June]; Available from: http://www.mathworks.com/matlabcentral/fileexchange/8277-fminsearchbnd.
38. Esfahanian, M., and Hamrock, B.J., *Fluid-film lubrication regimes revisited.* Tribology Transactions, 1991. **34**(4): p. 618-632.
39. Hamrock, B.J., *Fundamentals of fluid film lubrication*, ed. I. McGraw-Hill. 1994.
40. Bhushan, B., and Zhao, Z., *Macro- and microscale tribological studies of molecularly-thick boundary layer of perfluoropolyether lubricants for magnetic thin-film rigid disks.* J. Info. Storage Proc. Syst., 1999. **1**: p. 1-21.
41. Bhushan, B., *Introduction to Tribology*. 2002, New York: John Wiley & Sons.
42. Hornback, J.M., *Organic Chemistry*. 2006, Belmont, CA: Thomson.
43. Lai, K.-Y., *Liquid Detergents*. 2006, Boca Raton: Taylor & Francis.

44. Strandberg, L., *The effect of conditions underfoot on falling and overexertion accidents.* Ergonomics, 1985. **28**: p. 131-147.
45. Proctor, T.D.a.V.C., *Slipping, tripping and falling accidents in Great Britain - present and future.* Journal of Occupational Accidents, 1988. **9**: p. 269-285.
46. Strobel, C.M., et al., *Analysis of the Contribution of Adhesion and Hysteresis to Shoe-Floor Lubricated Friction in the Boundary Lubrication Regime.* Tribology Letters, 2012. **46**(3): p. 341-7.
47. Hamrock, B.J., S.R. Schmid, and B.O. Jacobson, *Fundamentals of fluid film lubrication*. Vol. 169. 2004: CRC press.
48. Lewis, G., *Finite element analysis of a model of a therapeutic shoe: effect of material selection for the outsole.* Bio-Medical Materials and Engineering, 2003. **13**(1): p. 75-81.
49. Bhowmick, A.K., *Rubber products manufacturing technology*. 1994: CRC.
50. Menezes, P.L. and S.V. Kailas, *Effect of roughness parameter and grinding angle on coefficient of friction when sliding of Al–Mg alloy over EN8 steel.* Journal of Tribology, 2006. **128**: p. 697.
51. Menezes, P.L., Kishore, and S.V. Kailas, *Studies on friction and transfer layer using inclined scratch.* Tribology International, 2006. **39**(2): p. 175-183.
52. Menezes, P.L., *Role of Surface Texture on Friction and Transfer Layer Formation – A Study Using Pin-on-Disk Sliding Tester*, in *Department of Materials Engineering*. 2007, Indian Institute of Science: Bangalore, India.
53. Greenwood, J.A. and J.B.P. Williamson, *Contact of Nominally Flat Surfaces.* Proceedings of the Royal Society of London. Series A, Mathematical and Physical Sciences (1934-1990), 1966. **295**(1442): p. 300-319.
54. Fu, S.Y., et al., *Effects of particle size, particle/matrix interface adhesion and particle loading on mechanical properties of particulate–polymer composites.* Composites Part B: Engineering, 2008. **39**(6): p. 933-961.
55. Le Gal, A., X. Yang, and M. Klüppel, *Evaluation of sliding friction and contact mechanics of elastomers based on dynamic-mechanical analysis.* The Journal of chemical physics, 2005. **123**: p. 014704.
56. Manning, D., C. Jones, and M. Bruce, *Boots for oily surfaces.* Ergonomics, 1985. **28**(7): p. 1011-1019.
57. Franyutti, S. and G. Williams, *New polyurethane systems for athetic footwear.* Journal of cellular plastics, 1992. **28**(1): p. 24-35.
58. Chandrasekaran, M. and A.W. Batchelor, *In situ observation of sliding wear tests of butyl rubber in the presence of lubricants in an X-ray microfocus instrument.* Wear, 1997. **211**(1): p. 35-43.
59. Beschorner, K., et al., *Modeling Mixed-Lubrication of a Shoe-Floor Interface Applied to a Pin-on-Disk Apparatus.* Tribology Transactions, 2009. **52**(4): p. 560-568.
60. Beschorner, K.E., et al., *Effects of slip testing parameters or measured coefficient of friction.* Applied Ergonomics, 2007. **38**: p. 773-80.
61. Hutchings, I.M., *Tribology: friction and wear of engineering materials.* 1992.
62. Cham, R. and M.S. Redfern, *Lower Extremity Corrective Reactions to Slip Events.* Journal of Biomechanics, 2001. **34**: p. 1439-1445.
63. Gronqvist, R., *Mechanisms of friction and assessment of slip resistance of new and used footwear soles on contaminated floors.* Ergonomics, 1995. **28**: p. 224-241.
64. Redfern, M.S., et al., *Biomechanics of Slips.* Ergonomics, 2001. **44**: p. 1138-1166.
65. Singh, G. and K. Beschorner, *A Method for Measuring Hydrodynamic Lubrication in the Shoe-Floor-Fluid Interface: Application to Shoe Tread Evaluation.* IIE Transactions on Occupational Ergonomics and Human Factors, 2014. **in press**.
66. Aschan, C., et al., *Development and validation of a novel portable slip simulator.* Applied Ergonomics, 2005. **36**: p. 585-593.

67. Cham, R. and M.S. Redfern, *Changes in gait when anticipating slippery floors.* Gait & Posture, 2002. **15**(2): p. 159-71.
68. Leamon, T.B. and D.H. Son, *The natural history of microslip.* Advances in Industrial Ergonomics and Safety I, 1989: p. 633-638.
69. Shan, L., et al., *Interfacial Fluid Mechanics and Pressure Prediction in Chemical Mechanical Polishing.* Journal of Tribology, 2000. **122**: p. 539.
70. International Standards Organization, *ISO 20871-2001: Footwear -- Test methods for outsoles -- Abrasion resistance*. 2012, ISO: Switzerland.
71. Li, K.W. and C.J. Chen, *The effect of shoe soling tread groove width on the coefficient of friction with different sole materials, floors, and contaminants.* Applied Ergonomics, 2004. **35**(6): p. 499-507.
72. Li, K.W., H.H. Wu, and Y.C. Lin, *The effect of shoe sole tread groove depth on the friction coefficient with different tread groove widths, floors and contaminants.* Applied Ergonomics, 2006. **37**(6): p. 743-748.
73. Strandberg, L., *The effect of conditions underfoot on falling and overexertion accidents.* Ergonomics, 1985. **28**(1): p. 131-147.
74. Tisserand, M., *Progress in the prevention of falls caused by slipping.* Ergonomics, 1985. **28**: p. 1027-1042.
75. Beschorner, K.E., et al., *Fluid pressures at the shoe–floor–contaminant interface during slips: Effects of tread & implications on slip severity.* Journal of biomechanics, 2014. **47**(2): p. 458-463.
76. Beschorner, K., M.S. Redfern, and R. Cham, *Earliest gait deviations during slips: Implications for recovery.* IIE Transactions on Occupational Ergonomics and Human Factors, 2013. **1**(1): p. 31-37.
77. Chambers, A.J. and R. Cham, *Slip-related muscle activation patterns in the stance leg during walking.* Gait & Posture, 2007. **25**(4): p. 565-572.
78. Moyer, B., M. Redfern, and R. Cham, *Biomechanics of trailing leg response to slipping-Evidence of interlimb and intralimb coordination.* Gait & posture, 2009. **29**(4): p. 565-570.
79. Moyer, B.E., et al., *Gait parameters as predictors of slip severity in younger and older adults.* Ergonomics, 2006. **49**(4): p. 329-343.
80. Singh, G. and K. Beschorner, *A Method for Measuring Hydrodynamic Lubrication in the Shoe-Floor-Fluid Interface: Application to Shoe Tread Evaluation.* Ergonomics, 2013. **in review**.
81. Proctor, T.D. and V. Coleman, *Slipping, Tripping and Falling Accidents in Great Britain-Present and Future*, in *Journal of Occupational Accidents*. 1988.
82. Chang, W.R., et al., *Measuring slipperiness- discussions on the state of the art and future research*, in *Measuring Slipperiness: Human Locomotion and Surface Factors*, W.R. Chang and T.K. Courtney, Editors. 2003, Taylor & Francis: London & New York.
83. ASTM, *ASTM F2913-11: Standard Test Method for Measuring the Coefficient of Friction for Evaluation of Slip Performance of Footwear and Test Surfaces/Flooring Using a Whole Shoe Tester*. 2011, ASTM International: West Conshohocken, PA.
84. European Standards and International Standards Organization, *EN ISO 13287: Personal protective equipment -- Footwear -- Test method for slip resistance*. 2012, Danish Standards: Charlottenlund, Denmark.
85. Chang, W.-R., et al., *A methodology to quantify the stochastic distribution of friction coefficient required for level walking.* Applied ergonomics, 2008. **39**(6): p. 766-771.
86. Cowap, M.J., et al., *Contributions of Adhesion and Hysteresis to the Coefficient of Friction Between Shoe and Floor Surfaces: Effects of Floor Roughness and Sliding Speed.* in review, 2014.
87. Burnfield, J.M. and C.M. Powers, *Prediction of slips: an evaluation of utilized coefficient of friction and available slip resistance.* Ergonomics, 2006. **49**(10): p. 982-995.

88. Siegmund, G.P., et al., *The effect of subject awareness and prior slip experience on tribometer-based predictions of slip probability.* Gait & posture, 2006. **24**(1): p. 110-119.
89. Tsai, Y.J. and C.M. Powers, *The Influence of Footwear Sole Hardness on Slip Initiation in Young Adults*.* Journal of forensic sciences, 2008. **53**(4): p. 884-888.

I.Publications

I.1. Peer-Reviewer Grants

Beschorner, K.E., Albert, D.L., Chambers, A.J., Redfern, M.S., [2014] Fluid Pressures at the Shoe-Floor-Contaminant Interface During Slips: Effects of Tread & Implications on Slip Severity, *Journal of Biomechanics* **47** (2), pp. 458-463.

Singh, G., Beschorner, K.E. [2014] A Method for Measuring Hydrodynamic Lubrication in the Shoe-Floor-Fluid Interface: Application to Shoe Tread Evaluation, *Institute of Industrial Engineers: Occupational Ergonomics and Human Factors*, in press.

Moore, C.T., Beschorner, K.E., Menezes, P., Lovell, M.R. [2012] Analysis of Shoe Friction during Sliding Against Floor Material: Role of Fluid Contaminant, *Journal of Tribology* **134** (4), p. 041104.

Strobel, C.M., Menezes, P., Lovell, M.R., Beschorner, K.E., [2012] Analysis of the Contribution of Adhesion and Hysteresis to Shoe-Floor Lubricated Friction in the Boundary Lubrication Regime, *Tribology Letters* 47 (3), 341-7.

I.2. Proceedings

Moghaddam, S.R., Beschorner, K.E. [2014] Finite Element Model of Shoe-Floor Hysteresis Friction, STLE Tribology Frontiers, Chicago, IL.

Beschorner, K.E., Chambers, A.J., Redfern, M.S. [2013] Effect of Shoe Tread Depth on Hydrodynamic Pressures in the Shoe-Floor Interface During Slipping. American Society of Biomechanics, Omaha, NE.

Albert, D., Ledgerwood, A., Chambers, A.J., Redfern, M.S. Beschorner, K.E. [2013] Effect of Shoe Tread Depth on Medial Lateral and Anterior-Posterior Foot Slipping Kinematics, American Society of Biomechanics, Omaha, NE.

Beschorner, K.E., Singh, G. [2012] A Novel Method for Evaluating the Effectiveness of Shoe-Tread Designs Relevant to Slip and Fall Accidents, Human Factors and Ergonomics Society, Boston, MA.

Singh, G., Beschorner, K.E. [2012] Influence of hydrodynamic fluid pressure and shoe tread depth on available coefficient of friction, ASME/STLE International Joint Tribology Conference, Denver, CO.

Singh, G. Beschorner, K.E. [2012] A 3-dimensional viscoelastic finite element model for predicting adhesion and hysteresis based on roughness, sliding speed and material properties, ASME/STLE International Joint Tribology Conference, Denver, CO.

Cowap, J. Beschorner, K.E. [2012] The Effects of Floor Roughness On Shoe-Floor Adhesion and Hysteresis, ASME/STLE International Joint Tribology Conference, Denver, CO.

Beschorner, K.E. [2012] Experimental and Modeling Studies for Understanding Shoe-Floor-Contaminant Friction and Designing for Slip-Resistance, ASME/STLE International Joint Tribology Conference, Denver, CO.
Moore, C.T., Beschorner, K.E., P.L. Menezes, M.R. Lovell [2011] Analysis of the Contribution of Adhesion and Ploughing to Shoe-Floor Lubricated Friction in the Boundary Lubrication Regime, ASME/STLE International Joint Tribology Conference, October 24-26, Los Angeles, CA.
Moore, C.T. and Beschorner, K.E. [2010] “Effects of varying shoe surface roughness on COF Between Shoe and Floor Material in the Presence of a Liquid Contaminant”. ASME/STLE International Joint Tribology Conference, March 31, 2010. San Francisco, CA. October 18-20, 2010.

I.3. Thesis:

Moore, C.T. [2011] Tribological contributions to slip and fall accidents: lubrication, adhesion and ploughing effects, M.S. Thesis, University of Wisconsin-Milwaukee.
Singh, G. [2012] Analysis of shoe-floor slipperiness through computational modeling and measurements of hydrodynamic pressures with robotic slip simulator, M.S. Thesis, University of Wisconsin-Milwaukee.
Moghaddam [2013] Finite Element Analysis of Contribution of Adhesion and Hysteresis to Shoe-Floor Friction, M.S. Thesis, University of Wisconsin-Milwaukee.

J.Inclusion Enrollment Table

Program Director/Principal Investigator (Last, First, Middle): Redfern, Mark S.

Inclusion Enrollment Report

This report format should NOT be used for data collection from study participants.

Study Title: Developing a Computational Model for Shoe-Floor Friction

Total Enrollment: 52 **Protocol Number:** PRO09090102

Grant Number: R01OH008986

PART A. TOTAL ENROLLMENT REPORT: Number of Subjects Enrolled to Date (Cumulative) by Ethnicity and Race				
Ethnic Category	**Females**	**Males**	**Sex/Gender Unknown or Not Reported**	**Total**
Hispanic or Latino	0	2	0	2 **
Not Hispanic or Latino	2	3	0	5
Unknown (individuals not reporting ethnicity)	24	21	0	45
Ethnic Category: Total of All Subjects*	26	26	0	52 *
Racial Categories				
American Indian/Alaska Native	0	0	0	0
Asian	3	3	0	6
Native Hawaiian or Other Pacific Islander	0	1	0	1
Black or African American	3	6	0	9
White	20	14	0	34
More Than One Race	0	2	0	2
Unknown or Not Reported	0	0	**0**	0
Racial Categories: Total of All Subjects*	26	26	0	52 *

PART B. HISPANIC ENROLLMENT REPORT: Number of Hispanics or Latinos Enrolled to Date (Cumulative)				
Racial Categories	**Females**	**Males**	**Sex/Gender Unknown or Not Reported**	**Total**
American Indian or Alaska Native	0	0	0	0
Asian	**0**	0	0	0
Native Hawaiian or Other Pacific Islander	0	1	0	**1**
Black or African American	0	0	0	0
White	0	1	0	1
More Than One Race	0	0	0	0
Unknown or Not Reported	0	0	0	0
Racial Categories: Total of Hispanics or Latinos**	0	2	0	2 **

* These totals must agree.
** These totals must agree.

K.Inclusion of Children

Children under 21 years of age were eligible and participated in this study.

L.Materials Available for Other Investigators

None.

TANGIBLE PERSONAL PROPERTY REPORT
Final Report SF-428- B

Federal Grant or Other Identifying Number Assigned by Federal Agency (Block 2 on SF-428).

5R01OH00 8986-03

1. **Report** (Select all that apply)

a. ___ Federally-owned Property (List on Supplemental Sheet SF-428S or recipient equivalent and complete Section 2a below.)

b. ___ Acquired Equipment with acquisition cost of $5,000 or more for which the awarding agency has reserved the right to transfer title (List on Supplemental Sheet SF-428S or recipient equivalent and complete Section 2b below.)

c. ___ Residual Unused Supplies with total aggregate fair market value exceeding $5,000 not needed for any other Federally sponsored programs or projects. *(Complete Section 2c below)*

d. ___ None of the above

2. Complete relevant section(s)	**For Agency Use Only**
2a. **Federally-owned Property** *(Select one or more.)* (i) ___ Request transfer to Award _____ (ii) ___ Request Federal Agency disposition instructions (iii) ___ Other *(Provide detail in Block **3** or attach request)*	Agency response to requested disposition of Federally owned property: (i) Recipient request approved___ denied ___ (ii) Dispose in accordance with attached instructions ___.
2b. **Acquired Equipment** *(Select one or more.)* (i) ___ Request unconditional transfer of title with no further obligation to the Federal Government. (ii) ___ Request Federal Agency disposition instructions Note: If the awarding agency does not provide disposition instructions within 120 days the recipient may continue to use the equipment for Federally supported projects or dispose in accordance with the applicable property standards.	Agency response to requested disposition of acquired equipment:: (i) Recipient request approved___ denied ___ (ii) Dispose in accordance with attached instructions ___ Authorized Awarding Agency Official Signature: / Date: Name: / Phone: Title / Email

2c. **Reportable Residual Unused Supplies**

(i) __ Sale proceeds or __ Estimate of current fair market value ..... $_____

(ii) Percentage of Federal participation ..... _____%

(iii) Federal share ..... $_____

(iv) Selling and handling allowance ..... $_____

(v) **Amount remitted to the Federal Government**..... $_____

3. Comments

Null

FINAL REPORT ATTACHMENT TO SF-428

Agency use only

OMB Approval Number: 3090-0289
Expiration Date: 4/30/2013

Form Approved Through 08/31/2015
OMB No. 0925-0002

Department of Health and Human Services

Final Invention Statement and Certification

(For Grant or Award)

DHHS Grant or Award No.

5R01OH00 8986-03

A. We hereby certify that, to the best of our knowledge and belief, all inventions are listed below which were conceived and/or first actually reduced to practice during the course of work under the above-referenced DHHS grant or award for the period

8/01/10 through 07/31/14 .

original effective date — *date of termination*

B. Inventions (Note: If no inventions have been made under the grant or award, insert the word *"NONE"* under Title below.)

NAME OF INVENTOR	TITLE OF INVENTION	DATE REPORTED TO DHHS
NONE		
(Use continuation sheet if necessary)		

C. Signature — This block ***must*** be signed by an official authorized to sign on behalf of the Institution.

Title
Associate Vice Provost for Research Operations

Typed Name
Jennifer Woodward, PhD

Signature
Jennifer E Woodward

Date
10/29/14

Name and Mailing Address of Institution
University of Pittsburgh
Office of Research
123 University Place
B21 University Club
Pittsburgh, PA 15213

FEDERAL FINANCIAL REPORT

DRAFT

1. Federal Agency and Organizational Element to Which Report is Submitted	2. Federal Grant or Other Identifying Number Assigned by Federal Agency	
NATIONAL INSTITUTE FOR OCCUPATIONAL SAFETY AND HEALTH	5R01OH008986-3	

3.Recipient Organization (Name and complete address, including Zip code)

UNIVERSITY OF PITTSBURGH AT PITTSBURGH
UNIVERSITY OF PITTSBURGH
OFFICE OF RESEARCH
PITTSBURGH PA 15213

4a. DUNS Number	4b. EIN	5. Recipient Account Number or Identifying Number	6. Report Type	7. Basis of Accounting
004514360	1250965591A6	117972A	☐ Quarterly ☐ Semi-Annual ☐ Annual ☒ Final	☒ Cash ☐ Accrual

8. Project/Grant Period From: (Month, Day, Year)	To: (Month, Day, Year)	9. Reporting Period End Date (Month, Day, Year)
08/01/2010	07/31/2014	07/31/2014

10. Transactions	Cumulative
(Use lines a-c for single or multiple grant reporting)	
Federal Cash (To report multiple grants, also use FFR Attachment):	
a. Cash Receipts	898,522.00
b. Cash Disbursements	898,522.00
c. Cash on Hand (line a minus b)	0.00
(Use lines d-o for single grant reporting)	
Federal Expenditures and Unobligated Balance:	
d. Total Federal funds authorized	898,522.00
e. Federal share of expenditures	898,522.00
f. Federal share of unliquidated obligations	0.00
g. Total Federal share (sum of lines e and f)	898,522.00
h. Unobligated balance of Federal funds (line d minus g)	0.00
Recipient Share:	
i. Total recipient share required	0.00
j. Recipient share of expenditures	0.00
k. Remaining recipient share to be provided (line i minus j)	0.00
Program Income:	
l. Total Federal program income earned	0.00
m. Program income expended in accordance with the deduction alternative	0.00
n. Program income expended in accordance with the addition alternative	0.00
o. Unexpended program income (line l minus line m or line n)	0.00

11. Indirect Expense	a. Type	b. Rate	c. Period From	Period To	d. Base	e. Amount Charged	f. Federal Share
	Predetermined	51.50	08/01/2010	07/31/2014	463,644.28	238,776.80	238,776.80
				g. Totals:	463,644.28	238,776.80	238,776.80

12. Remarks: Attach any explanations deemed necessary or information required by Federal sponsoring agency in compliance with governing legislation:

The original FFR was submitted for the period ending 07/31/13. This new FFR is being submitted for the NCE period through 07/31/14.

Prepared by Andrea Dunn
Ph: 412-624-5722
adunn@cfo.pitt.edu

13. Certification: By signing this report, I certify to the best of my knowledge and belief that the report is true, complete, and accurate, and the expenditures, disbursements and cash receipts are for the purposes and intent set forth in the award documents. I am aware that any false, fictitious, or fraudulent information may subject me to criminal, civil, or administrative penalties. (U.S. Code, Title 18, Section 1001)

a. Typed or Printed Name and Title of Authorized Certifying Official	c. Telephone (Area code, number and extension)
Mark Stolko Assistant Controller	412-624-6040
	d. Email address adunn@cfo.pitt.edu
b. Signature of Authorized Certifying Official	e. Date Report Submitted (Month, Day, Year) 10/27/2014
	14. Agency use only: